



University of Kentucky  
UKnowledge

---

Theses and Dissertations--Biosystems and  
Agricultural Engineering

Biosystems and Agricultural Engineering

---


2021

## IMPACT OF PREFERENTIAL FLOW, SOURCE WATER CONNECTIVITY, AND AGRICULTURAL MANAGEMENT PRACTICES ON SEDIMENT AND PARTICULATE PHOSPHORUS DYNAMICS IN MIDWESTERN TILE-DRAINED LANDSCAPES

Saeid Nazari

University of Kentucky, saeed\_nazari67@yahoo.com

Author ORCID Identifier:

 <https://orcid.org/0000-0002-9972-2737>

Digital Object Identifier: <https://doi.org/10.13023/etd.2021.367>

[Right click to open a feedback form in a new tab to let us know how this document benefits you.](#)

### Recommended Citation

Nazari, Saeid, "IMPACT OF PREFERENTIAL FLOW, SOURCE WATER CONNECTIVITY, AND AGRICULTURAL MANAGEMENT PRACTICES ON SEDIMENT AND PARTICULATE PHOSPHORUS DYNAMICS IN MIDWESTERN TILE-DRAINED LANDSCAPES" (2021). *Theses and Dissertations--Biosystems and Agricultural Engineering*. 82.

[https://uknowledge.uky.edu/bae\\_etds/82](https://uknowledge.uky.edu/bae_etds/82)

This Doctoral Dissertation is brought to you for free and open access by the Biosystems and Agricultural Engineering at UKnowledge. It has been accepted for inclusion in Theses and Dissertations--Biosystems and Agricultural Engineering by an authorized administrator of UKnowledge. For more information, please contact [UKnowledge@lsv.uky.edu](mailto:UKnowledge@lsv.uky.edu).

## **STUDENT AGREEMENT:**

I represent that my thesis or dissertation and abstract are my original work. Proper attribution has been given to all outside sources. I understand that I am solely responsible for obtaining any needed copyright permissions. I have obtained needed written permission statement(s) from the owner(s) of each third-party copyrighted matter to be included in my work, allowing electronic distribution (if such use is not permitted by the fair use doctrine) which will be submitted to UKnowledge as Additional File.

I hereby grant to The University of Kentucky and its agents the irrevocable, non-exclusive, and royalty-free license to archive and make accessible my work in whole or in part in all forms of media, now or hereafter known. I agree that the document mentioned above may be made available immediately for worldwide access unless an embargo applies.

I retain all other ownership rights to the copyright of my work. I also retain the right to use in future works (such as articles or books) all or part of my work. I understand that I am free to register the copyright to my work.

## **REVIEW, APPROVAL AND ACCEPTANCE**

The document mentioned above has been reviewed and accepted by the student's advisor, on behalf of the advisory committee, and by the Director of Graduate Studies (DGS), on behalf of the program; we verify that this is the final, approved version of the student's thesis including all changes required by the advisory committee. The undersigned agree to abide by the statements above.

Saeid Nazari, Student

Dr. William Ford, Major Professor

Dr. Donald Colliver, Director of Graduate Studies

IMPACT OF PREFERENTIAL FLOW, SOURCE WATER CONNECTIVITY, AND  
AGRICULTURAL MANAGEMENT PRACTICES ON SEDIMENT AND  
PARTICULATE PHOSPHORUS DYNAMICS IN MIDWESTERN TILE-DRAINED  
LANDSCAPES

---

DISSERTATION

---

A dissertation submitted in partial fulfillment of the  
requirements for the degree of Doctor of Philosophy in the  
College of Engineering and the College of Agriculture, Food, and Environment at the  
University of Kentucky

By  
Saeid Nazari  
Lexington, Kentucky

Director: Dr. William Ford, Assistant Professor of Biosystems and Agricultural  
Engineering  
Lexington, Kentucky  
2021

Copyright © Saeid Nazari 2021  
<https://orcid.org/0000-0002-9972-2737>

## ABSTRACT OF DISSERTATION

### IMPACT OF PREFERENTIAL FLOW, SOURCE WATER CONNECTIVITY, AND AGRICULTURAL MANAGEMENT PRACTICES ON SEDIMENT AND PARTICULATE PHOSPHORUS DYNAMICS IN MIDWESTERN TILE-DRAINED LANDSCAPES

Tile drainage is recognized as a significant transporter of sediment and particulate phosphorus (PP) in the Midwestern U.S., leading to proliferation of Harmful Algal Blooms (HABs). Numerous studies have focused on Dissolved Reactive Phosphorus (DRP) and Nitrogen (N) flux dynamics in tile-drained landscapes; however, the impact of preferential flow and agricultural management practices on fate and transport of sediment and PP has remained poorly understood. The overarching objective of this study was to improve understanding of sediment P delivery in tile-drained landscapes. This dissertation focuses on four studies.

In the first study, forms and flow pathway dynamics of total phosphorus (TP) loading in midwestern tile-drained landscapes was investigated. A dataset including 5 years of surface and tile discharge P and N concentrations from two Edge-of-Field (EOF) study sites with contrasting soil and management practices were investigated. Hydrograph recession techniques were coupled with multiple linear regression (MLR) for understanding hydrologic flow pathways, and empirical mode decomposition (EMD) time-series analysis was used to determine the significance of PP seasonality processes and the effect of management practices. The results showed that macropore flow plays a significant role in PP delivery to subsurface P loading which was significantly affected by environmental conditions and management practices.

In the second study, a new framework that couples hydrograph recession and specific conductance end-member mixing analysis (SC-EMMA) was developed to quantify both flow pathway dynamics and source connectivity of drainage water in tile-drainage. Statistical analysis was employed to evaluate the impact of pathway-connectivity dynamics on DRP concentrations. The results highlighted that pathway-connectivity hydrograph components improved prediction of DRP concentrations over hydrograph recession and SC-EMMA results in isolation. The findings also highlighted the importance of matrix-macropore exchange and preferential flow of new water to groundwater recharge to impact drainage hydrographs and DRP concentrations.

In the third study, our new pathway-connectivity framework was combined with high-frequency turbidity data to investigate sources and pathways of sediment delivery in tiles. MLR analysis was performed to evaluate impacts of pathway connectivity on sediment concentration and seasonal dynamics were assessed using hysteresis analysis. The results showed that new water that routes through quickflow reservoir is the main

hydrograph fraction for sediment and PP delivery in these landscapes. Results showed that hydrograph partitioning can improve prediction of sediment concentration and quickflow of new water was the major sediment and PP delivery pathway to tiles. Sediment concentrations were different in dry season with promoted macropores as compared to cold season with higher soil moisture and freezing and thawing effects.

In the fourth study, the impacts of drainage water management (DWM) on flow pathway-connectivity and PP dynamics were investigated. Before-After-Control-Impact (BACI) assessment, long-term EMD, and hysteresis analysis of data from a paired controlled (CD) and free-drainage (FD) field site was performed. The results showed that tile discharge, preferential flow and sediment P are significantly impacted by DWM at the event timescale. Results also suggested that DWM can change time-to-peak of hydrograph, preferential flow, thus impacting sediment pathway and transport processes in subsurface flow. Cumulatively, DWM was found to decrease sediment and PP concentration and loadings at the study site through enhancement of subsurface filtration and decreases in preferential transport of new water.

The processes elucidated in this study should be considered and used in agroecosystem models for improving representation of subsurface sediment delivery processes, and for model evaluation. Future studies should consider use of more robust tracers to elucidate spatial and temporal distribution of sediment sources and erosion mechanisms from subsurface pathways.

**KEYWORDS:** Tile Drainage, Preferential Flow, Source-connectivity, Sediment, Particulate P, Drainage water management.

---

Saeid Nazari

---

06/24/2021

---

Date

IMPACT OF PREFERENTIAL FLOW, SOURCE WATER CONNECTIVITY, AND  
AGRICULTURAL MANAGEMENT PRACTICES ON SEDIMENT AND  
PARTICULATE PHOSPHORUS DYNAMICS IN MIDWESTERN TILE-DRAINED  
LANDSCAPES

By  
Saeid Nazari

William Ford

---

Director of Dissertation

Donald Colliver

---

Director of Graduate Studies

06/24/2021

---

Date

## DEDICATION

This dissertation is dedicated to the almighty god who lifted us from miry clay, and to my beloved wife who is my best friend

## ACKNOWLEDGMENTS

I would like to thank to several individuals who helped and supported me throughout my PhD program. I would like to thank my advisor, Dr. William Ford, and rest of my committee members, Dr. Kevin King, Dr. Michael Montross, Dr. Ole Wendroth and Dr. Dwayne Edwards for helping me and supporting my research. First and foremost, I want to immensely appreciate my advisor and mentor, Dr. William Ford, for all his helps, supports, mentorships, encouragements, and patience. I personally believe that he is an incredible teacher, smart and knowledgeable researcher, and a great friend who knows the best way to provide a friendly and professional environment for doing research, making motivation, and pushing through new challenges. I would also like to thank Dr. Kevin King for all his helps and supports especially for timely provision of data and information, careful and insightful revision of our journal articles, being flexible about project materials and topics, and sharing his experience and knowledge about drainage research and field work with me. In addition, I would like to thank Dr. Michael Montross, chair of Biosystems and Agricultural Engineering Department, for providing a safe, appropriate, calm and friendly environment for all the staffs especially graduate students, so they can focus on their research work without any major interruptions. My gratitude also goes to Dr. Ole Wendroth, my PhD committee member, for providing insightful and positive comments, encouraging me, and letting me to use his expanded knowledge about soil science. I also want to thank Dr. Kelly Pennell, my outside examiner, for providing insightful comments and allocating her priceless time to both my M.Sc and Ph.D exams.

I gratefully acknowledge the support of the Biosystems and Agricultural Engineering department at the University of Kentucky. I would also like to thank the



landowners of the study sites who provided access to the field and management data; Jedediah Stinner, Katie Rumora, Marie Pollock, Phil Levison Christian Bower, and Sara Henderson for help in data collection and site maintenance; and Katie Emmett, Whitney Phelps and Eric Fischer for laboratory analysis of water samples, and Alex Fogle for all his helps in lab works. Funding for the edge of field research network was provided in part by several sources including: The 4R Research Fund (IPNI-2014-USA-4RN09); US EPA (DW-12-92342501-0); Ohio Farm Bureau, Conservation Innovation Grants (The Ohio State University – 69-3A75-12-231; Heidelberg University – 69-3A75-13-216); NRCS Mississippi River Basin Initiative; The Nature Conservancy; Ohio Corn and Wheat Growers Association; Ohio Soybean Association; NRCS Cooperative Conservation Partnership Initiative and NRCS Conservation Effects Assessment Project (CEAP). This work was partially supported by the National Institute of Food and Agriculture (NIFA), U.S. Department of Agriculture.

This dissertation could not be completed without the support and backing of my beautiful and lovely wife, who provides emotional support. Thank you, sweetheart, for giving me all of you and being my best friend. My words are not enough to express how kind you are and how much I love you.

My gratitude also goes to my parents for believing in me and guiding me through my early days in school and all their unconditional supports.

Finally, I am most grateful to Almighty god who saves lives and brings unreserved love, hope, and care.

## TABLE OF CONTENTS

<b>ACKNOWLEDGMENTS.....</b>	<b>iii</b>
<b>LIST OF TABLES .....</b>	<b>viii</b>
<b>LIST OF FIGURES .....</b>	<b>ix</b>
<b>CHAPTER 1. Introduction .....</b>	<b>1</b>
1.1 <i>Background Information.....</i>	<i>1</i>
1.2 <i>Conceptual Framework of PP delivery to Tiles .....</i>	<i>3</i>
1.3 <i>Overarching Objective.....</i>	<i>5</i>
<b>CHAPTER 2. IMPACTS OF PREFERENTIAL FLOW AND AGROECOSYSTEM MANAGEMENT ON SUBSURFACE PARTICULATE PHOSPHORUS LOADINGS IN TILE- DRAINED LANDSCAPES.....</b>	<b>7</b>
2.1 <i>Introduction.....</i>	<i>7</i>
2.2 <i>Methodology .....</i>	<i>12</i>
2.2.1 <i>Study Site and Materials.....</i>	<i>12</i>
2.2.2 <i>Nutrient Data Collection and Loading Analysis.....</i>	<i>13</i>
2.2.3 <i>Analytical Methodology .....</i>	<i>14</i>
2.2.3.1 <i>Explanatory analysis of TP—DRP loads and forms .....</i>	<i>14</i>
2.2.3.2 <i>Hydrograph Recession Analysis .....</i>	<i>15</i>
2.2.3.3 <i>Empirical Mode Decomposition (EMD) Time Series Analysis.....</i>	<i>16</i>
2.3 <i>Results.....</i>	<i>18</i>
2.3.1 <i>Exploratory analysis of TP – DRP loads and forms .....</i>	<i>18</i>
2.3.2 <i>Tile-drain Hydrograph Recession Analysis.....</i>	<i>20</i>
2.3.3 <i>Empirical Mode Decomposition Analysis.....</i>	<i>22</i>
2.4 <i>Discussion.....</i>	<i>24</i>
2.4.1 <i>Preferential Flow Dynamics in Tile Drainage .....</i>	<i>24</i>
2.4.2 <i>TP – DRP Forms and Pathways in Fine Textured Soils .....</i>	<i>25</i>
2.4.3 <i>Environmental and Management Effects on TP – DRP delivery to tile drains .....</i>	<i>27</i>
2.4.4 <i>Broader Implications .....</i>	<i>29</i>
2.5 <i>Figures and Tables.....</i>	<i>31</i>
<b>CHAPTER 3. QUANTIFYING HYDROLOGIC PATHWAY AND SOURCE CONNECTIVITY DYNAMICS IN TILE-DRAINAGE: IMPLICATIONS FOR P CONCENTRATIONS .....</b>	<b>36</b>
3.1 <i>Introduction.....</i>	<i>36</i>
3.2 <i>Materials and Methods .....</i>	<i>40</i>
3.2.1 <i>Study Site .....</i>	<i>40</i>
3.2.2 <i>Data Collection and Analysis .....</i>	<i>41</i>

3.2.3	Analytical Methodology .....	43
3.2.3.1	Hydrograph Recession and SC EMMA .....	43
3.2.3.2	Hydrograph Separation Framework .....	45
3.2.3.3	Comparison with Nutrient Concentration .....	46
3.3	<i>Results and Discussion</i> .....	48
3.3.1	Hydrograph Recession and SC-EMMA Results.....	48
3.3.2	Pathway-Connectivity Results.....	51
3.3.3	Implications for P delivery at the edge-of-field.....	55
3.4	<i>Conclusions</i> .....	58
3.5	<i>Figures and Tables</i> .....	60
<b>CHAPTER 4. THE ROLE OF FLOW PATHWAY, SOURCE WATER CONNECTIVITY, AND ENVIRONMENTAL GRADIENTS ON TILE-DRAIN SEDIMENT TRANSPORT DYNAMICS....71</b>		
4.1	<i>Introduction</i> .....	71
4.2	<i>Study Site and Materials</i> .....	76
4.3	<i>Analytical Methods</i> .....	79
4.3.1	Sediment and Particulate Phosphorus Concentration and Loading Estimates .....	79
4.3.2	Impact of flow pathway and water source connectivity on sediment loading .....	81
4.3.3	Tile sediment hysteresis analysis.....	83
4.4	<i>Results</i> .....	84
4.4.1	Sediment and Particulate P Loadings .....	84
4.4.2	Impact of Flow Pathway and Water Connectivity on Sediment Concentrations .....	85
4.4.3	Tile sediment hysteresis analysis.....	87
4.5	<i>DISCUSSION</i> .....	88
4.5.1	Field-scale tile sediment loading .....	88
4.5.2	Impact of pathway-connectivity and environmental drivers on tile sediment transport .....	90
4.5.3	Implications for Management.....	94
4.6	<i>Conclusion</i> .....	96
4.7	<i>Figures and Tables</i> .....	97
<b>CHAPTER 5. IMPACTS OF DRAINAGE WATER MANAGEMENT ON FLOW PATHWAY-CONNECTIVITY AND SEDIMENT PHOSPHORUS DYNAMICS IN A TILE-DRAINED AGROECOSYSTEM.....105</b>		
5.1	<i>Introduction</i> .....	105
5.2	<i>Methodology</i> .....	110
5.2.1	Study Site .....	110
5.2.2	Data Collection and Analysis .....	111
5.2.3	Analytical Methodology .....	114
5.2.3.1	Hydrograph Pathway Analysis.....	114
5.2.3.2	Before-After-Control-Impact Assessment .....	116
5.2.3.3	Time-series Analysis.....	116
5.2.3.4	High-frequency Pathway Connectivity and Hysteresis Analysis .....	117
5.3	<i>Results</i> .....	119
5.3.1	Hydrology and Hydrograph Recession Analysis .....	119
5.3.2	Before-After-Control-Impact (BACI) Analysis.....	121
5.3.3	Empirical Mode Decomposition (EMD) Analysis .....	122

5.3.4	High-Frequency Pathway-Connectivity and Sediment Hysteresis Analysis .....	124
5.4	<i>Discussion</i> .....	127
5.4.1	Impacts of DWM on Subsurface Flow Pathway and Water Source Connectivity.....	127
5.4.2	Impacts of DWM on Sediment and PP Dynamics in Tile-Drainage .....	130
5.5	<i>Conclusion</i> .....	132
5.6	<i>Figures and Tables</i> .....	134
<b>CHAPTER 6. Summary .....</b>		<b>144</b>
<b>CHAPTER 7. Future Work .....</b>		<b>147</b>
7.1	<i>Preliminary Findings</i> .....	147
<b>APPENDICES .....</b>		<b>154</b>
<i>APPENDIX 1. Supplemental Materials of Chapter 4</i> .....		154
<i>APPENDIX 2. Supplemental Materials of Chapter 5</i> .....		159
<b>REFERENCES .....</b>		<b>166</b>
<b>VITA.....</b>		<b>185</b>

## LIST OF TABLES

Table 2.1 Seasonal and annually averaged total tile flow (Q), slowflow ( $Q_{\text{slowflow}}$ ), and quickflow ( $Q_{\text{quickflow}}$ ) pathways results to tile drains for the clay and loam sites from 2015-2017. ....	31
Table 3.1 Summary of event timings, precipitations, total tile discharges, and flow partitioning results. ....	60
Table 3.2 Results of the multiple linear regression analysis for daily flow-weighted mean DRP concentrations. Estimated coefficient column shows estimated dissolved reactive P concentration (mg/L) associated with each flow fraction with standard error in parenthesis.....	62
Table 4.1 Seasonal and annual sediment yield, precipitation, and discharge for water year 2019.....	97
Table 4.2 Summary of discharge, event-based sediment yield, and HI values for pathway-connectivity indicators for the 31 monitored events.....	98
Table 4.3 Results of the multiple linear regression analysis for daily flow-weighted mean TSS concentrations. Estimated coefficient column shows estimated TSS concentration (mg/L) associated with $Q_{\text{quick-new}}$ and $Q_{\text{quick-old}}$ and $Q_{\text{slow}}$ fractions with standard error in parenthesis.....	99
Table 5.1 Control structure management periods for F2 and F4 in WY 16-19. ....	134
Table 5.2 Summary four years of surface and tile discharge, quickflow and slowflow for subsurface drain sites F2 and F4.....	135
Table 5.3 Before-After-Control-Impact (BACI) results. Effect of DWM on annual tile flow, quickflow and slowflow. The values in the table are observed values of F2 without DWM and predicted F2 values with DWM using F4 observed values and generated regression equations using data from water year 2016 and 2017. ....	136
Table 5.4 Event-to-event Pathway connectivity, sediment and TP-DRP loading and concentrations, and HI values for the two sites. ....	137
Table 5.5 Average values of flow pathway-connectivity, timing of peaks, sediment load and concentration, and HI values for different pathways for events where both sites were freely drained, and only the treatment site (F2) was freely drained. ....	138

## LIST OF FIGURES

Figure 1.1 a) Tile discharge from a USDA-ARS EOF site. b) Surface and Tile DRP Vs TP concentrations and loadings from 40 USDA-ARS EOF sites (Kevin King, unpublished).....2

Figure 1.2 Mechanisms and factors driving sediment delivery to subsurface for a) soil with desiccation cracks b) soil is saturated and macropores are visually closed.....4

Figure 2.1 Study site sampling locations in Ohio, USA. Picture of typical USDA-ARS edge-of-field monitoring platforms for surface and tile drainage are included.....32

Figure 2.2 Comparison of daily TP – DRP and TN – DIN loadings from surface and tile runoff at Site 1 (clay) and Site 2 (loam). Loadings are composited from both monitoring stations at each field.....33

Figure 2.3 Master Recession curves constructed over 5 years of subsurface flow from 18 recessions for (a) the clay site and from 24 recessions for (b) the loam site.....34

Figure 2.4 Five-year time series of TP – DRP concentration for the clay (a) and the loam (b) site. The raw TP – DRP timeseries is decomposed into a set of intrinsic mode functions (IMFs) in Step 1. In Step 2, the IMFs are tested to determine if trends are significantly differentiable from white noise. In Step 3, the significant IMFs representing seasonal trends (periods between 0.5-1.5 years) were summed and compared with management information.....35

Figure 3.1 Location of the tile-drained field located in Wood county, Ohio, USA. a) Aerial field delineation and monitoring location. b) Outlet of the tile network and its installed weir, and ISCO pump sampler. c) High-frequency sensing YSI EXO2 Sonde and its deployment in a drainage water management structure.....63

Figure 3.2 Separation of subsurface hydrograph to combined pathway-connectivity components including  $Q_{quick-old}$ ,  $Q_{quick-new}$ ,  $Q_{slow-old}$ , and  $Q_{slow-new}$ . Subsurface hydrograph is separated into quickflow ( $Q_q$ ) and slowflow ( $Q_s$ ) reservoirs using hydrograph recession analysis in Step 1 (a). Subsurface hydrograph is separated into new-water ( $Q_n$ ) and old-water ( $Q_o$ ) components using SC-EMMA approach (b). In Step 2, a set of equations are employed and calculated  $Q_{quick}$ ,  $Q_{slow}$ ,  $Q_{old}$  and  $Q_{new}$  (From Step 1) are used to separate hydrograph into pathway-connectivity components as shown in (c) and (d).....64

Figure 3.3 Master recession curve constructed from 18 subsurface flow recessions for water year 2019.....65

Figure 3.4 (a) Timeseries of data including 30-minute tile flow (mm) and 15-minute specific conductance ( $\mu\text{s}/\text{cm}$ ). Two events are highlighted at different times of year including (b) fall and (c) summer.....66

Figure 3.5 Tile discharge, quickflow calculated using hydrograph recession analysis and new water calculated using specific conductance end-member mixing analysis for each storm event (SE) at the study site during water year 2019.....	67
Figure 3.6 Results of pathway connectivity framework for a) SE26 and b) SE2. These two events were selected from summer and fall because they reveal seasonal differences in subsurface flow pathway and source connectivity.....	68
Figure 3.7 Flow-weighted daily mean DRP concentrations for the study site in water year 2019 plotted against tile discharge.....	69
Figure 3.8 Multiple Linear regression analysis results for daily flow-weighted mean concentrations of DRP as compared to a) hydrograph recession results, b) SC-EMMA results and c) the new pathway-connectivity framework results.....	70
Figure 4.1 a) Study site sampling locations in Ohio, USA; b) Typical USDA-ARS edge-of-field monitoring platforms for surface and tile; (c) YSI EXO sonde (with turbidity and conductivity sensors) were installed in the drainage water management structure; (d) Environmental conditions: macropores and snow-covered field.....	100
Figure 4.2 Regression of total suspended solids (TSS) and turbidity curve using log-transformed measures of TSS concentrations and turbidity values.....	101
Figure 4.3 Continuous timeseries for a) precipitation and tile discharge, b) temperature and specific conductance, and c) turbidity.....	102
Figure 4.4 Box-and-Whisker plots of HI values of $Q_{tile}$ , $Q_{quick-old}$ , $Q_{quick-new}$ , $Q_{quick}$ and $Q_{slow}$ against TSS concentrations. The dash and solid line within each box show mean and median HI values, respectively.....	103
Figure 4.5 Box-and-Whisker plots of HI values of $Q_{tile}$ , $Q_{quick-old}$ , $Q_{quick-new}$ , $Q_{quick}$ and $Q_{slow}$ against TSS concentrations. The dash and solid line within each box show mean and median HI values, respectively.....	104
Figure 5.1 a) Study site sampling locations in Ohio, USA; b) study site delineation with location of monitoring platforms, c) typical USDA-ARS edge-of-field monitoring platforms for surface and tile drain monitoring; and d) YSI EXO3 sonde.....	139
Figure 5.2 Time series of a) daily tile discharge, b) daily TP-DRP loading for 4 years; c) turbidity and d) specific conductance for WY 2019.....	140
Figure 5.3 Master recession curve for a) F2 and b) F4 constructed subsurface flow recessions for water year 2019.....	141
Figure 5.4 Four-year time series analysis of tile flow including a) sum of significant IMFs of tile for both sites; b) significant trends with frequencies less than one month; c) statistical significance test on IMFs of tile flow for F2, and d) Statistical significance test on IMFs of tile flow, slowflow and quickflow, respectively for F4.....	142

Figure 5.5 Four-year time series analysis of TP—DRP concentration a) sum of significant IMFs for F2 and F4, b) Monthly trends for F2 and F4 c) Statistical significance test on IMFs for F2, d) Statistical significance test on IMFs for F4.....	143
Figure 7.1 Comparison of daily flow-weighted mean concentration of total P (TP) – dissolved reactive P (DRP) and total N (TN) – dissolved inorganic N (DIN) from surface and tile runoff at the site.....	150
Figure 7.2 P:N ratio versus D <sub>50</sub> of transported sediment for surface and subsurface samples.....	151



## CHAPTER 1. INTRODUCTION

### 1.1 Background Information

Midwestern tile-drained landscapes export high levels of phosphorus (P), leading to proliferation of Harmful and Nuisance Algal Blooms (Blann et al., 2009; Smith et al., 2015 and Williams et al., 2016). Numerous studies have quantified dissolved reactive P (DRP) loadings and studied the mechanisms of DRP transport to subsurface drainage (e.g., Sims et al., 1998, Algoazany et al. 2007, Ruark et al., 2012; King et al., 2015; Smith et al., 2015; Williams et al., 2015; Christianson et al., 2016; Pease et al., 2017). Notwithstanding the importance of DRP, less emphasis has been placed on other forms of P in tile drains, resulting in their exclusion from agricultural water management models (e.g. Radcliffe et al., 2015; Christianson et al., 2016; Chen et al., 2018). Nevertheless, studies have shown much of the total P (TP) in subsurface drainage can be associated with particulate P (PP) (e.g. Schwab et al., 1977; Bottcher et al., 1989; Paasonen and Koivusalo, 2006; Enright and Madramootoo, 2004; Macrae et al., 2007; and Eastman et al., 2010; Christianson et al., 2016). As soils are eroded from the landscape and delivered to downstream waterbodies, P may be mobilized and can promote eutrophication and degradation of freshwater and marine sources (Zhu et al., 2018), or can fuel in-stream primary productivity (Brennan et al., 2017; Ford et al., 2018). Towards improved considerations of PP fluxes in management strategies, a need exists to evaluate the magnitudes and drivers influencing sediment and PP delivery to tile-drains.

The USDA-ARS SDRU in Ohio has established a series of Edge-of-Field (EOF) surface and subsurface monitoring platform across soil, management, and topographic gradients to quantify the impacts of practices on nutrient loadings in tile-drained landscapes. In these monitoring sites, surface runoff is measured using H-flumes, and a weir is installed in the outlet of tile drains. ISCO 6712 portable automatic samplers are used to collect water quality samples from surface and subsurface runoff. All water samples are analyzed for DRP, total P (TP), NO<sub>3</sub>-N, NH<sub>4</sub>-N, and total N (TN) concentrations. The compiled results (Kevin King, unpublished) from all the EOF sites indicates that subsurface DRP concentration and loading contributes 59% and 47% of TP concentration and loading, respectively. The TP—DRP may consist of Dissolved Organic P (DOP), Particulate Organic P (POP) and Particulate Inorganic P (PIP). Further investigation of drivers of these fluxes is critical given the impacts on TP loadings, particularly in spring, which has been linked to HABs in receiving water bodies (Macrae et al., 2010; King et al., 2015).

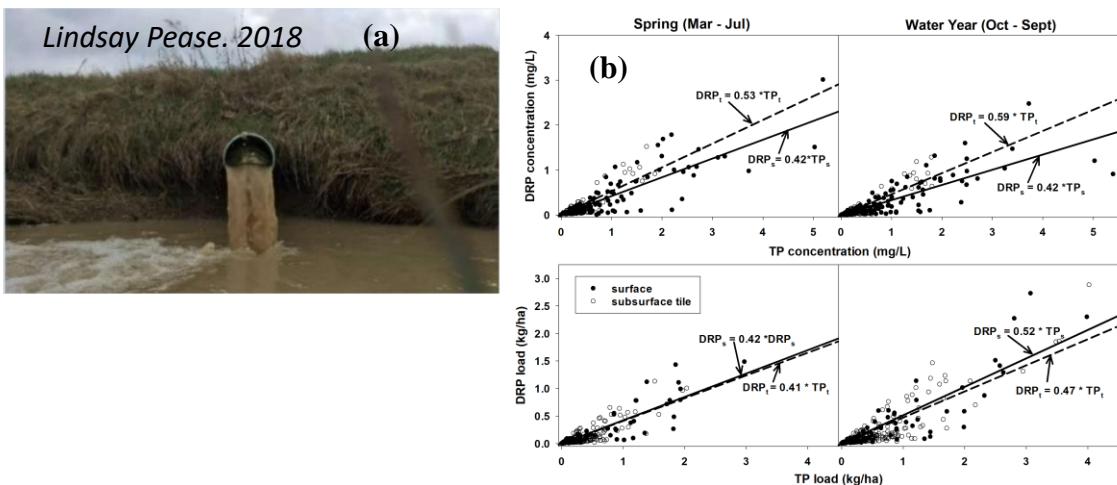


Figure 1.1 a) Tile discharge from a USDA-ARS EOF site. b) Surface and Tile DRP Vs TP concentrations and loadings from 40 USDA-ARS EOF sites (Kevin King, unpublished).

## 1.2 Conceptual Framework of PP delivery to Tiles

Studies that have previously measured PP delivery to tile drains suggest that soil characteristics, environmental conditions, and agricultural management practices all influence PP delivery to subsurface drainage (Figure 1.2). Regarding soil characteristics, finer sediments contain more Bioavailable Particulate P (BAPP) and may be preferentially transported during erosion (Michaud and Laverdiere, 2004; Collins et al., 2019). Likewise, soil texture is widely recognized to influence matrix and macropore flow. It is commonly assumed that TSS and PP delivery to tiles is through macropore flow and selective removal and transport of sediment from different parts of soil profile have shown macropore inner wall erosion (Oygarden et al., 1995; Unsitalo et al., 2001; Stone and Krishnappan, 2001; Paasonen and Koivusali, 2006, Schilling and Helmers, 2008). Regarding subsurface flow pathways, preferential flow is a function of soil matrix infiltration capacity, soil moisture, interaction between macropores and matrix and connectivity of macropores (Klaus et al., 2013; Tsuboyama et al., 1994; Sidle et al., 2001). Under low soil moisture conditions, water can quickly transport to tile via desiccation cracks (Williams et al., 2018; Ford et al., 2017). Under saturated soil moisture conditions, the rapid vertical flux through earthworm burrows, root channels and inter-aggregate voids can occur (Jarvis 2007, Deurer et al., 2009, Beven and Germann, 2013). In addition, when cracks are visually closed, a transition from preferential flow to matrix flow takes place and matrix flow starts at the top of the profile and progresses downward as moisture content exceeds field capacity. Regarding environmental conditions, raindrop impacts and intensity result in sediment detachment and transport of fine particles through macropores (Pilgrim and Huff, 1983, Heppell and Chapman 2006, Jarvis 2007) and TSS concentration and PP delivery in tiles can be different over seasons (Paasonen and Koivusalo, 2006; Schelde et al., 2006). Management is also perceived to be important as peak TSS concentrations in tile-drains have been observed following tillage (Paasonen and

Koivusalo, 2006). Further, the concentration of PP and BAPP bound to sediment is related to soil test P levels, and hence fertilization practices are perceived important (Poirier et al., 2012). Nevertheless, these perceptions are rarely robustly evaluated. For instance, studies that attribute TSS delivery to macropore flow have rarely quantified preferential flow contributions. Robust datasets that span the range of management conditions, soil textures, and environmental gradients are needed to test existing perceptions to better inform management practices.

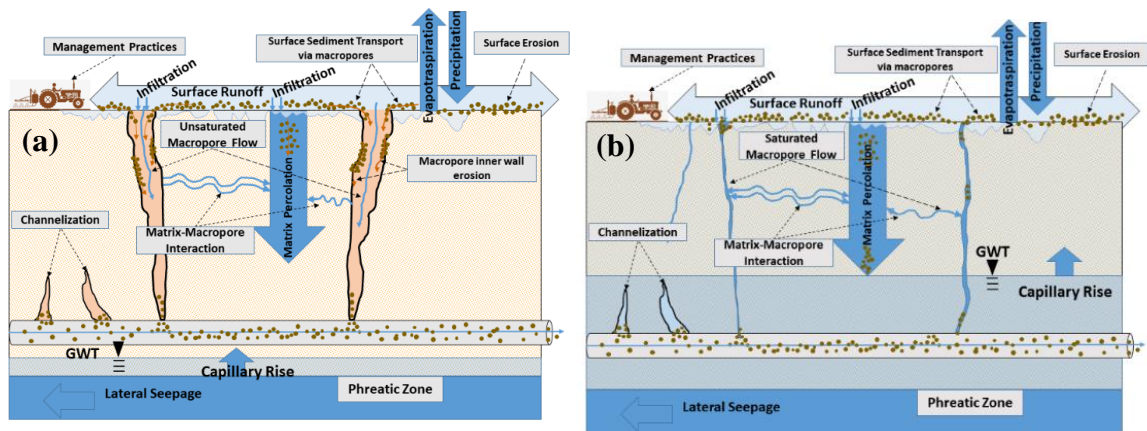


Figure 1.2 Mechanisms and factors driving sediment delivery to subsurface for a) soil with desiccation cracks b) soil is saturated and macropores are visually closed

Drainage Water Management (DWM) has been commonly used in tile-drained landscapes to regulate groundwater table and reduce subsurface drainage fluxes (Drury et al., 1999; Ghane et al., 2012). DWM structures are usually placed at the outlet of the tile network in order to regulate outlet elevation by adding and removing the stop logs within the structure. Depending on this regulation, here we define that when the stop logs are removed the outlet is free-drained (FD) which means that the hydraulic head in the tile drains is adjusted to be less than the hydraulic head of the water table in the surrounding soils. Under this condition gravitational flow and gradients are formed towards the drain

provided that water table is not lower than drain depth. Conversely, when the stop logs are in place we define that the tiles are under controlled drainage (CD) and the elevation of outlet is increased in order to retain more water in the field when needed. Several studies have shown that while controlled drainage (CD) is an effective practice in reducing subsurface flow and nutrient loading (Evans et al., 1995; Fausey, 2005; Strock et al., 2010; et al., 2012), it can increase surface runoff and consequently sediment loading from tile-drained fields (Singh et al., 2007; Ale et al., 2008; Cook and Verma 2012). Several previous studies have indicated that the reduced nutrient loading, especially nitrogen loading, is attributed to reduced water fluxes, and nutrient concentrations remain unchanged or slightly changed (Williams et al., 2015; Nash et al., 2015; Ross et al., 2016). DWM can also alter subsurface pathway dynamics such as increase of lateral seepage with CD (Ale et al. 2008, Thorp et al., 2008), and result in water loss via other pathways such as surface runoff and groundwater recharge (Ross et al. 2016). Hence, determining the efficiency of DWM is challenging due to limitations in characterization of all hydrological pathways (Cooke and Verma 2012). A need exists to quantify the effect of DWM on water lost in pathways such as preferential flow, surface runoff, groundwater recharge (Ross et al. 2016) and consequently impact of CD on sediment delivery in surface and subsurface of tile-drained field equipped with DWM.

### **1.3 Overarching Objective**

Numerous studies have focused on DRP and nitrogen flux dynamics in tile-drained landscapes, and automated samplers have been used in EOF monitoring programs to capture flow and dissolved and total nutrient event flow concentrations. However, less emphasis has been placed on PP. Therefore, a need exists to study fluxes and dynamics of sediment and PP to improve our understanding of sediment P delivery in tile-drained landscapes with the ultimate goal of advancing agricultural water quality models and

providing effective management solutions that minimize downstream impacts. The following objectives have been outlined towards achieving our overall goal:

Objective 1: Characterizing subsurface flow pathways and P forms to evaluate impacts of preferential flow, environmental conditions, and management practices on particulate P delivery in tile-drained landscapes.

Objective 2: Develop and evaluate a novel framework to partition subsurface flow based on both flow pathway and source connectivity descriptors and elucidate their impact on P concentration dynamics in tile drainage.

Objective 3: Quantify sediment loading dynamics for a subsurface drained agroecosystem and assess the governing flow pathway and water source impacts on tile sediment loads.

Objective 4: Identify impacts of Drainage Water Management (DWM) on flow pathway-connectivity and sediment phosphorus dynamics in a tile-drained agroecosystem.

This dissertation is organized in seven chapters, chapter 1 establishes the focus of this research, current research gaps, and general rationale of this dissertation. Chapters 2, 3, 4, and 5 focus on objectives 1, 2, 3 and 4, respectively. Chapter 6 provides a summary from findings of all chapters. Finally, Chapter 7 addresses future research needs and preliminary results of a tracer-based approach for partitioning sediment source provenance. The second chapter is published in Journal of Environmental Quality and is adapted by editor's permission to be incorporated in this dissertation.

## CHAPTER 2. IMPACTS OF PREFERENTIAL FLOW AND AGROECOSYSTEM MANAGEMENT ON SUBSURFACE PARTICULATE PHOSPHORUS LOADINGS IN TILE-DRAINED LANDSCAPES

Adapted with permission from Nazari, S., Ford, W. I., King, K. W. 2020. *Impacts of preferential flow and agroecosystem management on subsurface particulate phosphorus loadings in tile-drained landscapes*, Journal of Environmental Quality, Vol. 49, No. 5, pp. 1370-1383.

Copyright © 2020 John Wiley & sons, Ltd.

### 2.1 Introduction

Midwestern tile-drained landscapes export significant levels of phosphorus (P) that contribute to the proliferation of harmful and nuisance algal blooms (Blann et al., 2009; Smith et al., 2015 and Williams et al., 2016). While numerous studies have quantified dissolved reactive P (DRP) loadings and studied the mechanisms of DRP transport to subsurface drainage systems, less emphasis has been placed on other forms transported through tile drains such as particulate P (PP) and dissolved unreactive P (DUP) (Radcliffe et al., 2015; King et al, 2015; Christianson et al., 2016; Chen et al. 2018). In particular, as PP is lost from the landscape and delivered to downstream waterbodies, bioavailable P may be mobilized, promoting eutrophication and degradation of freshwater and marine sources or fueling in-stream primary productivity (Brennan et al. 2017; Ford et al., 2018; Zhu et al, 2018).

Field-scale nutrient studies in tile-drained agroecosystems have evolved over the past 50 years and now focus on methodologies for continuous monitoring of flow-weighted mean concentrations (FWMC) of dissolved and total nutrient species using automated samplers on surface flumes and subsurface tile mains (Williams et al., 2016; Harmel et al., 2018). Temporal and economic constraints often limit analyses that can be performed on samples and, as a result, most long-term monitoring programs typically

only analyze bioavailable nutrients (orthophosphate, nitrate and ammonium) and total nutrient concentrations (Williams et al., 2016; Christianson et al., 2016; Macrae et al., 2007; Reba et al., 2013; Macrae et al., 2019). Regarding total nutrients, both alkaline and alkaline/acid persulfate digestions on unfiltered samples have been used for coupled measurements of total P (TP) and total (TN); although the alkaline persulfate digestions are recognized to underpredict TP when suspended sediment concentrations are significant (Koroleff et al., 1983; Patton and Kryskalla, 2003; Dayton et al., 2017).

We postulate that the P:N ratios of non-soluble reactive forms will provide insight to forms and sources of P in edge-of-field studies. The difference between TP and DRP (TP – DRP) reflects the sum of inorganic PP, organic PP, and DUP (Macrae et al., 2019), while the difference between TN and dissolved inorganic N (DIN) (TN – DIN) reflects organic (both particulate and dissolved) nitrogen species (Patton and Kryskalla, 2003). Organic compounds have predictable P:N ratios in soil organic matter that are significantly less than P:N ratios of the bulk soil pool in row-cropping systems, which stems from accrual of inorganic P in soils (Cleveland and Liptzin, 2007; Froussard et al., 2016). We perceive that comparing ratios of TP – DRP to TN – DIN can aid in informing forms of P delivered to tile drains and provide insight into where PP is mobilized in the soil profile.

Several studies have shown that much of the TP in subsurface drainage may be associated with PP that is delivered to tile drains through preferential flowpaths (Eastman et al. 2010; Christianson et al., 2016; Turunen et al., 2017). The occurrence and magnitude of preferential flow varies as a function of soil matrix infiltration capacity, soil moisture, matrix-macropore interaction and hydrologic connectivity of macropores to



subsurface pathways (Sidle et al., 2001; Klaus et al., 2013). Under both low and high antecedent moisture, water may quickly transport to tiles via desiccation cracks, earthworm burrows, root channels and inter-aggregate voids (Beven and Germann, 2013; Ford et al., 2017; Williams et al., 2018). As a result, preferential flow has high temporal variability. The increasing availability of continuous, long-term flow records from tile-drains illustrate the need for empirically-based methods to quantify preferential and diffuse flow contributions to tile runoff hydrographs.

Hydrograph recession analysis is an empirically-based flow partitioning approach used in karst springs that has applicability to tile-drained landscapes (Schilling and Helmers, 2008; Jarvie et al., 2014; Husic et al., 2019; Ford et al., 2019). In hydrograph recession, the receding limb of the hydrograph is conceptualized as the drainage of a series of reservoirs that have variable hydraulic conductivities and storage volumes (Husic et al., 2019). These reservoirs often recede exponentially, resulting in distinct log-linear regions. A master recession curve can be generated for a site by compiling events from long-term monitoring data to determine the number of statistically differentiable reservoirs in a system (Gregor and Malik, 2012). Hydrograph recession can also be applied on an event-by-event basis to quantify temporal variability in flow pathway dynamics (Jarvie et al., 2014; Ford et al., 2019). The applicability of hydrograph recession to tile-drained landscapes is recognized given that reservoir-style hydrologic models have been applied to tile-drain hydrographs to reflect quick preferential flow through macropores and slow diffuse percolation through the soil matrix (Brauer et al. 2014; Ford et al., 2018). While hydrograph recession has been successfully applied at the

watershed scale in tile-drained landscapes, applications at edge-of-field scales are lacking (Schilling and Helmers, 2008).

In addition to flow pathways, P dynamics in tile drains are complicated by variability in environmental conditions and agricultural management practices. Regarding environmental conditions, precipitation intensity and magnitude influence sediment detachment and transport through macropores and PP delivery in tiles has been shown to vary seasonally (Paasonen and Koivusalo, 2006; Schelde et al., 2006; Jarvis, 2007). Sediment and PP delivery through tile-drains is well recognized to be impacted by tillage, but the documented impacts are inconsistent due to confounding factors (Coelho et al. 2012). For example, tillage can increase the soil losses via surface disturbance but may also decrease macropore continuity, thus decreasing preferential flow from overland flow (Paasonen and Koivusalo, 2006; Williams et al., 2016). The relative roles of hydroclimatic variability and management practices on P delivered to tile drains is not well understood (Macrae et al., 2019). Time-series analysis of long-term concentration records has provided insight into controlling drivers of P transport from subsurface flow pathways in watershed-scale studies and may be valuable in identifying governing mechanisms at the field scale now that long-term records of continuous flow and nutrient data are available (Jarvie et al., 2017; Ford et al., 2018; 2019).

Empirical Mode Decomposition (EMD) is a time-series analysis method that has high perceived utility for tile-drain water quality studies given its flexibility for detecting trends in complex datasets. In tile-drained landscapes of the Western Lake Erie basin, nonstationary and non-linear phosphorus delivery may stem from changes in runoff patterns and land management practices (Jarvie et al., 2017; Pease et al. 2017, Williams

et al. 2018). Among time-series analysis approaches used in environmental studies, EMD does not have limitations of Fourier-based and regression approaches which assume linear and stationary time-series (Wu et al., 2007; Ford et al. 2015). Instead of selecting fixed functional forms of trends, the trends are adaptive over time (Wu et al. 2007; Ford et al., 2015). As a result, the method has recently been applied to nutrient concentration and flow datasets in karstic and tile-drained watersheds (Ford et al. 2015, Ford et al. 2018, Ford et al. 2019). While there is perceived utility for analyzing tile-drain nutrient signals, application at the field scale has been limited, in part, due to a lack of continuous long-term datasets.

In this study, we characterize subsurface flow pathways and P forms to evaluate impacts of preferential flow, environmental conditions, and management practices on particulate P delivery in tile-drained landscapes. Specific objectives of this study were to a) use continuous edge-of-field monitoring data and P:N ratios of non-soluble reactive nutrient species to assess the forms and magnitudes of TP – DRP transported in tile-drains; b) assess the utility of hydrograph recession analyses to quantify preferential flow dynamics in tile drains; and c) perform time-series analysis of long-term TP – DRP data to identify the impact of management and environmental drivers on TP – DRP delivery to tile drains. To meet these objectives, we employed exploratory analysis of N and P datasets, continuous and master recession curve hydrograph recession analysis on tile flow, and empirical mode decomposition (EMD) time-series analysis at two study sites with contrasting soil characteristics in Ohio, USA.

## 2.2 Methodology

### 2.2.1 Study Site and Materials

We selected two sites from the USDA-ARS Soil Drainage Research Unit edge-of-field monitoring network for detailed study. The sites are comparable in terms of slope (<0.5% to 3%), average annual precipitation ( $1045 \pm 151$  mm) and crop rotations (corn-soy-wheat) (Williams et al. 2016; Figure 2.1). However, the sites differ in soil texture (clay vs. loam), depth to drainage network (0.7- 1 m), and tillage and fertilization practices. These soil textures, drainage depths, and management practices typify end-members for the region (Williams et al., 2016). Both sites consist of two surface ( $C_{S-A}$  and  $C_{S-B}$  for the clay site and  $L_{S-A}$ ,  $L_{S-B}$  for the loam site) and two tile ( $C_{T-A}$  and  $C_{T-B}$  for the clay site and  $L_{T-A}$ ,  $L_{T-B}$  for the loam site) monitoring stations. The drainage areas of surface monitoring stations were delineated by micro-topographical differences and were 7.33 ha, 1.5 ha, 3.24 ha, and 2.35 ha for  $C_{S-A}$ ,  $C_{S-B}$ ,  $L_{S-A}$ , and  $L_{S-B}$ , respectively. Tile drainage areas were delineated by subsurface drainage maps and were found to be 8.71 ha, 1.13 ha, 3.69 ha, and 5.87 ha, for  $C_{T-A}$ ,  $C_{T-B}$ ,  $L_{T-A}$ , and  $L_{T-B}$ , respectively. The clay site is tilled following each harvest. Inorganic fertilizer was applied typically after planting. Historic management practices have resulted in soil test P levels in the maintenance range in the plow layer (M3P= 29.6 ppm in 0-15 cm) that decrease with depth (M3P= 5.8 ppm in 15-61 cm). The loam site was strip tilled before planting in 2012, 2016 and 2017 and disk tilled after manure application in 2016. Inorganic and organic fertilizers were applied during the monitoring period. In contrast to the clay site, historic management practices at the loam site have resulted in high soil test P levels in

the plow layer (M3P=113.6 ppm in 0-15 cm) that decrease with depth (M3P= 33.5 ppm in 15-61 cm).

## 2.2.2 Nutrient Data Collection and Loading Analysis

The study sites were a part of the USDA-ARS Soil Drainage Research Unit edge-of-field monitoring network and methodology for field data collection and analysis used previously published methods (Williams et al., 2016; Pease et al., 2017). Tile mains were equipped with a weir insert (Thel-Mar, Brevard, NC), ISCO 4230 Bubbler Flow Meters (Teledyne Isco, Lincoln, Nebraska), and ISCO 2150 Area Velocity Sensor, which measured discharge under submerged conditions. Surface monitoring stations on each field were equipped with H-Flumes and a bubbler flow meter, which measured water depth in the flumes in order to calculate surface volumetric discharge using stage-discharge curves. The tile and surface monitoring stations were instrumented with ISCO 6712 portable automatic samplers in order to collect nutrient samples. Water samples were collected from surface runoff using a flow-proportional strategy. A flow-proportional approach could not be used for subsurface drainage; thus, daily time-compositing was used. Tipping bucket rain gages were used to measure rainfall duration, intensity, and depth, and were corrected using a standard rain gage (Macrae et al., 2019).

All water samples were analyzed for DRP, TP, NO<sub>3</sub>-N, NH<sub>4</sub>-N, and TN concentrations for the entire monitoring duration at all sites. Dissolved splits were vacuum filtered (0.45 μm), analyzed for N according to US Environmental Protection Agency (USEPA) method 353.3 and for P according to USEPA method 365.1. TP and TN concentrations were determined from unfiltered samples using alkaline persulfate method of Koroleff et al. (1983) prior to 2015 and the USGS method of Patton and

Kryskalla (2003) thereafter. The differences in analytical methods is important to note given the findings of Dayton et al. (2017), which found that average total phosphorus percent recovery of USGS and alkaline persulfate methods were 76.1% and 24.5%, respectively, using suspensions derived from soils in agricultural landscapes of Ohio. Samples rarely fell below method detection limits, with the exception of  $\text{NH}_4\text{-N}$ , which was below detection for approximately 4% of samples. For these samples, we assumed  $\text{NH}_4\text{-N}$  concentrations were equal to zero. Most of these measurements occurred at low flow conditions and hence had limited impact on loading dynamics. Further, as a result of analytical and handling error, DRP concentrations would occasionally exceed TP. When this occurred, we assumed TP concentrations were equal to DRP.

### 2.2.3 Analytical Methodology

#### 2.2.3.1 Explanatory analysis of TP—DRP loads and forms

Surface and subsurface daily TP, DRP, TN, and DIN loadings were calculated using the approach of Williams et al. (2015). Briefly, we determined the midpoint of all sample time steps for each bottle. We then used linear interpolation between measured values at the mid-point to estimate the concentration for each interval when flow was measured. Loading was estimated as the product of interpolated concentrations and flowrate. We also estimated average daily FWMC by dividing average daily loads by daily discharge for the measured water quality parameters. We summarized loadings using annual and seasonal averages. Seasons were defined as winter (January-March), Spring (April-June), Summer (July-September), and Fall (October-December) for our analysis.

In order to infer the dominant forms of P in tile-drained fields, we analyzed P:N ratios of non-soluble reactive nutrients. First, we calculated TN and DIN loadings, analogous to the methodology for TP and DRP. We generated a linear regression between daily tile TP – DRP and TN – DIN loading for samples measured using the alkaline persulfate digestion (prior to 2015) and for the alkaline/acid persulfate digestion (post 2015). Next, we compared the results to typical P:N ratios for organic matter in agroecosystems which have been found to range from 0.034 to 0.083 (Frossard et al., 2016). These ratios for organic matter have been found to show limited variability across comparable landcovers (Cleveland and Liptzin, 2007). Therefore, deviation from organic matter P:N ratios would indicate sediments high in inorganic P (e.g., surface derived sediments).

#### 2.2.3.2 Hydrograph Recession Analysis

Master recession curve analysis was performed by compiling subsurface hydrograph recessions from events throughout the monitoring period. Recession curves were manually fit to the compiled recession events to produce a line of best fit. Calibrations were performed by modifying recession coefficients for a user-selected number of reservoirs to generate a master recession curve that provided the best visual fit to the data. For tile-drains, two reservoirs were assumed, representing matrix and macropore flowpaths. Reservoir recession coefficients in the literature vary, however studies typically show that distinct reservoirs differ by a factor of three, or greater (Schilling and Helmers, 2008; Rimmer and Hartmann, 2012; Husic et al., 2019). For our study, we generated a master recession curve using three years of tile hydrology data. We

selected 18 recessions from  $C_{T-A}$  and 24 recessions from  $L_{T-A}$  to create a single master recession curve using RC 4.0 software (HydroOffice; Malik and Vojtkova, 2012; Gregor and Malik, 2012). More recessions existed for each field, but they were not included in the analysis since they were either comprised of days with zero flow (associated with no flux or tile backwater) or had non-linear recessions associated with disruption of initial recession with secondary flow peaks.

Continuous time-series estimates of flow pathways for  $C_{T-A}$  and  $L_{T-A}$  were estimated using event-based hydrograph separation methodology for three years of study. The methodology is described in detail elsewhere (Husic et al., 2019; Ford et al., 2019). Briefly, for each hydrologic event, we plotted the falling limb of the subsurface discharge hydrograph on logarithmic scale and manually fit linear curves on reservoirs and determined the inflection points of the linear trends. In the next step, a linear increase in slow flow was then assumed from the beginning of the rising limb of the hydrograph, which represented the start of quickflow, to the determined inflection point on the falling limb from previous step, and this point signified the separation of quick and slow flow (Husic et al., 2018). Finally, event contribution by each pathway was calculated as the area between the two curves for the quick flow pathway and the area under the curve for the slow flow pathway (Ford et al. 2019). To quantify the impact of flowrate and quickflow on TP – DRP concentrations, we performed a multiple linear regression analysis. The model response variable, daily TP – DRP (mg/l), was regressed against flowrate and fraction of flow associated with quickflow using RStudio (RStudio, inc, 2011).

#### 2.2.3.3 Empirical Mode Decomposition (EMD) Time Series Analysis



In this study, the main goal of employing EMD was to use it as a dyadic filter to remove noise from data and determine intra-annual to inter-annual trends and compare the trends with timing of management practices that are perceived to impact TP – DRP delivery in tiles. The process of time series analysis using the EMD may be summarized in three steps. In step 1, the EMD decomposes the time series (raw data) into a series of Intrinsic Mode Functions (IMFs), in which the lowest frequency IMF is identified as the base residual trend and the highest frequency trend is considered noise for well-sampled datasets (Wu et al., 2007). The EMD uses an iterative procedure called sifting to generate IMFs. Briefly, the algorithm finds all local maxima and minima in the time series, then computes the corresponding interpolations as upper and lower envelopes of the signal using a cubic spline function. Next, the average of the lower and upper envelope is subtracted from the data signal (related to the current iteration). The process is repeated until the average envelope converges to a specified threshold. The converged envelope is subtracted from the original dataset and the steps are repeated until all extremes are removed. We used a previously published code in Matlab that conducts EMD and generates IMFs (Rato et al. 2008). The model was run from 2013 to 2017 for TP – DRP FWMC at both study sites.

In step 2, a statistical significance test was performed on IMFs based on the method explained by Wu et al. 2007 to determine if IMFs were significantly different from white noise. The first IMF, which typically reflects noise for well-sampled datasets, was considered as base noise. Then, a negative linear relationship of  $\log_{10}$  of variance and  $\log_{10}$  of period with a slope of -1 was plotted with  $\log_{10}(\text{Var}) \pm \log_{10}(3)$  as upper and lower bounds for confidence intervals. A log-log plot of variance versus mean period was

plotted for each IMF on the same graph. Finally, the IMFs that plotted outside of the specified interval were considered statistically different from white noise, reflecting a significant trend in the data.

In step 3, the significant IMFs were aggregated at environmentally relevant timescales. For the present study we focused on the seasonal timescales given the implication for seasonal eutrophication and HABs (Ford et al. 2018). Statistically significant frequencies with mean period between six to eighteen months were included as a seasonal trend since trends may not have been pronounced in certain years (resulting in a frequency greater than 12 months), or may experience a secondary intra-annual oscillation in some years (resulting in a frequency less than twelve months). If such a phenomenon is commonly occurring, leading to frequencies outside of the specified bounds, it would suggest that the result is likely due to a non-seasonal fluctuation. The seasonal IMFs were summed and compared with timing of management practices.

## **2.3 Results**

### **2.3.1 Exploratory analysis of TP – DRP loads and forms**

The clay and loam sites displayed contrasting hydrologic behavior and timing, despite similar precipitation patterns. The average annual precipitation was 1057 mm at the clay site and 1033 mm at the loam site. Rainfall was greatest in spring and summer and least in fall and winter at both sites. Similarly, average total runoff (surface plus subsurface) for both fields was comparable (257 mm for the clay site and 307 mm for the loam site). For the clay site, 44% of discharge was through surface runoff, which was greatest in spring and least in fall, and 56% through subsurface runoff, which was

greatest in spring and least in summer. Conversely, for the loam site, surface runoff was negligible (<3% of total runoff), while subsurface runoff was greatest in winter and least in summer.

Annual loading results highlight similar total P loadings through combined overland and subsurface flow paths but contrasting P forms at the clay and loam sites. Similar to total runoff, TP loadings for the clay and loam site were comparable and averaged  $1.6 \text{ kg ha}^{-1} \text{ yr}^{-1}$  and  $1.9 \text{ kg ha}^{-1} \text{ yr}^{-1}$ , respectively. Contrasting TP, annual DRP loading was an order of magnitude less at the clay site ( $0.12 \text{ kg ha}^{-1} \text{ yr}^{-1}$ ) as compared to the loam site ( $1.25 \text{ kg ha}^{-1} \text{ yr}^{-1}$ ). As a result, annual subsurface TP – DRP loading constituted 93% and 34% of TP in the clay and loam site, respectively. Regarding seasonality, TP – DRP loadings were greatest in spring (TP – DRP =  $0.35 \text{ kg ha}^{-1} \text{ yr}^{-1}$ ) and summer (TP – DRP =  $0.27 \text{ kg ha}^{-1} \text{ yr}^{-1}$ ) for the surface pathway, but were greatest in winter (TP – DRP =  $0.22 \text{ kg ha}^{-1} \text{ yr}^{-1}$ ) and spring (TP – DRP =  $0.34 \text{ kg ha}^{-1} \text{ yr}^{-1}$ ) for the subsurface pathway at the clay site. TP – DRP loadings were greatest in winter (TP – DRP =  $0.22 \text{ kg ha}^{-1} \text{ yr}^{-1}$ ) and fall (TP – DRP =  $0.21 \text{ kg ha}^{-1} \text{ yr}^{-1}$ ) for the subsurface pathway and were, comparatively, negligible for the surface pathway at the loam site.

The slopes of the regression line between TP – DRP and TN – DIN loadings provide the average P:N ratios of non-soluble reactive nutrients in surface and tile runoff at the study sites (Figure 2.2). To compare these findings with P:N ratios of organic matter, we included two lines that represent the range of P:N ratio for organic matter reported in agroecosystems (0.034-0.083). Analysis of the P:N ratios prior to 2015 differed from those following 2015 at both sites. For the clay site, we found a surface P:N ratio of 0.1068 and subsurface P:N ratio of 0.054 prior to 2015. After 2015, the P:N

ratio increased four-fold in both surface and subsurface pathways to 0.38 and 0.23, respectively. For the loam site, we found a surface P:N ratio of 0.076 and subsurface P:N ratio of 0.043 prior to 2015. After 2015, the P:N ratio increased three-fold in both surface and subsurface pathways to 0.25 and 0.13, respectively. The difference in P:N ratios prior to, and after 2015 stems from differences in percent P recovery of the alkaline persulfate method (Koroleff et al., 1983) and the alkaline/acid persulfate method (Patton and Kriskala, 2003) for TP analysis, which is further discussed in section 4.2. These results show higher P:N ratios in surface runoff as compared to subsurface runoff at both sites, which reflects connectivity to surface soils with high inorganic P content. Interestingly, higher P:N ratios at the clay site as compared to the loam site in both surface and subsurface pathways was somewhat surprising given the soil test P levels at the loam site were greater than the clay site.

### 2.3.2 Tile-drain Hydrograph Recession Analysis

Results from the master recession curves and continuous recession analysis at the subsurface outlet of each field identified two discernible slopes, confirming two reservoirs, with reservoir 1 (R1) representing a steep recession and reservoir 2 (R2) a mild recession. The recession coefficients ( $\alpha$ ) of the clay site for R1 and R2 were 2 and 0.25 day<sup>-1</sup>, respectively (Figure 2.3.a). The recession coefficients ( $\alpha$ ) of the loam site for R1 and R2 were 0.95 and 0.35 day<sup>-1</sup>, respectively. On average, results of the master recession curve suggest that R1 and R2 account for 66% and 34% of subsurface flow at the clay site and 36% and 64% of the subsurface flow for the loam site.

Results of the continuous recession analysis provide insight into seasonal flow pathway dynamics and how they compare between the clay and loam sites (Table 2.1).

The results of continuous recession analysis yielded similar results to the master recession curve, with R1 and R2, respectively, accounting for 65% and 34% of the subsurface discharge at the clay site, and 36% and 64% of the subsurface discharge at the loam site. The greatest portion of flow for R1 occurred in summer at the clay site, comprising 82% of the total subsurface flow. At the loam site, R1 was greatest in fall, comprising 57% of the total subsurface flow. The greatest subsurface flow volume to tiles from R1 occurred in spring at the clay site, constituting 40% of total annual quickflow. The greatest subsurface flow to tiles from R1 occurred in winter at the loam site, constituting 37% of total annual quickflow. The least contribution of R1 to annual subsurface flow to tiles occurred in summer at both fields.

The multiple linear regression model comparing TP – DRP concentration to flow parameters was significant for both fields; however, the model explained only a small fraction of the variance in the TP – DRP dataset. For the clay site we found coefficients for flow rate ( $7 \times 10^{-4}$ ) and fraction of flow associated with quickflow (0.31) were positively related to TP – DRP and were significant ( $p < 0.001$ ). Likewise, the overall model was significant ( $p < 0.001$ ) and had an adjusted  $R^2$  of 0.24, suggesting the predictors described 24% of TP – DRP variability. Similar results were found for the loam site in which coefficients for  $Q_t$  ( $5.2 \times 10^{-4}$ ) and  $F_t$  (0.08) were positively related to TP – DRP and were significant ( $p < 0.001$ ). The overall model was significant ( $p < 0.001$ ) and also had an adjusted  $R^2$  of 0.24, suggesting the predictors described 24% of TP – DRP variability. Comparing the two sites, the coefficients for  $Q_t$  were comparable, however the quickflow coefficient at the clay site was four-fold greater than the loam

site, highlighting the importance of quickflow contributions in exerting enhanced controls on TP – DRP concentrations at the clay site.

### 2.3.3 Empirical Mode Decomposition Analysis

Empirical mode decomposition results for TP – DRP loading for both the clay and loam site from 2013-2017 are provided in Figure 2.4. The raw data time series for TP – DRP loading was first decomposed into IMFs using the aforementioned sifting process, which are shown in step 1 for the clay (Figure 2.4.a) and loam (Figure 2.4.b) sites. The analysis generated nine IMFs and a residual trend for the clay site and eight IMFs and a residual trend for the loam site. Next, the statistical significance of the IMFs was tested (Step 2) and we found that five out of nine and two out of eight IMFs were statistically significant, at the clay and loam site, respectively. This means that these IMFs have variances that were greater than what would be expected from noise and indicated a physical trend in the data. In Step 3, we summed the significant IMFs that had a mean period between 0.5-1.5 years (reflecting seasonal trends) and compare the timing of maxima-minima dynamics to management information to identify how practices and flow drivers influence these statistically significant trends. We focus on the results from Step 3.

The sum of significant IMFs showed differences in amplitudes coinciding with the TP method utilized (Figure 2.4, Step 3). TP – DRP concentrations at both sites had more subtle oscillations prior to 2015 when using the Koroleff persulfate digestion procedure. For the clay site, max-min differences in the sum of statistically significant IMFs varied over a 0.2 mgP/L range prior to 2015, but more than 0.6 mgP/L range after 2015. Similarly, the loam site varied over a 0.1 mgP/L range prior to 2015 and 0.5 mgP/L range

after 2015. These findings indicate that the significant trends are associated with particulate P.

Regarding the impact of flow and crops, we found that for both sites the peak TP – DRP concentrations occurred in fallow seasons that had the greatest flow, and that minimum TP – DRP concentrations occurred in late-fall, following harvest (Figure 2.4, Step 3). Generally, in both fields, TP – DRP concentration gradients decreased when the field was cultivated and increased when the field was fallow. The majority of TP – DRP maximum peaks occurred in spring for the clay field and winter for the loam field when average subsurface discharge, macropore flow, and consequently TP – DRP and DRP loadings were greatest. On the other hand, the occurrence of most of the minimum peaks in late fall for both sites show that the occurrence of minima were not correlated with discharge since tile discharge was minimum in summer for both sites.

Regarding tillage practices, vertical tillage was used at the clay site following each harvest, while conservation tillage was used at the loam site. We found that TP – DRP concentrations increased to a local maximum in three out of the four years (2014, 2015, and 2017), in the early winter following tillage, before decreasing to a local minimum in mid to late winter. Conversely, conservational tillage and use of cover crops at the loam site showed no discernable impacts on TP – DRP concentrations.

The impact of cover crops when the field is typically fallow was also recognized to influence significant seasonal trends. Wheat was present at the clay site in 2013, and on the loam site in late 2014 through summer 2015. For the clay site, in the year with wheat we found that TP – DRP minima occurred during spring coinciding with wheat cover on the field during a period that the field is typically fallow, and as a result the maxima

shifted to summer following harvest. Likewise, TP – DRP peaks at the loam site showed a smaller winter maximum while wheat was on the field in 2015, followed by a large, instantaneous spike in TP – DRP concentration following wheat harvest in summer.”

## **2.4 Discussion**

### **2.4.1 Preferential Flow Dynamics in Tile Drainage**

Results of the hydrograph recession analysis indicate distinguishable quick and slow flow reservoirs at both the clay and loam sites that reflect preferential flow through macropores and diffuse flow through soil matrix percolation. The recession coefficient for R1 was eight-fold greater than R2 at the clay site and three-fold greater than R2 at the loam site. Reservoirs are often determined distinguishable when recession coefficients are more than three-fold different (e.g., Husic et al. 2019). Further, for the loam site, we found 36% of the subsurface flow transport to tiles occurred via the quick flow reservoir, R1. This result falls within uncertainty bounds of macropore flow estimates (both seasonally and annually) in a recent macropore modeling publication from the loam site (Ford et al., 2017), suggesting R1 represents preferential flow via macropores. Regarding slow flow, the inverse of the recession coefficient represents the time it would take to drain the reservoir without any additional discharge and a constant recession slope. This time would be 4 and 2.8 days for the clay and loam site, respectively which is comparable to expected matrix transit times reported in similar tile-drained landscapes of Indiana (Vidon and Cuadra, 2010). Collectively, these results suggest hydrograph recession provides a data-driven method for quantifying preferential flow and diffuse matrix percolation contributions to tile hydrology.



Our results provide insight into how preferential flow contributions are impacted by desiccation crack networks that bypass the drainage layer during the growing season. Surface runoff was second greatest in the summer, which agrees well with other recent studies that have shown that high-intensity rainfall on clay soils can trigger infiltration-excess surface flow with either simultaneous or zero tile response (e.g., Kokulan et al. 2019; Macrae et al., 2019). We found that quickflow contributions constituted 80% of tile flow during summer months, suggesting simultaneous connectivity of surface and tile pathways, which has been highlighted to occur in spring and summer in clay soils (Macrae et al., 2019). Nevertheless, tile flow was least in the summer, suggesting a disconnection between macropore flow through these desiccation crack pathways and the tile drains. Water that infiltrates via desiccation crack flow may bypass the drainage system if crack networks extend deep into the vadose zone and recharge the seasonably low ground water table (Mirus and Nimmo, 2013), or may infiltrate into the unsaturated matrix. The latter is likely small given hydrophobicity of macropore walls is recognized to increase under low moisture conditions (Nimmo, 2012), which suggest a fate of deep percolation. Collectively these results suggest that groundwater recharge could be an important regulator in timing and flow pathway dynamics of tile discharge.

#### 2.4.2 TP – DRP Forms and Pathways in Fine Textured Soils

Results of our study suggest TP – DRP concentrations in tile and surface flow pathways are predominantly associated with PP. Results of the P:N analysis showed significantly greater P:N ratios in both surface and subsurface pathways of the clay and loam sites when using the USGS persulfate digestion methodology (Patton and Kriskala, 2003) as compared to the alkaline persulfate digestion (Koroleff, 1983). Studies in

cultivated row-cropping soils have shown fairly stable ratios for P:N of organic matter (Figure 2.2), with greater P:N ratios attributed to the presence of inorganic P bound to soil surfaces (Frossard et al., 2016). Dayton et al. (2017) suggested that the USGS persulfate digestion method captures approximately 76% of total P for edge-of-field tile drain samples when sediment concentrations are high, whereas the alkaline persulfate method of Koroleff (1983) captures only 25%. Similarly, our results show that P:N is approximately three to four times higher when using the USGS method providing further support that particulate P is the primary contributor to TP – DRP loadings from the study sites. This result was not surprising given several studies measuring both TP and PP fluxes have shown PP can dominate TP loadings in tile drainage (e.g. Paasonen and Koivusalo, 2006; Enright and Madramootoo, 2004; Macrae et al., 2007; and Eastman et al., 2010; Christianson et al., 2016).

Comparison of results for TP – DRP loadings, concentrations and P:N ratios for the clay and loam sites highlight differences in sediment sources and pathway dynamics. We hypothesized that TP – DRP would be greater for the loam site as compared to the clay site given the greater tile flow volumes and soil test P levels at the loam site. Contrary to this we found greater TP – DRP concentrations, loadings, and P:N ratios at the clay site. We postulate differences in source contributions and flow pathway dynamics explain, at least some of these differences. Regarding sediment sources, sediment erosion from surface soils was greater at the clay site, but negligible at the loam site. The prominence of simultaneous pathway activation in the clay site (Macrae et al. 2019) would suggest greater connectivity of overland sediments to tile, which is partially supported by P:N ratios that deviate from organic signature that would be expected from

macropore wall erosion. The low P:N ratios in surface runoff of the loam site support a lack of surface erosion. Furthermore, in loamy soils, overland flow often requires saturation-excess conditions that limit simultaneous connectivity of surface runoff and tile flow (Macrae et al. 2019) suggesting that surface sediment sources would not be a prominent contributor to TP – DRP loadings in tile drains. Second, macropore flow at the clay site was a greater percentage of tile flow and occurred over a much shorter duration (e.g.,  $\alpha = 2$  at the clay site) as compared to the loam site. Macropore flows are well recognized to span a gradient of laminar to highly turbulent flow regimes (Beven and Germann, 2013; Williams et al., 2016). The rapid transport of flow through larger desiccation cracks (especially in spring and summer) at the clay site suggest turbulent flow regimes with greater transport carrying capacities and shear stresses. Conversely, the loam site likely had less turbulent flow in macropore pathways. This result is supported by findings from Ford et al. (2017), which was conducted at the same loam site as the present study. In their study, a numerical model that assumes macropore flow occurs as laminar films along macropore walls was successfully applied to estimate preferential flow. This would suggest less erosive flows with less transport carrying capacities. These findings underscore the potential importance of flow regimes (in addition to preferential flow volumes) in order to adequately predict delivery of sediment and particulate P to tiles.

#### 2.4.3 Environmental and Management Effects on TP – DRP delivery to tile drains

Our results highlight the coupled effects of flow dynamics and landcover to regulate seasonal maximum-minimum variability of TP – DRP concentrations. Peak TP – DRP concentrations generally occurred in seasons with the maximum quick flow

contributions at both sites. Likewise, at both sites we found decreases in TP – DRP concentrations following planting, reaching a minimum in fall, corresponding with harvest. The only deviations in these max-min dynamics were years with wheat in the rotation in which the presence of wheat during the wet season resulted in delaying peak TP – DRP concentrations in runoff. Decreasing values of TP – DRP during the growing season may reflect decreasing turbulent intensity in macropore flow. As ET increases during the growing season, desiccation cracking increases and may decrease shear stress on macropore walls given the increased surface area for transporting preferential flow. This is compounded by lesser flow volumes to tile drains during the growing season as well as lesser contributions from the soil matrix. Further, surface erosion may decrease because of vegetation cover, however we saw the second greatest contribution of TP – DRP in surface runoff during summer at the clay site, so we do not suspect that is a major mechanism leading to decreased concentrations of TP – DRP in tile drainage.

Our results suggest long-term impacts of disruption of macropore connectivity to influence TP – DRP concentrations in tiles. We found intra-annual fluctuations in TP – DRP concentrations at the clay site following conventional tillage practices, but no discernable effects on the loam site using conservation tillage practices. For the clay site we found that after tillage, TP – DRP concentrations increased to a local maximum in early January before decreasing slightly to a local minimum in mid-winter and then increasing again to the annual maxima in spring. This occurred in three years (2014, 2015, and 2017). Williams et al. (2016) found that soil disturbance resulting from tillage can significantly reduce peak event flows and may reduce delivery of DRP to tile drains. However, for DRP, the effect of tillage diminishes rapidly, and raindrop impact and wet

and drying cycles after tillage result in reformation of cracks in the soil surface, which consequently leads to more subsurface macropore flow (Mapa et al., 1986; Messing and Jarvis, 1993). Our results suggest that as cracks reform, PP may be impacted over longer timeframes as peak flows through macropores increase. Increasing peak flows will result in greater shear stresses and inner-wall macropore erosion and sediment delivery to tiles. The decrease to a local minimum late in winter may be associated with re-wetting. As the clay soil becomes saturated, macropores decrease due to soil swelling and TP – DRP reaches a local minimum. Shortly after the occurrence of local minimums, macropore pathways reform due to an increase of ET, and TP – DRP increases from a local minimum to a maximum when subsurface and macropore discharge peaks in spring.

#### 2.4.4 Broader Implications

Our study highlights the potential for P:N to be a useful tracer of PP sources given that the P:N ratios in surface soils differ from subsurface due to stratification of soil P in the profile. Sediment fingerprinting is a commonly used approach for quantifying sediment sources in agricultural landscapes (e.g., Davis and Fox, 2009); however, P:N atomic ratios are not included in fingerprinting studies to the authors' knowledge. We postulate P:N should be included in future unmixing models for quantifying sediment source provenance. One such application is to quantify differences in inner-wall macropore erosion and transport to tile-drains, from surface-derived erosion. As highlighted in Wilson et al. (2018), datasets are lacking to evaluate subsurface erosion processes, and novel utilization of this existing edge-of-field data may help to fill this data gap. Such applications will ultimately lead to improved simulation tools that can be

coupled with agroecosystem management models in order to provide more holistic P management plans.

Preferential flow has been identified as one of the significant pathways of P delivery, and a wide-range of methods have been used to quantify subsurface flow pathway dynamics ranging from dual-porosity numerical models, to data-driven hydrograph separation techniques using hydrochemical and isotope tracers (Schilling and Helmers, 2008; Vidon and Cuadra 2010; Klaus et al., 2013; Williams et al., 2016; Smith and Capel, 2018; Jarvis 2007; Deurer et al. 2009; Ford et al., 2017). While each of these methods provides insight into macropore flow and subsurface P delivery pathways, most long-term monitoring programs have continuous flow measurements, but may lack long-term measures of tracers. Likewise, numerical models are often complex, and their use is limited to specialists. The application of hydrograph recession analysis used in this study provides a promising, easy-to-use tool for partitioning flow pathway dynamics in tile-drains and compares well with previous macropore modeling estimates.

Our study confirmed the effectiveness of EMD in detecting trend in long-term TP – DRP datasets from tile-drains and is likely transferable to other contaminants of interest. While crop, tillage practices and fertilizer application varied year to year at our study sites, we were able to detect management induced trends for TP – DRP using EMD. Although Fourier filters can remove noise of linear data with distinct frequency scales, these filters fail when the processes are either nonlinear or nonstationary (Huang et al. 1998). Likewise, statistical significance tests (e.g., Kruskal-Wallis) can help to identify the seasonal differences in median or average value of P concentrations (Pease et al. 2017), however these differences may be masked by noisy time-series. Previous

studies on transport of subsurface nutrients in tile-drained landscapes shows that change of crop rotation, rainfall pattern, tillage practices and fertilization can have a significant effect on a variety of subsurface nutrient concentrations (King et al. 2015; Williams et al., 2016; Ford et al., 2018). These findings suggest that EMD can be successfully applied across a broader class of signals for detecting important management impacts at the field scale.

## 2.5 Figures and Tables

Table 2.1 Seasonal and annually averaged total tile flow (Q), slowflow ( $Q_{\text{slowflow}}$ ), and quickflow ( $Q_{\text{quickflow}}$ ) pathways results to tile drains for the clay and loam sites from 2015-2017.

		<b>Tile (clay)</b>	<b>Tile (loam)</b>
<b>Q (mm)</b>	<b>Annual</b>	143.7	299
	<b>Winter</b>	48.4	128.3
	<b>Spring</b>	62.1	74.3
	<b>Summer</b>	13.3	40.7
	<b>Fall</b>	19.9	55.6
<b><math>Q_{\text{quickflow}}</math>(mm)</b>	<b>Annual</b>	93.4	107.6
	<b>Winter</b>	31.00	39.8
	<b>Spring</b>	36.6	26.0
	<b>Summer</b>	10.9	13.8
	<b>Fall</b>	14.1	32.3
<b><math>Q_{\text{slowflow}}</math>(mm)</b>	<b>Annual</b>	50.3	191.3
	<b>Winter</b>	17.4	88.5
	<b>Spring</b>	25.5	48.3
	<b>Summer</b>	2.4	26.9
	<b>Fall</b>	5.8	23.4



Figure 2.1 Study site sampling locations in Ohio, USA. Picture of typical USDA-ARS edge-of-field monitoring platforms for surface and tile drainage are included



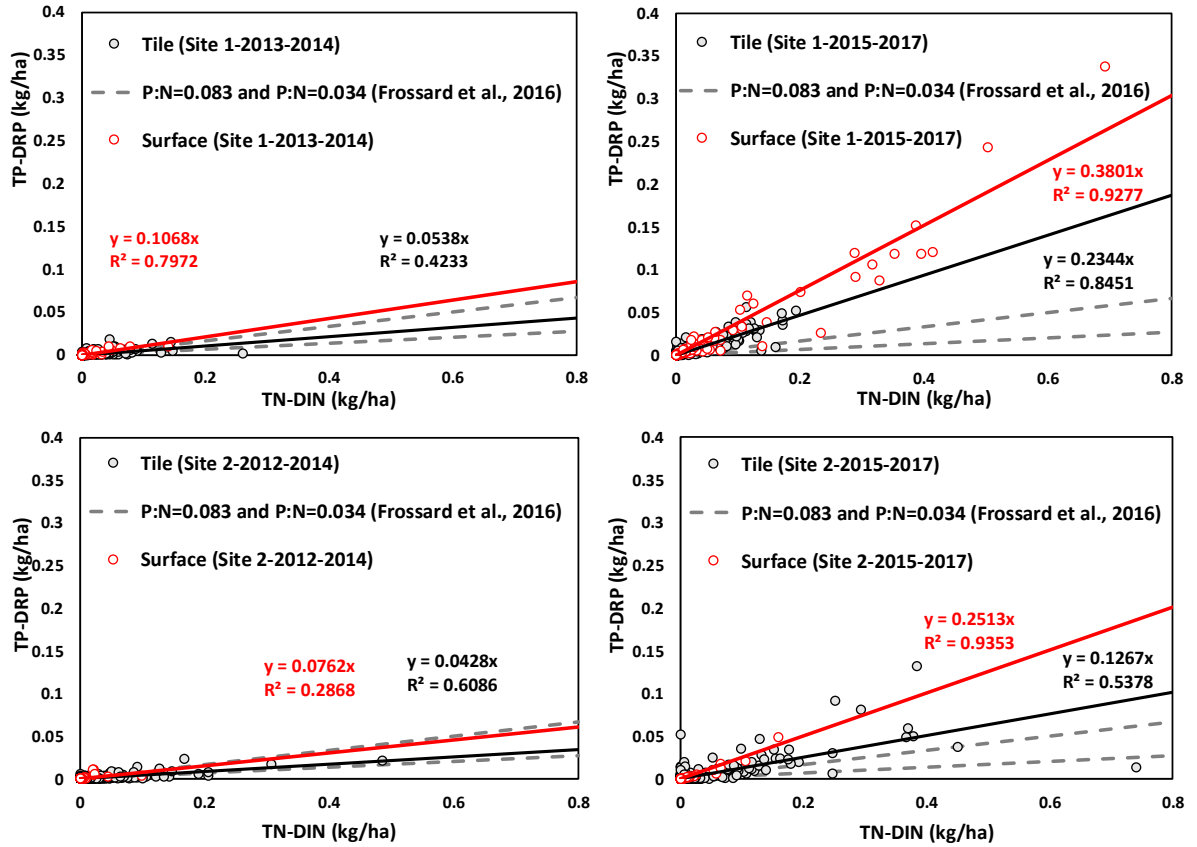


Figure 2.2 Comparison of daily TP – DRP and TN – DIN loadings from surface and tile runoff at Site 1 (clay) and Site 2 (loam). Loadings are composited from both monitoring stations at each field.

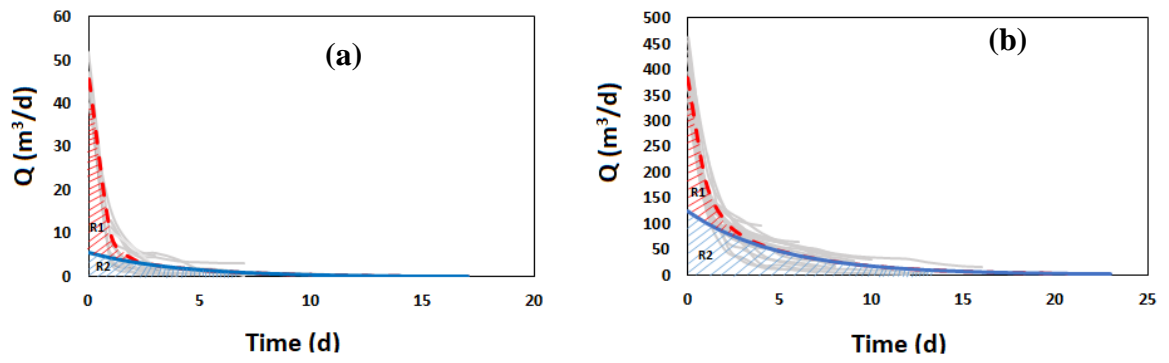


Figure 2.3 Master Recession curves constructed over 5 years of subsurface flow from 18 recessions for (a) the clay site and from 24 recessions for (b) the loam site

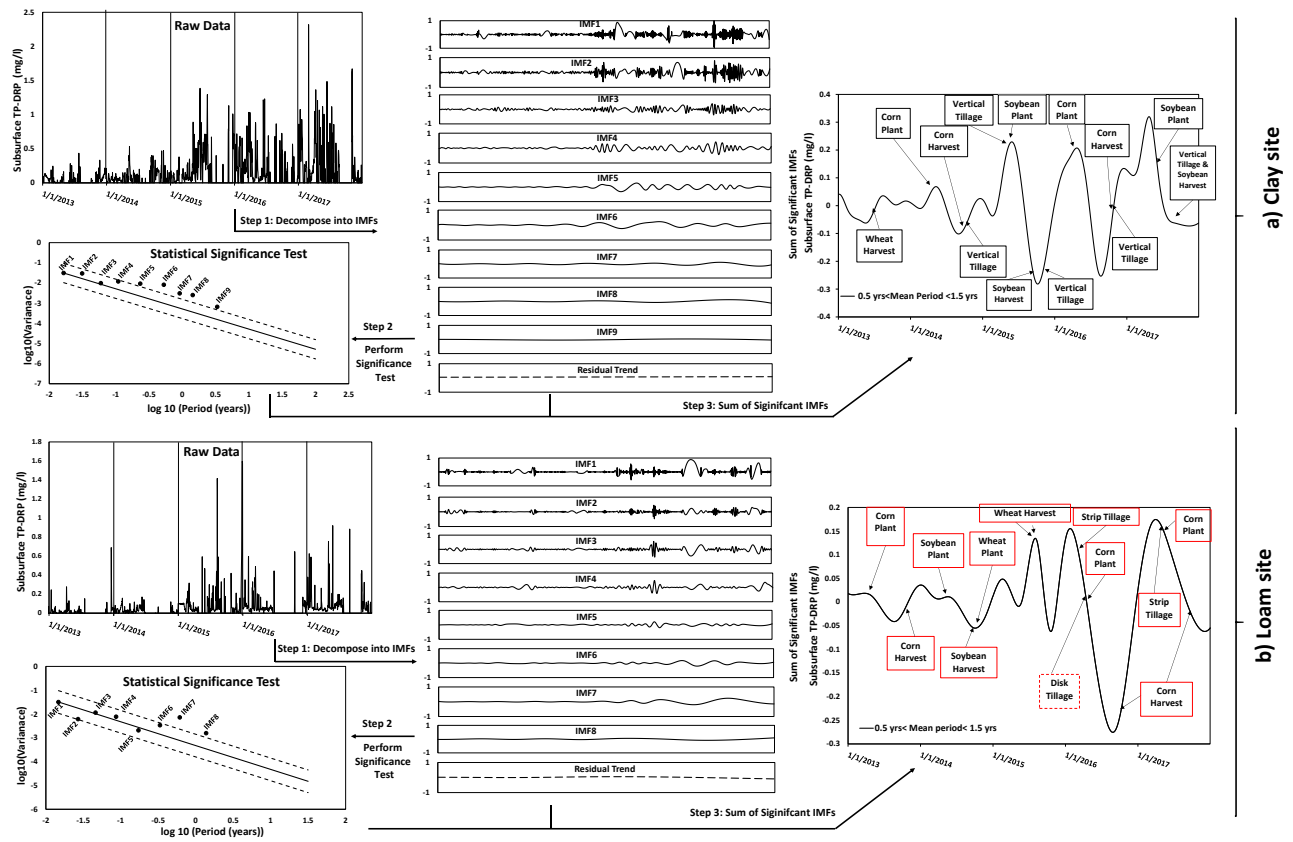


Figure 2.4 Five-year time series of TP – DRP concentration for the clay (a) and the loam (b) site. The raw TP – DRP timeseries is decomposed into a set of intrinsic mode functions (IMFs) in Step 1. In Step 2, the IMFs are tested to determine if trends are significantly differentiable from white noise. In Step 3, the significant IMFs representing seasonal trends ‘periods between 0.5-1.5 years) were summed and compared with management information.

## CHAPTER 3. QUANTIFYING HYDROLOGIC PATHWAY AND SOURCE CONNECTIVITY DYNAMICS IN TILE-DRAINAGE: IMPLICATIONS FOR P CONCENTRATIONS

Adapted from a revised resubmission to *Vadose Zone Journal*: Nazari, S., Ford, W. I., King, K. W. 2021. *Quantifying Hydrologic Pathway and Source Connectivity Dynamics in Tile-Drainage: Implications for P Concentration*.

### 3.1 Introduction

Agricultural subsurface tile-drainage across the midwestern US has increased eutrophication and the persistence of harmful and nuisance algal blooms (Simard et al., 2000; Kleinman et al., 2015; Van Esbroeck et al., 2016). Tile-drainage networks in fine-textured soils are often the primary field-scale discharge pathway during stormflows and can disproportionately impact watershed-scale water and nutrient budgets (King et al., 2014; Williams et al., 2015; Schilling et al., 2020). Tile-drainage nutrient loadings during stormflows reflect variability in flow pathway dynamics and source water connectivity (King et al., 2015; Smith et al., 2018; Puer et al., 2020; Jiang et al., 2021; Ortega-Pieck et al., 2020). For the purposes of this study, flow pathway refers to the subsurface flow domain such as percolation through micropores in the soil matrix or preferential transport through macropores, and source connectivity refers to sources of water such as event water (e.g., precipitation or irrigation water), or pre-event water (e.g., water residing in the soil matrix prior to stormflows). Existing methodologies to quantify flow pathway dynamics and source connectivity during storm events have limitations ranging from short temporal domains and coarse sampling resolutions, when using chemical and isotopic tracers (Puer et al., 2020; Nazari et al., 2020), to uncertainties and long-term data requirements associated with field-scale numerical models (Ford et al., 2017). Development and evaluation of a framework that considers both flow pathway

and source connectivity dynamics at the field point of discharge (referred to herein as ‘edge-of-field’) to assess the implications for tile-drain water quality is a major need and research gap.

Soils in tile-drained fields have been conceptualized as two-domain hydrologic systems including diffuse percolation through the soil matrix and preferential flows through macropore networks, with interactions occurring between the domains (Klaus et al., 2013; Gerke et al., 2013; Brauer et al., 2014; Bishop et al., 2015; Frey et al., 2016). Diffuse flow through matrix percolation is associated with slow and delayed seepage of water from the soil matrix to tile drains. Preferential flow through macropores reflects the rapid transfer of water to tiles via desiccation cracks, root channels, worm holes, fractures, and other bio pores that bypass percolation through the soil matrix (Flury et al., 1994; Beven and Germann, 2013). There is widespread recognition of bi-directional matrix-macropore interaction during events in tile-drained fields that has been found to significantly impact contaminant loadings (Klaus et al., 2013; Bishop et al., 2015; Williams et al., 2015; Callaghan et al., 2017; Ford et al., 2018). Recent advancements in field-scale hydrology and water quality models (e.g., Hydrus, MACRO, APEX, and DRAINMOD) have been important for representing these dynamics and water sources for agroecosystem management (Beven and Germann, 2013; Ford et al., 2017; Askar et al., 2020). However, in agroecosystem models, they often require long-term records for rigorous calibration and validation and neglect or over-simplify simulation of processes including matrix-macropore interaction, resulting in uncertainties during model evaluation (Djabelkhir et al., 2018; Pferdmenges et al., 2020).

Utilization of hydrograph recession analysis has been identified as an effective method to quantify event-scale matrix and macropore pathway contributions (Ford et al., 2019; Husic et al., 2019; Nazari et al., 2020). In hydrograph recession, hydrographs are conceptualized as the drainage of a series of reservoirs that have variable hydraulic conductivities and storage volumes (Husic et al., 2019). These reservoirs often recede exponentially, resulting in distinct log-linear regions of the hydrograph. The hydrograph recession method has been successfully applied in subsurface drained landscapes with lateral preferential pathways including karst and tile-drained landscapes to partition flow into diffuse and preferential flowpaths with varying hydraulic conductivities (Schilling and Helmers 2008; Mellander et al., 2013; Ford et al., 2019; Husic et al., 2019; Nazari et al., 2020).

Regarding tile drainage source dynamics during storm flows, studies have applied various chemical and isotopic tracer methods (Keinzler and Naef 2008; Vidon and Cuadra 2010; Klaus et al. 2013; Williams et al. 2015; Ford et al. 2018). Most studies that assess source water dynamics partition tile-drainage water into ‘new’ and ‘old’ water components, in which ‘old’ water reflects storage in the soil prior to the event, and ‘new’ water reflects either precipitation or irrigation inputs during an event (Schilling and Helmers, 2008; Vidon and Cuadra 2010; Klaus et al., 2013; Williams et al., 2016). These studies have found that preferential flow can consist of both new and old water sources (Vidon and Cuadra, 2010; Williams et al., 2016; Smith et al., 2018). While these techniques have been effective at identifying source water dynamics at the field to watershed scale within-events, these approaches are often limited to coarse resolution

sampling of a few events due to data collection and analytical expense (Williams et al., 2016; Puer et al., 2020).

Studies have employed high-frequency conductance-based measurements as an inexpensive means to continuously monitor source connectivity dynamics during tile-drain hydrologic events at the watershed scale (e.g., Heppell and Chapman, 2006; Schilling and Helmers, 2008; Vidon and Cuadra 2010; Kronholm and Capel, 2015) and more recently at the field scale (Smith et al., 2018; Puer et al., 2020). Specific conductance (SC) can be used as a general indication of runoff age due to change of drainage water ion concentrations during residence within the soil profile. Typically, waters with extended residence times are likely to have a greater ionic content and SC values (Pilgrim et al., 1983). In recent years, advances in the robustness and reliability of inexpensive *in-situ* water quality sensors have enabled scientists and practitioners to continuously monitor SC (Snyder et al., 2018). As a result, studies are now deploying these technologies in tile-drains at the edge-of-field and coupling these measurements with end-member mixing analyses (EMMA) to quantify the contribution of preferential flows of new water (Smith et al., 2018; Puer et al., 2020). To date, studies have not coupled hydrograph recession and SC-EMMA approaches for investigating flow pathway and source connectivity dynamics simultaneously.

Several studies have postulated that flow pathway and source connectivity dynamics impact dissolved reactive phosphorus (DRP) loadings in tile-drained agroecosystems. Water extractable P from soils correlates well with tile drain DRP concentrations during storm events, hence, event-water that is rapidly transported to tile via preferential flowpaths is often cited as a driver of tile DRP concentrations (Stamm et al., 1998;

Heathwaite and Dils, 2000). Other studies have illustrated that matrix water may be rapidly transported from variable depths in the soil column to tile during events, which alters DRP concentration dynamics (Klaus et al., 2013; Williams et al., 2016; Ford et al., 2018). We postulate that combining hydrograph recession analysis of tile flow and SC-EMMA will improve quantification of flow pathway and source water connectivity dynamics, and consequently improve correlations with nutrient concentrations in tile-drainage.

The overall objective of this study was to develop a new approach to partition subsurface flow based on both flow pathway and source connectivity descriptors and elucidate their impact on P concentration dynamics in tile drainage. Specific objectives of this chapter are to: 1) apply hydrograph recession analysis of subsurface discharge to partition the tile hydrograph into quickflow and slowflow pathways, and SC-EMMA to partition new-water and old-water; 2) develop and apply a new hydrograph separation framework that describes both hydrologic pathway (i.e., matrix flow vs. preferential macropore flow) and source connectivity (e.g., new-water vs. old-water) in tile drainage; and 3) investigate the relationship between separated hydrograph fractions and tile-drain DRP concentrations.

## **3.2 Materials and Methods**

### **3.2.1 Study Site**

A field site from the USDA-ARS Soil Drainage Research Unit edge-of-field monitoring network (Williams et al., 2016) was secured for this study. The field site (0.158 km<sup>2</sup>) is a systematically tile drained field in Wood County, Ohio U.S.A.



Systematic tile drainage was implemented at 0.9 m (3 ft) below the soil surface with a lateral spacing of 15.2 m (50 ft). Laterals were routed to a 0.3 m (12 in) tile main which was equipped with a drainage water management structure before discharging to a downstream ditch (Figure 3.1a). During our monitoring period, the structure remained open as part of a before-after-control-impact assessment, thus the field was always freely drainage during our monitoring period. The soils were characterized as silty-clay-loams consisting of Nappanee (NpA) and Hoytville (HcA) soil series (SSURGO soil data base, NRCS USDA, 2019). Soil P levels were measured using Mehlich-3 P soil tests at various depths and locations for the field and were found to average 80.6 mg kg<sup>-1</sup> in the upper surface layer (0-5 cm), 36.5 mg kg<sup>-1</sup> from 5-15 cm, and averaged 6.3 mg kg<sup>-1</sup> at depths of 15-60 cm. The typical crop rotation was corn-soybean-wheat, managed with conservation-tillage. At the onset of monitoring (October 1, 2018), the field contained soybean that was harvested on 10/17/2018. The field remained fallow until wheat was planted the following season (10/11/2019).

### 3.2.2 Data Collection and Analysis

Precipitation and discharge were collected by the USDA-ARS using well-accepted edge-of-field monitoring practices (Williams et al., 2016; Figure 3.1b). Tipping bucket rain gages were used to measure 10-minute rainfall intensity, depth, and duration. Tile mains were equipped with a weir insert (Thel-Mar, Brevard), and an ISCO 4230 Bubbler Flow Meter (Teledyne Isco, Lincoln, Nebraska). Additionally, the tile outlet was equipped with an ISCO 2150 Area Velocity sensor for 30-minute discharge measurements under submerged conditions. Similarly, a surface monitoring site was equipped with a 61-cm (2-ft) H flume and a bubbler flow meter to measure 10-minute

discharge. Discharge was reported from the standard flume or weir stage-discharge relationships or as the product of area and velocity for the tile outlet when submerged. During water year 2019 (October 1, 2018-September 30, 2019), total tile discharge was 522 mm, or 41% of precipitation (1263 mm). Surface runoff was only 8.3 mm (< 1% of precipitation) highlighting the importance of the subsurface flow pathway. Mean 30-minute tile discharge throughout the monitoring period was 0.0025 m<sup>3</sup>/s, while maximum discharge was 0.0343 m<sup>3</sup>/s.

A YSI EXO3 water quality sonde (Xylem/YSI Incorporation, 2020) was installed in the drainage water management structure to continuously (15-minute interval) measure specific conductance (see Figure 3.1c). The sonde was equipped with a conductivity/temperature sensor, which uses four internal pure-nickel electrodes to measure solution conductance. Two of the electrodes are current driven, while the other two are used to measure voltage drop (EXO User Manual). Monthly maintenance was performed on the instrument per manufacturer recommendations, and was consistent with other studies (Snyder et al., 2018). A one-point calibration approach was performed using KorEXO software and a calibration standard with conductivity equal to 1000  $\mu\text{s}/\text{cm}$ .

Surface and tile water samples were collected using a Teledyne ISCO 6712 portable sampler and accessories. Surface samples were collected using a flow proportional methodology; that is, a 200 mL aliquot was collected for every 1mm volumetric depth. Ten composited aliquots made up one sample. Due to periodic submergence, a time-proportional approach was used to collect water samples. A 100-ml aliquot was collected every six hours for 48 hours and composited into a single sample bottle reflecting a two-

day composite sample. During rainfall events, samples were collected at higher frequencies (samples collected every 15 minutes and composited hourly). Collected water samples were analyzed for dissolved reactive P (DRP) throughout the monitoring period by first vacuum filtration (0.45 $\mu$ m) and then analyzing for P using the ascorbic acid reduction method (Murphy and Riley, 1962). Samples rarely fell below method detection limits. Specific conductance was also measured on all Isco collected samples using a calibrated SC sensor in the laboratory.

### 3.2.3 Analytical Methodology

#### 3.2.3.1 Hydrograph Recession and SC EMMA

Hydrograph recessions from events throughout the monitoring period were compiled to develop a master recession curve. We assumed two flow pathways reflecting reservoirs for matrix and macropore flow, consistent with previous studies (Schilling and Helmers 2008; Vidon and Cuadra 2010; Williams et al., 2016; Nazari et al., 2020). Recession coefficients ( $k$ ) for a linear reservoir are defined by the equation  $Q=Q_0e^{-kt}$  (Gregor and Malik, 2012). The master recession curve (MRC) was automatically created using a Genetic Algorithm (GA) incorporated in RC 4.0 software (HydroOffice; Gregor and Malik, 2012; Malik and Vojtkova, 2012). We omitted events that were either comprised of days with zero flow (i.e., associated with no flux or tile backwater) or had nonlinear recessions associated with disruption of the initial recession and/or secondary flow peaks. For MRC creation, we selected 18 recessions from the site. Then we selected two linear reservoirs and fit two recession curves so that the two recessions provided

optimal fit to the data. The goodness-of-fit was tested using the Nash-Sutcliffe Efficiency (NSE) value (Moriiasi et al., 2007).

Hydrograph recession analysis was performed for each storm event using methods described by Husic et al. (2019) and Ford et al. (2019) (Figure 3.2a) which has been recently applied in tile-drained landscapes (Nazari et al., 2020). Briefly, for each hydrologic event, we graphed the falling limb of the subsurface discharge hydrograph on a logarithmic scale and manually fit linear curves to distinct log-linear regions (reflecting drainage of two reservoirs) to determine the inflection points of the linear trends. Then, a linear increase in slow flow was assumed from the beginning of the rising limb of the hydrograph, which represents the start of quickflow ( $Q_{quick}$ ), to the determined inflection point on the falling limb from the previous step, which represents the maximum of the slow flow reservoir (Husic et al., 2019). To test the impact of the assumption of linear increase of slowflow reservoir on flow pathway results we evaluated two alternative approaches for calculation of the slowflow hydrograph for eight events. We used a non-linear two-parameter digital filter method (Eckhardt, 2005), in which parameters were calibrated so that slowflow reservoir non-linearly increased to the maximum slowflow value near or before the hydrograph peak and then its value remained constant to the inflection point on the falling limb. We also used a non-linear one-parameter digital filter method (Lyne and Hollick, 1979) in which the recession constant was calibrated so that slowflow non-linearly increased slowly early in the event and then increased rapidly towards the inflection point on the falling limb of the hydrograph. Comparing the results of these two approaches showed limited impact on results (1-4% difference), and the timing of flow pathway peaks remained unchanged. Given the insensitivity of this

assumption, we present results using the simplified linear assumption for the 27 events. The area between the hydrograph and the slow flow curve represented  $Q_{quick}$ , and the area underneath the slow flow reservoir curve represented  $Q_{slow}$ . We performed this analysis on 27 storm events (SEs) from water year 2019.

New-water and old-water fractions were quantified using specific conductance end-member mixing analysis (SC-EMMA; Figure 3.2b). Following the approach of Smith et al. (2018), we solved the following system of equations at each timestep to estimate the pre-event (old) and event (new) flow contributions to tile drainage.

$$(Q_{Tile})_t = (Q_{old})_t + (Q_{new})_t \quad (1a)$$

$$(SC_{Tile})_t(Q_{Tile})_t = SC_{old}(Q_{old})_t + SC_{new}(Q_{new})_t \quad (1b)$$

where,  $(Q_{Tile})_t$ ,  $(Q_{old})_t$ ,  $(Q_{new})_t$  were total, old-water and new-water tile discharges at time  $t$ , respectively.  $(SC_{Tile})_t$  was the measured specific conductance of subsurface tile water at time  $t$ , and  $(SC_{old})_t$  and  $(SC_{new})_t$  were specific conductance of old-water and new-water at time  $t$ , respectively. We assumed that  $SC_{new}$  was the average specific conductance of surface water runoff samples collected from the surface site, and  $SC_{old}$  was the specific conductance of subsurface water at the beginning of each event and varied from one event to the next, a result of variable soil water conditions.

### 3.2.3.2 Hydrograph Separation Framework

We developed a new hydrograph separation framework that considers both flow pathway and water source connectivity (Figure 3.2c-d). Once  $Q_{quick}$ ,  $Q_{slow}$ ,  $Q_{new}$  and  $Q_{old}$ , were calculated, we developed the following piecewise functions for each time step ( $t$ ) to estimate the portion of old-water that drains to the quickflow reservoir ( $Q_{quick-old}$ ), portion

of new-water that drains to the quickflow reservoir ( $Q_{quick-new}$ ), portion of new-water that drains through the slowflow reservoir ( $Q_{slow-new}$ ), and the portion of old-water that drains to the slowflow reservoir ( $Q_{slow-old}$ ). In deriving this framework, we assumed that 1) if quickflow exceeded new-water, all new-water was attributed to the quickflow pathway, and 2) if new-water exceeded quickflow, then all quickflow was attributed to new-water. Based on these assumptions, each pathway-source component of the hydrograph can be calculated as follows.

$$\begin{cases} (Q_{quick-old})_t = (Q_{quick} - Q_{new})_t & \text{if } (Q_{quick})_t \geq (Q_{new})_t \\ (Q_{quick-old})_t = 0 & \text{if } (Q_{quick})_t < (Q_{new})_t \end{cases}$$

(2.a)

$$\begin{cases} (Q_{quick-new})_t = (Q_{new})_t & \text{if } (Q_{quick})_t \geq (Q_{new})_t \\ (Q_{quick-new})_t = (Q_{quick})_t & \text{if } (Q_{quick})_t < (Q_{new})_t \end{cases}$$

(2.b)

$$\begin{cases} (Q_{slow-old})_t = (Q_{total} - Q_{quick})_t & \text{if } (Q_{quick})_t \geq (Q_{new})_t \\ (Q_{slow-old})_t = (Q_{total} - Q_{new})_t & \text{if } (Q_{quick})_t < (Q_{new})_t \end{cases}$$

(2.c)

$$\begin{cases} (Q_{slow-new})_t = 0 & \text{if } (Q_{quick})_t \geq (Q_{new})_t \\ (Q_{slow-new})_t = (Q_{new} - Q_{quick})_t & \text{if } (Q_{quick})_t < (Q_{new})_t \end{cases}$$

(2.d)

We partitioned the tile flow into  $Q_{quick-new}$ ,  $Q_{quick-old}$ ,  $Q_{slow-new}$ , and  $Q_{slow-old}$  for the entire 2019 water year. For each selected event (27 events), we calculated total water volume and fractions for each partitioning.

### 3.2.3.3 Comparison with Nutrient Concentration

Dissolved reactive P concentrations ( $DRP_{tile}$ ) in tile-drainage will reflect mixing of flow contributions and their associated nutrient compositions, which can be described using a linear mass-balance mixing model. Based on our pathway-connectivity framework, we conceptualized tile drain nutrient concentrations to be influenced by the four hydrograph fractions as follows.

$$DRP_{tile}Q_{tile} = DRP_{quicknew}Q_{quicknew} + DRP_{quickold}Q_{quickold} + DRP_{slownew}Q_{slownew} + DRP_{slowold}Q_{slowold} \quad (3)$$

where,  $DRP$  is the daily flow-weighted mean nutrient concentration (mg/l), and  $Q$  is the tile flowrate for each partition (mm/d). We used a daily, as opposed to event-based timestep since cumulative event dynamics will smooth out some variability in pathway dynamics. We also disregarded the sorption/desorption effects along the pathways for simplification and because the time scale of the events was short. Hence our analysis reflects average  $DRP$  concentrations for each pathway across events.

Dividing both sides of the equation 3 by  $Q_{Tile}$ , the equation can be written as a multiple linear regression (MLR) model, with  $DRP_{tile}$  as the measured dependent variable, fractions of pathway-source contributions as independent variables, and concentrations of the sources as unknowns:

$$DRP_{tile} = F_{quicknew} \times DRP_{quicknew} + F_{quickold} \times DRP_{quickold} + F_{slownew} \times DRP_{slownew} + F_{slowold} \times DRP_{slowold} \quad (4)$$

where,  $F$  is the fraction of total tile discharge for each partition at a given timestep.

Daily subsurface  $DRP$  loadings and flow from the tile drainage network were calculated for all events throughout the monitoring period. We determined the midpoint of all sample time steps for each collected water sample, then used linear interpolation between measured values at the midpoint to estimate the concentration for each interval, and finally estimated loading as the product of interpolated concentrations and flow rate (Williams et al., 2015). We calculated daily  $Q_{quick-new}$ ,  $Q_{quick-old}$ ,  $Q_{slow-new}$  and  $Q_{slow-old}$  by

summing calculated 30-minute flow components. Daily flow-weighted mean concentrations of DRP were calculated by dividing daily nutrient load by daily tile discharge. Daily flow-weighted mean concentration of DRP was used for MLR analysis in equation 4.

We performed a multiple linear regression at a daily timestep in order to estimate ‘best-fit’ concentrations for the partitioned hydrograph sources. The MLR models were performed in RStudio software. The F-statistic was used to test the null hypothesis that individual coefficients (DRP values in equation 4) were not equal to zero, as well as the null hypothesis that the overall MLR model provided a superior fit to a mean trend. P-values were calculated for the F-statistics in both hypothesis testing scenarios, and significance results are reported for  $p < 0.05$ ,  $p < 0.01$ ,  $p < 0.001$ , and  $p < 0.0001$ . We performed an analogous analysis using only  $Q_{quick}/Q_{slow}$  and  $Q_{new}/Q_{old}$  to assess the improvement in predictions when using our new coupled hydrograph separation framework over each isolated hydrograph separation method.

### **3.3 Results and Discussion**

#### **3.3.1 Hydrograph Recession and SC-EMMA Results**

Master recession curve analysis for the 2019 water year data resulted in two discernable reservoirs reflecting preferential flow through macropores and diffuse drainage through the soil matrix (Figure 3.3). Reservoir 1 (R1) reflected a steeply recessing quickflow pathway, while Reservoir 2 (R2) was characteristic of a mildly recessing slowflow pathway. The recession coefficients for R1 and R2 were 0.9 and 0.25  $d^{-1}$ , respectively (Figure 3.3). The NSE value was equal to 0.81, suggesting very good fit



(Moriassi et al., 2007). Given that the recession coefficients vary by greater than three-fold (Schilling and Helmers, 2008; Rimmer and Hartmann, 2012; Husic et al., 2019), these findings are indicative of two distinct flow pathways. Results of the master recession curve suggest that R1 accounted for 54% of the subsurface flow while the remainder, or 46% was attributed to R2. These values were consistent with ranges reported for preferential and diffuse flow at nearby loam and clay fields with similar long-term management practices (Ford et al., 2017; Nazari et al., 2020) and indicated that both preferential and matrix flow are significant contributors to subsurface drainage.

Specific conductance (SC) measurements during storm events showed a consistent pattern of maximum values occurring prior to the event, a decrease to minimum values slightly before or after peak discharge, and then increasing values on the receding limb toward pre-event levels (Figure 3.4). Pre-event SC averaged 566.5  $\mu\text{s}/\text{cm}$  for the twenty-seven events. Minimum event SC averaged 240.5  $\mu\text{s}/\text{cm}$ , reflecting decreases towards values reported for precipitation (e.g., 12  $\mu\text{s}/\text{cm}$  in Smith et al., 2018) and measured SC in the surface runoff samples (15  $\mu\text{s}/\text{cm}$  from 55 surface runoff samples). Interestingly, the time to minimum SC values differed significantly for fall and winter events (mean = 698 minutes; with range of 165 to 1260 minutes) compared to spring and summer events (mean = 183 minutes; with a range of 60 to 390 minutes). Similar quick responses (141 min) from spring and summer events on silty clay loam sites in Iowa (Smith et al., 2018) have been reported and may be associated with differences in management practices, precipitation patterns, and seasonal differences in preferential flowpaths (Graham and Lin, 2011; Williams et al., 2016; Plier et al., 2020).

Based on our results, we postulate seasonal differences and precipitation pattern dynamics both play an important role in timing of new water delivery to tile drains. Regarding precipitation patterns, our results showed that average event precipitation intensity (PI) in summer and spring (PI=9.8 mm/day) were two-fold greater than for the events in fall and winter (PI= 4.2 mm/day). With regard to seasonal environmental conditions, previous studies in tile-drained landscapes suggest that during the growing season, low-moisture conditions promote desiccation crack expansion, which enables water to rapidly transfer to tiles or bypass the drainage system (e.g. Nazari et al. 2020). Conversely, during winter a large amount of infiltration can occur via preferential flow because under partially saturated conditions a considerable portion of macropores remain air-filled (Granger et al., 1984; Stadler et al., 2000, Pittman et al., 2020; Mohammed et al., 2018 and 2020). Nevertheless, infiltrated meltwater may freeze due to matrix-macropore heat and water transfer, and the frozen water can block the macropore pathway, and consequently reduce infiltration of event water (Stadler et al., 1997; Watanabe and Kugisaki, 2017; Demand et al., 2019; Mohammed et al., 2020). Cumulatively, these seasonal environmental factors in precipitation and soil dynamics are likely drivers of short time to peaks in spring and summer and longer time to peaks in fall and winter.

Results of the event-based continuous recession and SC-EMMA analysis illustrated noticeable differences in magnitude and timing of the quick flow and new water fractions, challenging the assumption that new-water is equivalent to preferential flow (Table 3.1; Figure 3.5). Cumulatively,  $Q_{quick}$  was estimated to be 172 mm (48% of total tile discharge) and  $Q_{new}$  was estimated to be 176 mm (49% of total tile discharge).

For individual events, we found quickflow contribution to total subsurface flow varied from 8 to 77%, and new-water contributions varied from 3 to 82% (Table 3.1). However, new-water and quickflow hydrographs often differed in terms of peak timing and magnitude between events (Figure 3.5). The peak of  $Q_{quick}$  often occurred before  $Q_{new}$  except for SE12 and SE26. The difference between time to peak of  $Q_{quick}$  and  $Q_{new}$  averaged 164 minutes for fall and winter events, and 87 minutes for spring and summer events. Studies have often assumed the amount of preferential flow is equated to the amount of new-water transported to tile (Klaus et al., 2013). For example, Smith et al. (2018) and Puer et al. (2020) interpreted conductance-based unmixing results as separation of preferential flow and slow flow. Similarly, Williams et al. (2016) used  $\delta^{18}O$  to define event and pre-event water to tile drains and assumed that event water transported to tile drains within a storm event was only possible through macropore flows. Our findings suggest new-water during storm flows may be transported to tile through both preferential and diffuse flow paths, suggesting caution should be used with tracer-based approaches.

### 3.3.2 Pathway-Connectivity Results

Results of the pathway-connectivity framework indicates all four hydrograph components had a significant, but variable contribution to tile hydrology. Cumulatively,  $Q_{quick-old}$ ,  $Q_{quick-new}$ ,  $Q_{slow-old}$  and  $Q_{slow-new}$  contributed 9%, 39%, 42% and 10% of tile discharge for the analyzed events (Table 3.1).  $Q_{quick-old}$  contributions ranged from 0.05% to 27%,  $Q_{quick-new}$  contributions ranged from 1.86% to 66%,  $Q_{slow-new}$  contributions ranged from 0.7% to 33%, and  $Q_{slow-old}$  contributions ranged from 13% to 98% of total tile

discharge. Many agroecosystem water management models make simplifying assumptions that limit their ability to represent the aforementioned pathway-connectivity dynamics. For instance, APEX, DRAINMOD-P, ADAPT, RZWQM2-P, SimplyP, SWAP, and SWAT, do not actively simulate matrix-macropore processes explicitly through dual porosity or dual permeability frameworks (Pferdmenges et al., 2020). This is important not only for hydrologic simulations, but also contaminant transport given source connectivity has a major impact on nutrient, pesticide and sediment transport processes, as will be discussed in section 3.3.3. As modeling frameworks in agroecosystems evolve to incorporate robust hydrologic processes, the coupled hydrograph-recession SC-EMMA framework proposed herein may be useful for quantitative model evaluations given the heterogeneity observed at the event-scale in pathway-connectivity dynamics.

Results for  $Q_{quick-new}$  support existing perceptions that preferential transport of surface water occurs through both saturated and unsaturated conditions through macropores in fine-textured, tile-drained soils.  $Q_{quick-new}$  for the 27 events had a positive linear relationship with event precipitation ( $R^2 = 0.4$ ), and a weak negative correlation with 10-day antecedent rainfall ( $R^2 = 0.12$ ). Further, under low antecedent conditions in summer (Figure 3.6a), two  $Q_{quick-new}$  peaks were observed, one of which occurred 60 minutes into the event, and the other occurred 210 minutes into the event. This finding illustrates that fine-textured tile-drained landscapes are not solely drained by binary flow reservoirs, but instead reflect a spectrum of slow to rapid flows. For example, Schilling et al. (2008) illustrated recessions in tile-drained landscapes of Iowa may be separated into quick, intermediate, and slow flow regimes. The timing of the second peak is

reflective of the time to peak for  $Q_{quick-new}$  in fall as evidenced by similar magnitude drainage events with greater antecedent moisture (Figure 3.6b). While further work is needed to illustrate the prominence and mechanisms driving these early-event peaks, one potential mechanism is that desiccation crack networks may be more prominent during these low antecedent moisture periods, promoting unsaturated film flow to tiles (e.g., Nimmo, 2012; Mirus and Nimmo, 2013; Ford et al., 2017). Regardless, these findings support a growing body of research in tile-drained landscapes that suggest macropore flows of surface-derived water sources are significant under a range of antecedent moisture conditions (Tokunga and Wan, 1997; Cey and Rudolph, 2009; Ford et al, 2017; Smith et al., 2018).

Results for quickflow of old water ( $Q_{quick-old}$ ) highlight the importance of intrinsic event properties to control the magnitude of matrix-macropore flow. The  $Q_{quick-old}$  component of the hydrograph, by definition, reflects matrix water that is transported to tile-drains via macropore flowpaths, and was found to be activated throughout the year, even under drier antecedent conditions. Like  $Q_{quick-new}$ , we found a positive linear relationship between  $Q_{quick-old}$  and precipitation ( $R^2 = 0.52$ ), and a weak negative relationship with 10-day antecedent rainfall ( $R^2=0.08$ ). We also found  $Q_{quick-old}$  to have a positive linear relationship with  $Q_{quick-new}$  ( $R^2 = 0.40$ ). Klaus et al. (2013) performed irrigation experiments on a tile-drained hillslope and found old-water was mobilized through shallow surface soil depths (20-40 cm) and transported through macropores because macropore–matrix interaction leads to an initiation of macropore flow after a moisture threshold was exceeded. Several other studies have highlighted macropore flow under porewater tension conditions and associated importance of macropore–matrix

interaction in controlling this flow (e.g. Tokunaga and Wan 1997; Cey and Rudolph 2009; Bishop et al., 2015; Callaghan et al., 2017). The findings of our study support that increasing preferential flow of new-water enhances mixing with the soil matrix (i.e., bi-directional matrix-macropore interaction). Likewise, our findings support that larger precipitation events will result in greater saturation of soils and thus greater rates of matrix-macropore exchange. Contrary to anticipated outcomes, antecedent rainfall had little impact on matrix-macropore exchange. This finding suggests that antecedent conditions may be insensitive when compared to intrinsic storm event hydrologic characteristics with regards to magnitude of matrix-macropore exchange.

Apart from near-surface initiation of macropore flow, rapid transport of old water to tile drains could occur because of rapid transition of the capillary fringe from tension saturation to positive pressure (Sklash and Farvolden 1979). In tile-drained systems, the groundwater elevation is at or near the tile drain elevation, therefore it is possible that part of the correlation between macropore flow and matrix-macropore exchange is associated with the rapid transition of the capillary fringe tension saturation to positive pressure near tile drains. Nevertheless, as will be discussed in section 3.3.3, we do not feel this is a prominent source for our study since regression analyses with DRP concentrations indicated high levels of DRP in the  $Q_{quick-old}$  pathway.

Our findings show contributions of both new-water and old-water to the slow flow pathways suggesting groundwater recharge of new-water plays an important role in tile-drainage fluxes. The average time to peak of  $Q_{slow-new}$  for all the events was  $32 \pm 4$  hours. Using a one-dimensional form of Darcy's law in which we assumed area weighted hydraulic conductivity averaged  $5.5 \text{ cm day}^{-1}$  and 45% of porosity for our site (NRCS,

2019; Vidon and Cuadra, 2010), we found that for new stormwater to reach tile drains through diffuse percolation alone could take on the order of a week. This result suggests that new-water, at least to some degree, bypasses portions of the soil matrix before ultimately draining through the soil drainage reservoir. Previous studies have indicated that unsaturated-zone preferential flow can significantly contribute to groundwater recharge (Lee et al., 2006; Mirus and Nimmo 2013; Cuthbert et al., 2013). For tile-drained landscapes, Frey et al. (2012) highlighted that under partially saturated conditions water transport via macropores to subsurface can then be laterally transmitted to tiles via short slowflow pathways in the vicinity of tile lines. Although we did not measure groundwater level and its responsiveness to preferential flow, we found that there was a negative relationship between  $Q_{slow-new}$  time to peak and 10-day antecedent rainfall ( $R^2 = 0.19$ ). This finding is consistent with Lee et al. (2006) where the authors found that groundwater recharge with preferential flow is dependent on both thickness and degree of saturation of the unsaturated zone. Collectively, these results suggest that groundwater recharge could be an important regulator of timing and flow pathway dynamics in tile discharge.

### 3.3.3 Implications for P delivery at the edge-of-field

Daily flow-weighted mean DRP concentrations were poorly correlated with discharge, stemming primarily from significant variability at low tile discharges (Figure 3.7). We found that tile drainage only predicted about 10% of the variability in DRP. The simple regression underestimates DRP concentrations at low-flow conditions where DRP concentration was highly variable, and overestimated DRP concentrations at high-flow conditions when concentrations were less variable. This finding suggests that during

high-flow conditions, subsurface discharge can be a more reliable predictor of DRP concentration while under low-flow conditions other environmental factors may influence DRP such as P (de)sorption, redox conditions, and water source (Wright et al., 2001; Kleinman and Sharpley, 2002; King et al., 2015).

Multiple linear regression (MLR) analysis suggests that including both pathway and connectivity partitioning was important for estimating tile drainage DRP concentrations (Table 3.2; Figure 3.8). The p-value of the F-statistic for all three models was  $< 2 \times 10^{-16}$ , suggesting all models were significant predictors of tile DRP concentrations. Further, all beta coefficients were found to be significant at a 0.05 significance level. Comparing the visual results of predicted DRP values and measured DRP values (Figure 3.8) illustrates that our new pathway-connectivity framework provided improvements at low-moderate DRP concentrations ( $< 0.05$ ) as evidenced by datapoints converging on the 1:1 line (Figure 3.8c). Further indication of improvement of prediction using our pathway-connectivity framework is evidenced by increases in the NSE (0.46; see Moriasi et al., 2007), as compared to SC-EMMA (0.41) (Figure 3.8.b), and hydrograph recession (0.27) results (Figure 3.8.a). While the improvement may partially reflect additional variables in the regression analysis, all regression variables were significant (Table 3.2), and the coefficients differed between each of the hydrograph partitions. This methodology may become particularly important for understanding dynamics at sites where matrix exchange of old water to macropores constitutes a greater proportion of the tile hydrograph. Further, this methodology may help with evaluating drivers of DRP delivery to tile at sites where new water is a poor predictor of DRP concentrations (Pluer et al., 2020). While predictions could be improved by accounting



for variability in individual source compositions, our results support the importance of considering both hydrologic source and pathway to accurately predict DRP concentration dynamics. Furthermore, our analysis reflects an average DRP concentration from pathways, however between events there are likely complex sorption/desorption dynamics that result in variability in each pathway. Considering redox or other conditions that can effect sorption/desorption dynamics between events can reduce uncertainty associated with our MLR analysis and improve the NSE value.

Best-fit concentrations from the regression model provide insight into sources of DRP in the soil profile and the impacts of preferential flow on groundwater recharge. Results of the regression analysis showed  $DRP_{quick-old}$  was slightly less than  $DRP_{quick-new}$ . This result suggests  $DRP_{quick-old}$  was initiated from near-surface matrix waters, given that water extractable P is highly stratified at the study site (see study site description). Such stratification and subsurface labile P accumulation is typical of tile-drained agroecosystems in the region (King et al., 2015; Xu et al., 2020). Additionally, concentrations for  $DRP_{slow-new}$  were high, similar to quick flow pathways. This finding was somewhat surprising considering the slow-new source ultimately drains through the matrix reservoir. In part this finding may partially reflect uncertainties in the new water SC end-member, particularly later in the event when SC values may be non-conservative (Vidon and Cuadra 2010). Nevertheless, the finding is of interest because it suggests groundwater recharge through preferential flowpaths is an important source of greater DRP concentrations in tile drainage, which is rarely emphasized in tile DRP studies (King et al., 2015) and merits further consideration in future tile-drainage water quality

research, particularly when studying practices such as drainage water management which directly impacts water table dynamics.

The results of this study highlight that coupled characterization of flow pathway and water source are important for predicting DRP concentrations in tile-drainage. Few studies have assessed the impact of flow pathway and source connectivity dynamics on tile P concentrations during storm events (Jiang et al., 2021). Previous studies have either used total Q, preferential flow or new/old water estimates to predict P concentrations and loading in tiles. For instance, Puer et al. 2020 found that preferential flow (estimated by conductivity based unmixing) was weakly correlated with P concentration, although the relationship between P and preferential flow was positive suggesting that preferential flow was a significant driver of P transport to tiles (Puer et al. 2020, Grant et al. 2019). Given the relatively low cost of specific conductance, flow and temperature sensors, widespread application of pathway-connectivity frameworks across environmental and management gradients has significant potential for advancing our understanding of contaminant transport in tile-drainage.

### **3.4 Conclusions**

A new method was presented that combines Specific Conductance-End-Member Mixing Analysis (SC-EMMA) and hydrograph recession approaches to describe both hydrologic pathways and source connectivity by separation of subsurface hydrograph into  $Q_{quick-new}$ ,  $Q_{quick-old}$ ,  $Q_{slow-new}$ ,  $Q_{slow-old}$ . Results highlight event-to-event and seasonal variability in dominant source-pathway dynamics. New-water and quickflow hydrographs often differed in terms of peak timing and magnitude between events. Our

results support that new-water through macropore flow can occur under both dry and saturated conditions. Likewise, matrix-macropore exchange occurs under a range of antecedent conditions. Contributions of new-water in the slowflow reservoir highlighted that groundwater recharge plays a significant role in tile-drainage fluxes.

Using the pathway-connectivity flow components as descriptors of DRP delivery in a multiple linear regression (MLR) model improved prediction of DRP concentrations in tiles as compared to tile flow or hydrograph recession results, although it provided comparable results to new-water and should be evaluated elsewhere at sites where matrix-macropore exchange constitute a larger percentage of the tile water budget. We found that new-water that routes through quickflow and slowflow reservoirs play a significant role in delivery of DRP in tiles as compared to old-water. Results show that DRP concentrations associated with matrix-macropore exchange revealed initiation of this water source from the near-surface matrix. This study highlights a data-driven approach using inexpensive sensors to assess flow pathway and connectivity dynamics and can be used to help inform numerical model evaluations and assess environmental gradients across sites in future work.

### 3.5 Figures and Tables

Table 3.1 Summary of event timings, precipitations, total tile discharges, and flow partitioning results.

Event #	Event start time	Event ending time	Event Precip (mm)	$Q_{Tile}$ (mm)	$Q_{quick}$ (mm)	$Q_{slow}$ (mm)	$Q_{new}$ (mm)	$Q_{old}$ (mm)	$Q_{quick-old}$ (mm)	$Q_{quick-new}$ (mm)	$Q_{slow-old}$ (mm)	$Q_{slow-new}$ (mm)
SE1	11/1/18 1:00	11/9/18 10:00	49.91	33.2 (870)*	21.5 (870)	11.7 (4020)	13.1 (1380)	20.1 (690)	8.9 (690)	12.6 (1380)	11.2 (3750)	0.5 (4020)
SE2	11/9/18 13:30	11/12/18 3:30	8.43	4 (300)	0.5 (300)	3.5 (1230)	0.1 (990)	3.9 (300)	0.4 (300)	0.1 (300)	3.5 (1140)	0 (1200)
SE3	11/26/18 1:00	11/30/18 4:00	23.86	21.8 (780)	13.5 (780)	8.2 (2850)	12.3 (840)	9.5 (510)	2.2 (510)	11.4 (840)	7.4 (2190)	0.9 (2850)
SE4	12/1/18 11:00	12/5/18 22:30	14.21	16.9 (930)	7.9 (900)	9 (2880)	7.7 (960)	9.2 (900)	1.2 (900)	6.7 (960)	8 (2310)	1 (2880)
SE5	12/20/18 12:30	12/27/18 4:00	22.4	16.4 (990)	7.8 (960)	8.5 (2610)	6.2 (1080)	10.2 (930)	2.7 (720)	5.2 (1080)	7.5 (2100)	1 (2610)
SE6	12/27/18 13:00	12/31/18 7:00	6.44	5.5 (1440)	0.9 (1410)	4.6 (2640)	0.4 (1560)	5.2 (1410)	0.7 (1410)	0.3 (1560)	4.5 (2550)	0.1 (2580)
SE7	12/31/18 7:30	1/5/19 23:30	24.56	21.9 (540)	12.7 (540)	9.2 (2850)	12.1 (660)	9.8 (450)	1.8 (450)	10.9 (660)	8 (2010)	1.2 (2820)
SE8	1/22/19 22:30	1/31/19 7:00	39.55	34.8 (570)	26.8 (2580)	8 (6000)	24.2 (2730)	10.7 (2310)	3.8 (300)	23.1 (720)	6.9 (3060)	1.1 (3960)
SE9	2/12/19 10:30	2/14/19 12:00	14.18	5.7 (1080)	1.8 (1080)	3.9 (1860)	2.3 (1140)	3.4 (990)	0.3 (990)	1.5 (1140)	3.2 (1230)	0.7 (1860)
SE10	2/14/19 23:30	2/19/19 17:00	1.23	9.7 (990)	3.9 (990)	5.8 (2160)	4.4 (990)	5.3 (210)	0.2 (180)	3.6 (990)	5.1 (1140)	0.7 (2160)
SE11	2/20/19 14:30	2/21/19 10:04	8.44	4.4 (570)	2.7 (540)	1.7 (990)	3.6 (570)	0.8 (300)	0.2 (300)	2.5 (540)	0.6 (420)	1.1 (990)
SE12	2/23/19 16:30	2/26/19 3:30	6	12.6 (1050)	8.3 (1400)	4.4 (2490)	7.2 (1110)	5.4 (750)	1.5 (750)	6.8 (1110)	4 (1980)	0.4 (2490)
SE13	3/9/19 16:30	3/13/19 8:00	21.38	12.4 (660)	5 (660)	7.4 (1530)	8 (690)	4.4 (330)	0.3 (330)	4.8 (660)	4.1 (750)	3.2 (1530)
SE14	3/14/19 15:30	3/20/19 9:00	11.43	25 (1890)	8.2 (1890)	16.8 (3660)	9.7 (1980)	15.3 (1830)	1.2 (1830)	7.1 (1940)	14.2 (2730)	2.6 (3630)
SE15	3/20/19 18:00	3/26/19 17:30	17.4	11 (600)	2.7 (600)	8.3 (2880)	1.8 (870)	9.2 (480)	1.4 (480)	1.3 (870)	7.8 (2250)	0.5 (2880)
SE16	3/28/19 5:30	4/4/19 3:30	37.18	27.2 (2370)	13.4 (4080)	13.8 (6630)	13.8 (4200)	13.5 (3450)	2.2 (1740)	11.2 (2490)	11.2 (3360)	2.6 (4320)
SE17	4/18/19 15:30	4/20/19 4:04	33.71	16.1 (900)	6.3 (900)	9.8 (1590)	11.2 (960)	4.9 (480)	0.4 (480)	6 (900)	4.5 (780)	5.3 (1590)
SE18	4/20/19 5:00	4/25/19 7:26	13.92	23.2 (210)	8.5 (300)	14.7 (30)	13.7 (330)	9.5 (210)	0 (210)	8.5 (300)	9.5 (180)	5.2 (450)
SE19	4/27/19 18:30	4/29/19 15:30	17.02	12.7 (390)	5.2 (630)	7.6 (1620)	5.3 (690)	7.4 (540)	0.6 (300)	4.5 (450)	6.8 (870)	0.8 (1380)

Table 3.2 (Continued) Summary of event timings, precipitations, total tile discharges, and flow partitioning results.

Event #	Event start time	Event ending time	Event Precip	$Q_{Tile}$	$Q_{quick}$	$Q_{slow}$	$Q_{new}$	$Q_{old}$	$Q_{quick-old}$	$Q_{quick-new}$	$Q_{slow-old}$	$Q_{slow-new}$
SE20	4/30/19 14:00	5/1/19 13:30	6.04	4.4 (240)	0.6 (270)	3.8 (810)	0.7 (360)	3.8 (240)	0.2 (270)	0.4 (360)	3.5 (570)	0.3 (780)
SE21	5/13/19 6:30	5/16/19 22:00	3.7	4.4 (210)	0.5 (210)	4 (1170)	0.5 (330)	3.9 (180)	0.2 (180)	0.3 (330)	3.7 (810)	0.3 (1140)
SE22	5/28/19 4:00	5/31/19 12:28	8.27	10.1 (150)	2.5 (150)	7.7 (60)	5.3 (210)	4.9 (150)	0 (150)	2.5 (210)	4.9 (150)	2.8 (60)
SE23	6/13/19 19:00	6/14/19 23:30	2.18	3.9 (120)	1.4 (240)	2.5 (600)	2.1 (270)	1.8 (210)	0.3 (60)	1 (120)	1.4 (90)	1.1 (450)
SE24	6/15/19 10:30	6/19/19 13:30	5.45	11.6 (1140)	5.6 (1140)	6 (2220)	6.1 (1170)	5.5 (1140)	0.6 (540)	5 (1170)	4.9 (1140)	1.1 (2220)
SE25	7/6/19 19:30	7/10/19 9:30	16.77	0.6 (90)	0.1 (90)	0.6 (210)	0 (150)	0.6 (90)	0 (90)	0 (150)	0.6 (270)	0 (210)
SE26	9/21/19 15:00	9/22/19 19:00	22.91	1 (120)	0.5 (120)	0.5 (600)	0.3 (60)	0.7 (90)	0.25 (90)	0.25 (120)	0.47 (540)	0.03 (600)
SE27	9/30/19 2:00	9/30/19 23:30	32.76	6.2 (300)	3.1 (240)	3.1 (870)	3.5 (570)	2.7 (270)	1.2 (270)	1.9 (480)	1.6 (480)	1.5 (870)
<b>Sum</b>			469.33	356.83	171.87	184.96	175.32	181.5	32.54	139.13	148.98	35.99
<b>Mean</b>			17.38	13.21	6.37	6.86	6.50	6.73	1.21	5.16	5.52	1.33
<b>SD</b>			±12.5	±9.5	±6.5	±4.1	±5.8	±4.67	±1.8	±5.27	±3.47	±1.41

\*The numbers in parentheses show time-to-peaks of flow components in minutes

Table 3.3 Results of the multiple linear regression analysis for daily flow-weighted mean DRP concentrations. Estimated coefficient column shows estimated dissolved reactive P concentration (mg/L) associated with each flow fraction with standard error in parenthesis.

	<i>Estimated Coefficients</i>	<i>P-Value of flow fractions</i>	<i>P-Value of Overall Model</i>
<b>Regression using new pathway-connectivity framework</b>			
<i>DRP<sub>quick-old</sub></i>	0.076 (0.02)**	0.00033	$<2 \times 10^{-16}$
<i>DRP<sub>quick-new</sub></i>	0.091 (0.008)***	$<2 \times 10^{-16}$	
<i>DRP<sub>slow-old</sub></i>	0.028 (0.003)***	$2.65 \times 10^{-12}$	
<i>DRP<sub>slow-new</sub></i>	0.153 (0.019)***	$8.8 \times 10^{-13}$	
<b>Regression using only Hydrograph Recession Analysis</b>			
<i>DRP<sub>quick</sub></i>	0.088 (0.006)***	$<2 \times 10^{-16}$	$<2 \times 10^{-16}$
<i>DRP<sub>slow</sub></i>	0.043 (0.003)***	$<2 \times 10^{-16}$	
<b>Regression using only SC-EMMA Analysis</b>			
<i>DRP<sub>new</sub></i>	0.108 (0.007)***	$<2 \times 10^{-16}$	$<2 \times 10^{-16}$
<i>DRP<sub>old</sub></i>	0.034 (0.003)***	$<2 \times 10^{-16}$	

P=0.05, \*P=0.01, \*\*P=0.001, \*\*\*P=0.0001

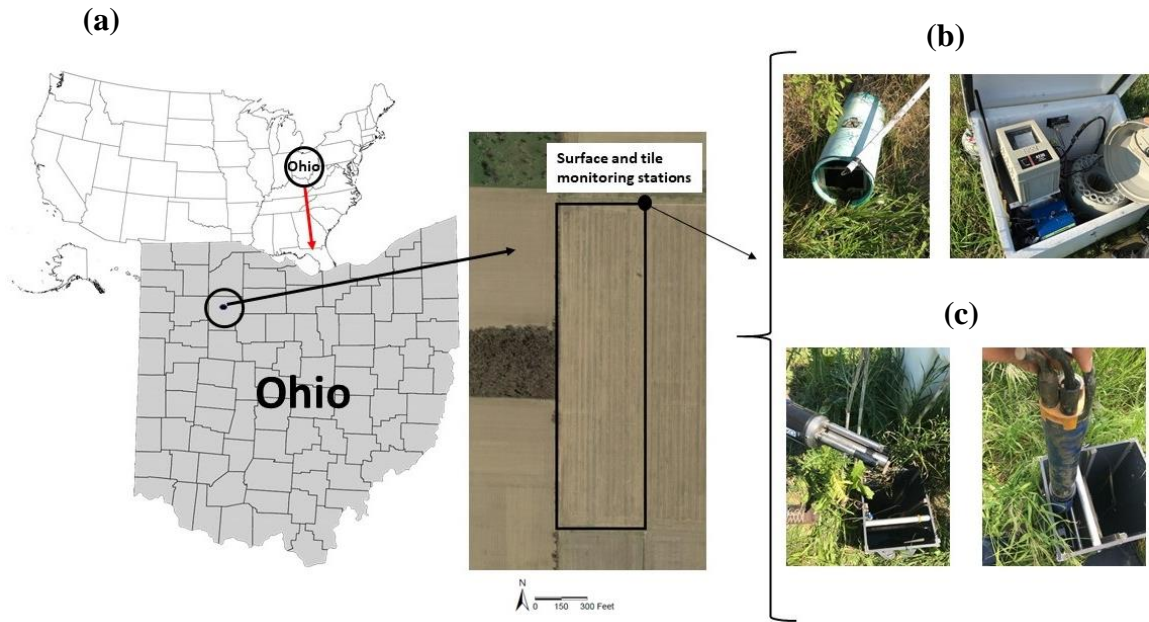


Figure 3.1 Location of the tile-drained field located in Wood county, Ohio, USA. a) Aerial field delineation and monitoring location. b) Outlet of the tile network and its installed weir, and ISCO pump sampler. c) High-frequency sensing YSI EXO2 Sonde and its deployment in a drainage water management structure.

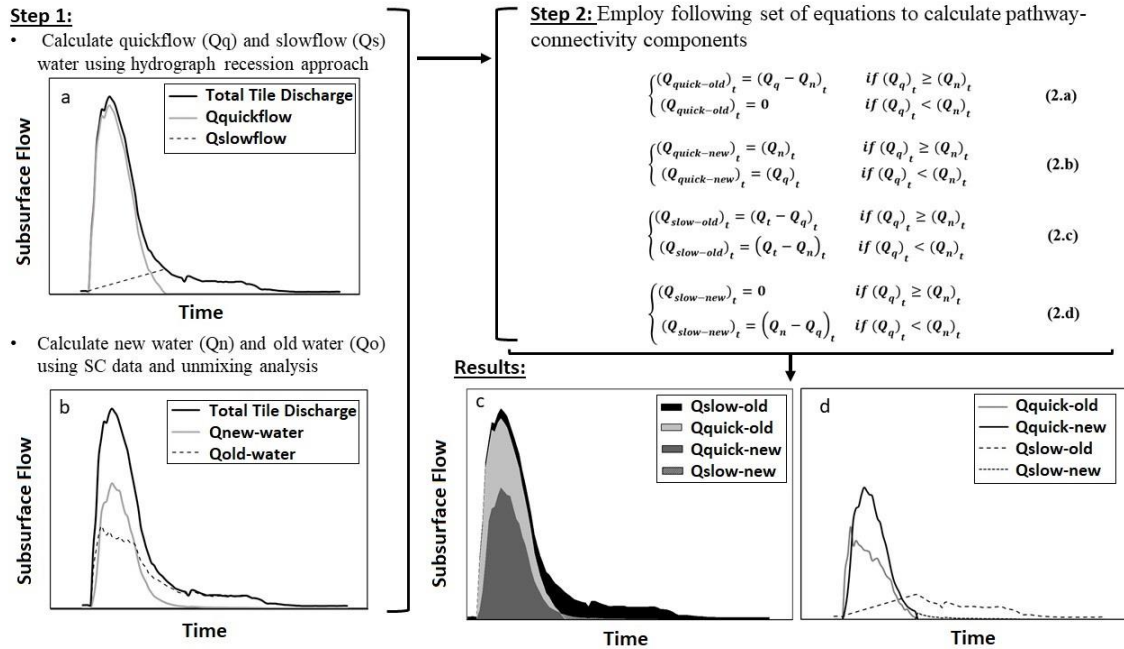


Figure 3.2 Separation of subsurface hydrograph to combined pathway-connectivity components including  $Q_{quick-old}$ ,  $Q_{quick-new}$ ,  $Q_{slow-old}$ , and  $Q_{slow-new}$ . Subsurface hydrograph is separated into quickflow ( $Q_q$ ) and slowflow ( $Q_s$ ) reservoirs using hydrograph recession analysis in Step 1 (a). Subsurface hydrograph is separated into new-water ( $Q_n$ ) and old-water ( $Q_o$ ) components using SC-EMMA approach (b). In Step 2, a set of equations are employed and calculated  $Q_{quick}$ ,  $Q_{slow}$ ,  $Q_{old}$  and  $Q_{new}$  (From Step 1) are used to separate hydrograph into pathway-connectivity components as shown in (c) and (d).



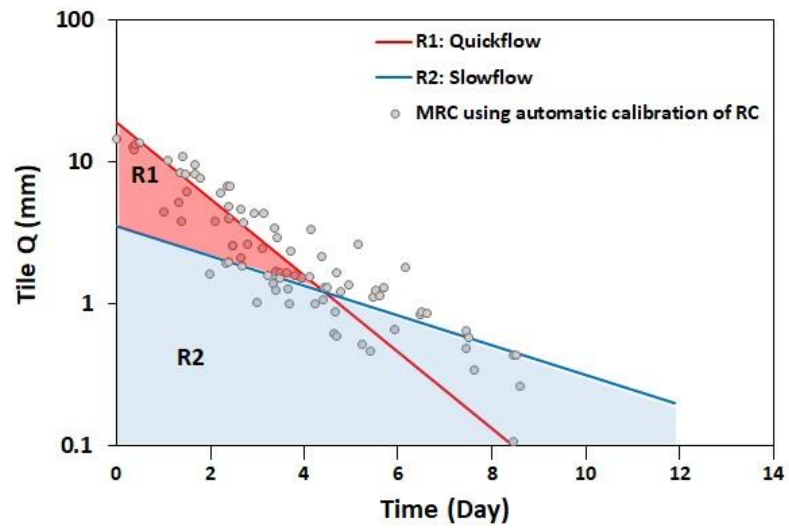


Figure 3.3 Master recession curve constructed from 18 subsurface flow recessions for water year 2019.

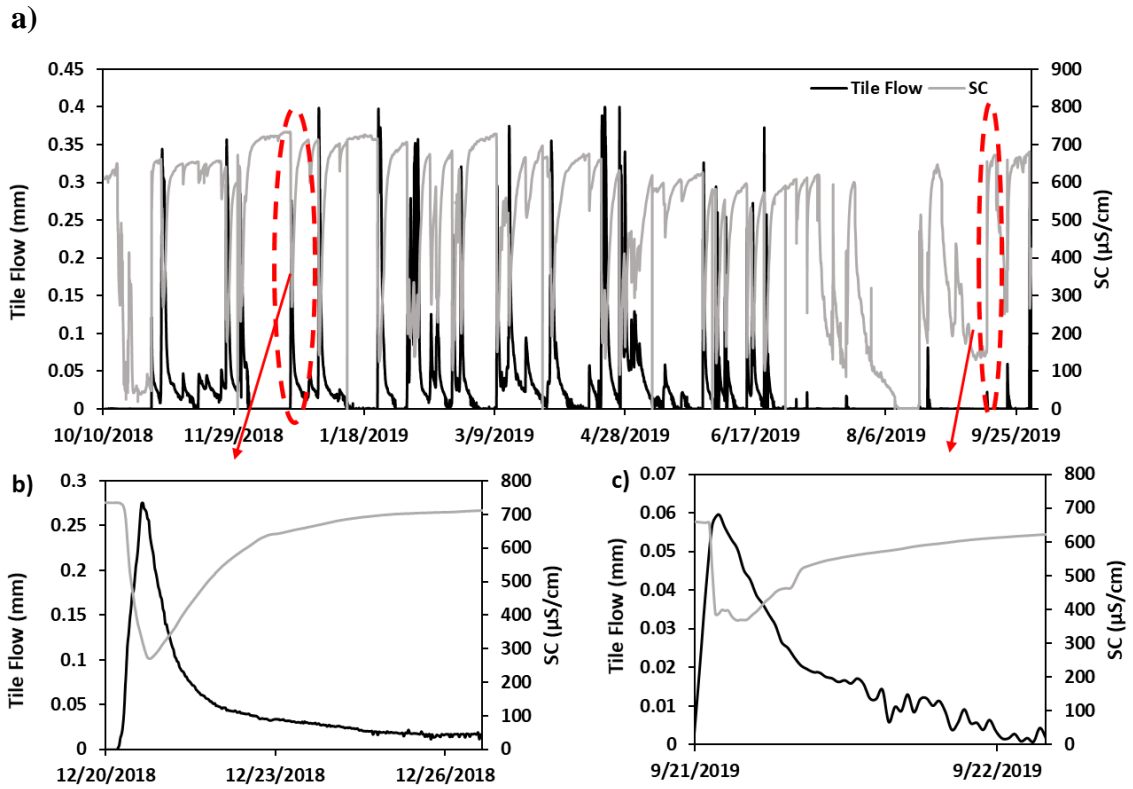


Figure 3.4 (a) Timeseries of data including 30-minute tile flow (mm) and 15-minute specific conductance ( $\mu\text{S}/\text{cm}$ ). Two events are highlighted at different times of year including (b) fall and (c) summer.

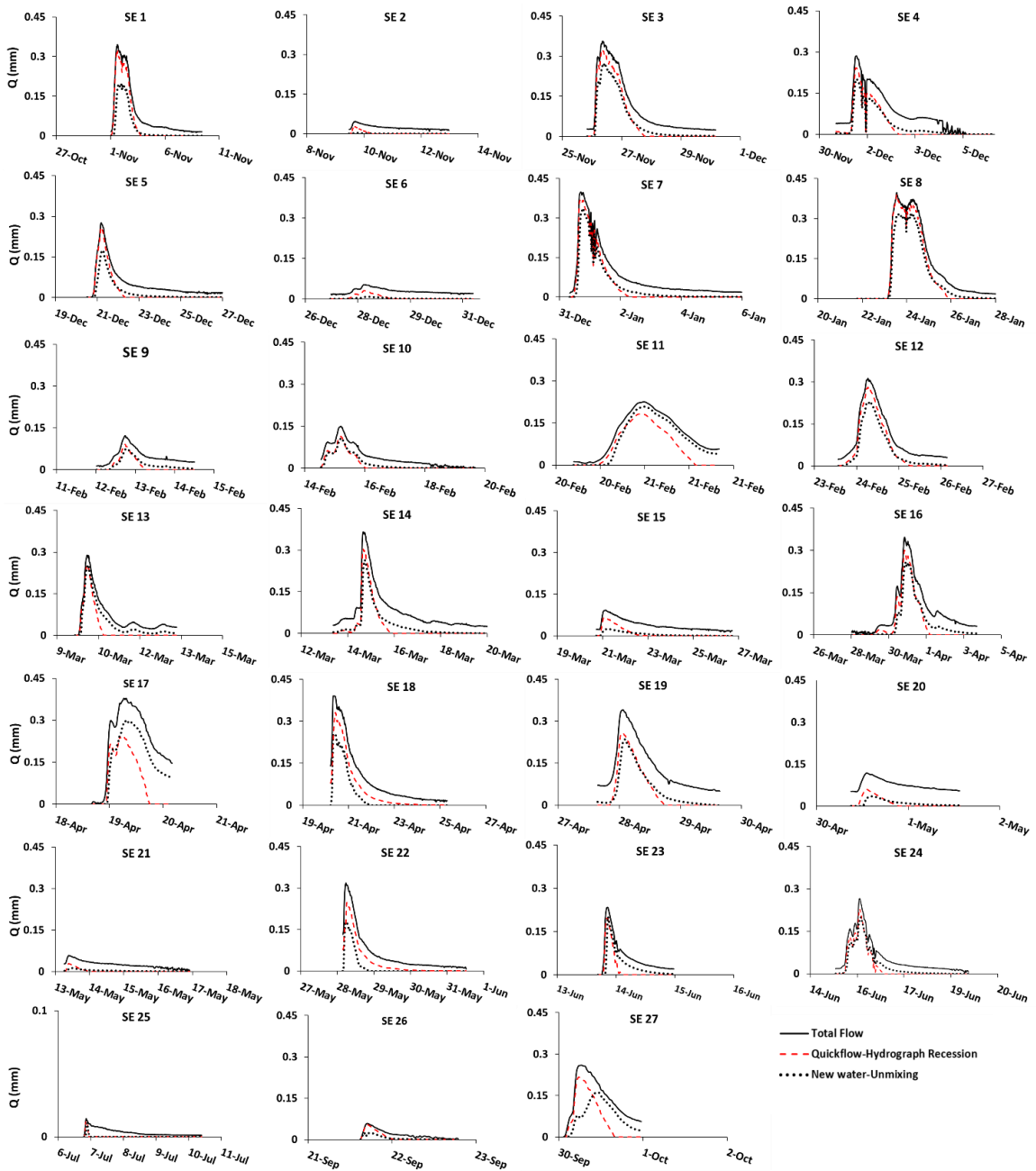


Figure 3.5 Tile discharge, quickflow calculated using hydrograph recession analysis and new water calculated using specific conductance end-member mixing analysis for each storm event (SE) at the study site during water year 2019.

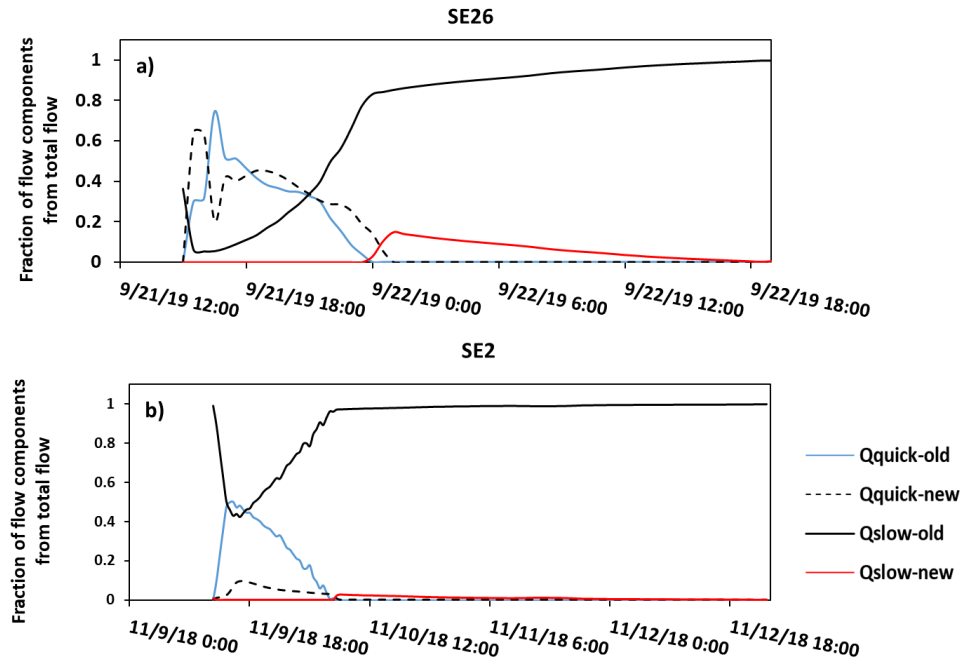


Figure 3.6 Results of pathway connectivity framework for a) SE26 and b) SE2. These two events were selected from summer and fall because they reveal seasonal differences in subsurface flow pathway and source connectivity.

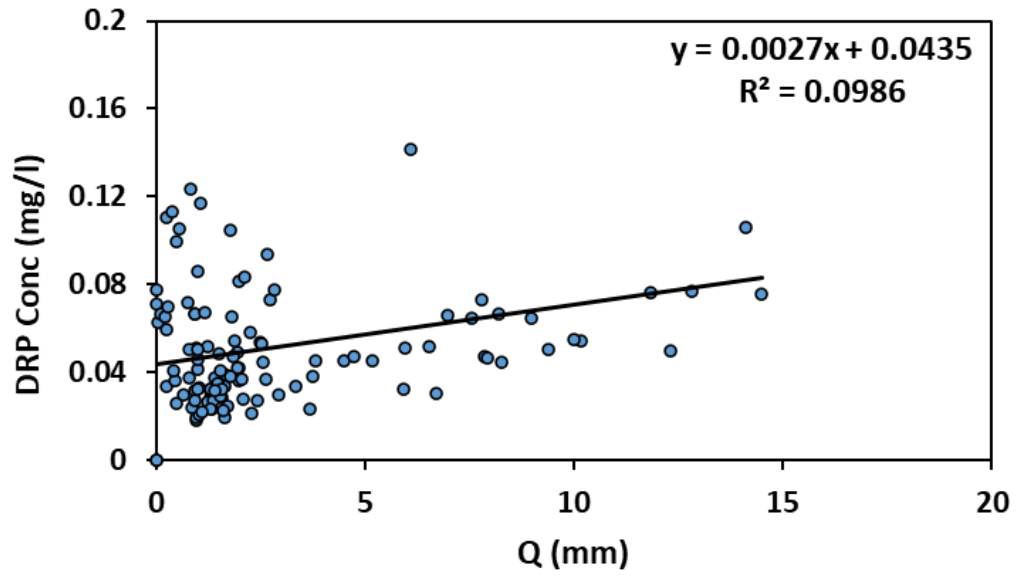


Figure 3.7 Flow-weighted daily mean DRP concentrations for the study site in water year 2019 plotted against tile discharge.

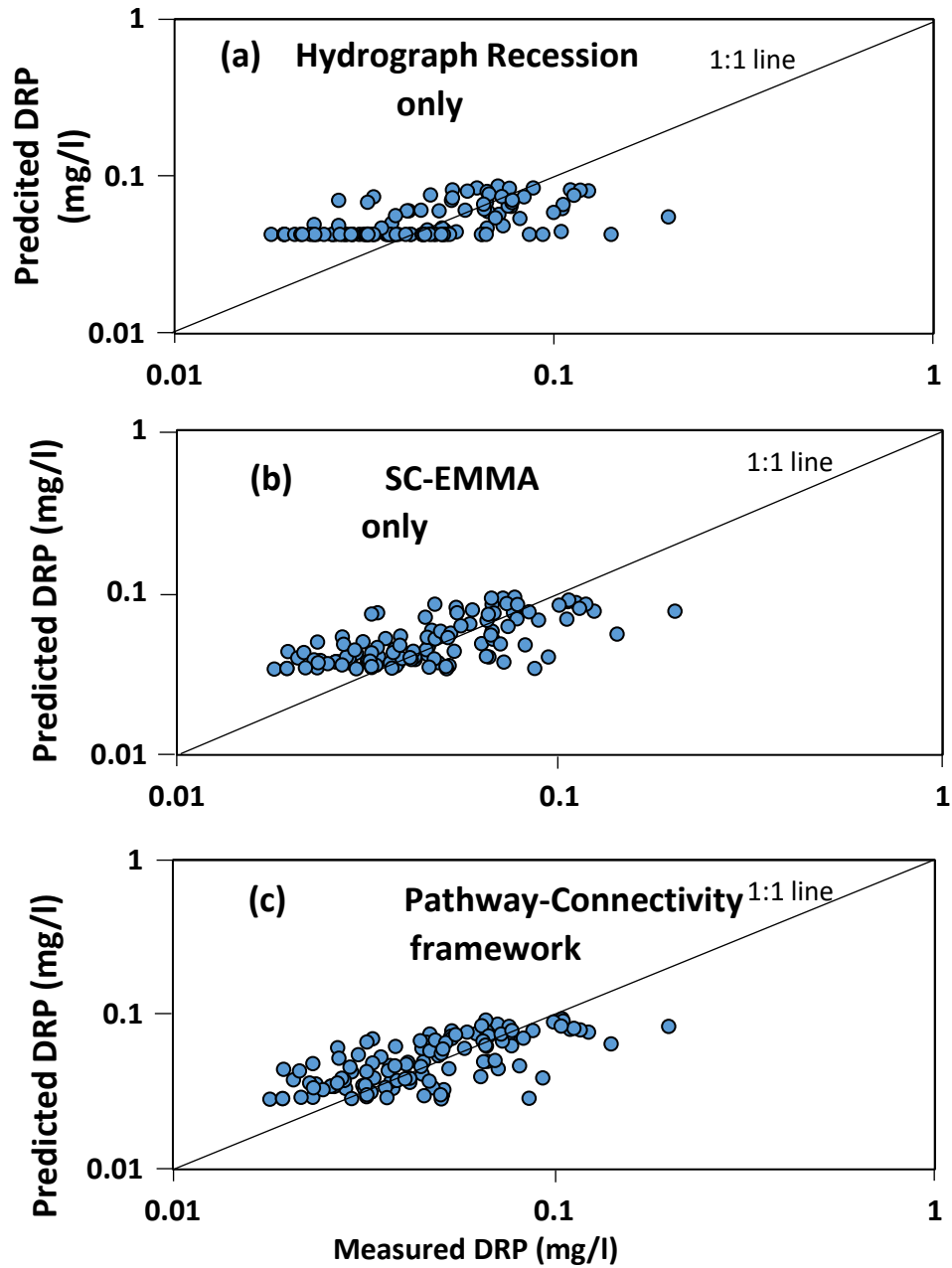


Figure 3.8 Multiple Linear regression analysis results for daily flow-weighted mean concentrations of DRP as compared to a) hydrograph recession results, b) SC-EMMA results and c) the new pathway-connectivity framework results.

## CHAPTER 4. THE ROLE OF FLOW PATHWAY, SOURCE WATER CONNECTIVITY, AND ENVIRONMENTAL GRADIENTS ON TILE-DRAIN SEDIMENT TRANSPORT DYNAMICS

### 4.1 Introduction

Quantifying sediment and particulate phosphorus (PP) transport dynamics is of increasing interest in tile-drained landscapes given recent findings that PP fate plays an important role in eutrophic conditions of receiving waterbodies (e.g., Casillas-Ituarte et al., 2020). The impact of hydrologic and sediment transport processes on PP loadings at the field-scale in tile-drained landscapes remains poorly understood (Jiang et al., 2021). Studies have traditionally attributed fine sediments in tile-drains to erosion from surface soils during storm events that are transported to tile drains *via* preferential flowpaths, thus partially bypassing the filtration capacity of the soil matrix (Michaud and Laverdiere, 2004; Turunen et al., 2017; Collins et al., 2019). Nevertheless, laboratory studies of preferential flow through undisturbed soil cores have indicated that subsurface flow, ionic strength of water, and matrix-macropore interaction may also result in subsurface sediment erosion and transport, suggesting potential impacts on tile sediment loadings (Hendrick et al., 1993; Jacobsen et al., 1997; Schelde et al., 2002; Rousseau et al., 2004; Wilson et al., 2018). There is a pressing research need for sediment and PP databases from tile drained agroecosystems to improve understanding of flow pathway and water source impacts on PP loadings from tiles (Christianson et al., 2016; Jiang et al., 2021).

Subsurface flow pathways have been identified as significant drivers of subsurface sediment erosion and transport. It is postulated that preferential flow paths play a significant role because macropores provide rapid connectivity from surface to tiles, in contrast with micropore pathways in the soil matrix that are usually considered

too small for conveyance of sediment particles (Turunen et al., 2017; Akay and Fox, 2007; Frey et al. 2016). The connectivity of surface to subsurface via macropores provides a rapid pathway for detached surface particles to bypass soil filtration capacity and move from surface to tiles through turbulent conduits (Stone and Wilson, 2006; Poirier et al., 2012; Grangeon et al., 2021). Sediments eroded from the subsurface are derived from particle detachment from macropore walls or from seeping from matrix to macropores (Wastra et al., 2013; Wilson et al., 2018). Highly turbulent flow in macropores can result in a positive feedback loop in which erosion of macropore walls enlarges macropore conduits, creating higher volumes of flow and shear stresses and thus a subsequent increase in erosion (Kaplan et al., 1993; Wilson et al., 2016 and 2020; Bernatek-Jakiel et al., 2020). In order to better understand subsurface sediment erosion and transport processes within tile drained fields it is critical to study subsurface flow pathways and dynamics in these landscapes.

Source water properties have also been identified to play a key role in subsurface sediment erosion and transport. Macropore walls are envisioned to have chemical exchange/interactions with water and can release or retain particles depending on source water chemical properties (Majdalani et al., 2007). Water sources with lower ionic strength are more erosive as compared to water with high ionic content because the lower ionic strength results in higher osmotic potential and therefore higher total potential of soil water which results in weaker links between soil particles, thus increasing particle detachment by mechanical pressure (Miyazaki, 1993; Tessier et al., 1999; Rousseau et al., 2004). It is also now well established that preferential flows contain both low ionic strength event water and high ionic strength soil water (Klaus et al., 2013; Williams et al.,



2016; Smith et al., 2018; Puer et al., 2020; see Chapter 3). Seepage of matrix water to preferential flow paths (i.e., matrix-macropore exchange) can result in translocation of sediment from the soil matrix to preferential flowpaths (Wilson et al., 2018) and therefore may impact sediment loads to tile. These findings highlight that assessing sediment transport drivers to tile require hydrograph separation techniques that consider not only the flow pathway (e.g., quick and slow flow paths), but also water source (e.g., rainfall event water vs. pre-event soil water).

Gradients in climatic drivers will impact subsurface flow pathway and water source connectivity dynamics as well as erodibility of tile sediment sources. Increases in precipitation intensity and magnitude have generally resulted in increases in surface erosion (Warsta et al., 2014; Perks et al., 2015; Sherriff et al. 2016; Turunen et al., 2017; Beczek et al., 2019) and increases in preferential flow of low ionic strength water (See Chapter 3). These findings suggest both surface and subsurface sources are expected to have increased loadings with increases in precipitation. Regarding antecedent conditions, studies have shown that the subsurface erosion sources experience higher initial peak concentrations with increasing time between events due to regeneration of easily detachable particles along macropore walls (Schelde et al., 2002; Majdalani et al., 2007; Van den Bogaert et al., 2016). Similarly, temporal variability in erodibility of surface sources that are delivered to tile drains have also been postulated (Turunen et al., 2017). For instance, a large amount of preferential flow can occur in winter under unsaturated and partially saturated conditions (Stadler et al., 2000, Pittman et al., 2020; Mohammed et al., 2018 and 2020), but infiltrated water may freeze due to exchange of heat and water with soil matrix, and the frozen water can block the macropore pathway and reduce

infiltration of event water (Watanabe and Kugisaki, 2017; Demand et al., 2019; Mohammed et al., 2020). Previous studies have reported higher preferential flow fractions under dryer conditions of summer and spring due to shrink-swell cracks that progressively could develop from the end of winter to become fully developed in summer and form larger subsurface conduits (Kladivko et al., 1991; Øygarden and Jenssen, 1997; Grangeon et al., 2021).

Given the complexity of flow pathway, source water connectivity dynamics, and surface/subsurface erosion, robust datasets are needed to evaluate tile sediment loading dynamics. Continuous measurements of tile flowrates and electrical conductance have enabled separation of both flow pathway and water source connectivity dynamics in tile-drains using data-driven approaches. Hydrograph recession analysis has been successfully applied in subsurface drained landscapes for partitioning quick and slow flow pathways of water during storm events (Schilling and Helmers 2008; Mellander et al., 2013; Ford et al., 2019; Husic et al., 2019; Nazari et al., 2020). Further, continuous conductance measurements in tile-drain waters have been increasingly reported in recent years and have been coupled with end-member unmixing models for partitioning event and pre-event water sources during stormflows (e.g., Smith et al., 2018; Plier et al., 2020). In the previous chapter of this dissertation, these methodologies were coupled into a flow pathway-connectivity framework that discretizes hydrographs into rapid transport of event water, rapid transport of pre-event water, slow transport of event water, and slow transport of pre-event water (see Chapter 3). Given the importance of both water source and flow pathways on erosion and transport processes, coupling these

hydrograph partitions with sediment measurements from tiles could provide new insights to governing processes controlling tile sediment loadings.

Continuous *in situ* sensor measurements of turbidity have rarely been applied in tile-drainage despite their widespread use as a reliable surrogate for measuring sediment concentration dynamics at high-frequencies in many watershed-scale applications. Turbidity sensors have become robust and economically feasible for use as a surrogate of suspended sediment concentrations in fluvial environments (Sherriff et al., 2016; Snyder et al., 2018; Pickering and Ford, 2021). Continuous monitoring of turbidity has been used to assess sediment hysteresis dynamics, which can provide insights into sediment peaks and source exhaustion, sediment storage availability and mobilization pathways, and lag time between discharge and peak sediment concentration (Williams 1989; Duvert et al., 2010; Lloyd et al. 2016; Sherriff et al., 2016, Grangeon et al., 2021). Performing hysteresis analysis on separated hydrograph fractions have not been reported to our knowledge but may improve insights into tile sediment loading dynamics and prevailing flow pathways and water sources impacting sediment delivery.

The overarching objective of this study was to quantify sediment loading dynamics for a subsurface drained agroecosystem and assess the governing flow pathway and water sources impacting tile sediment loads. Specific aims of the study were to: 1) quantify sediment concentration and loading dynamics in a systematically-drained field characteristic of fine-textured midwestern agroecosystems, 2) assess the impact of flow pathway and water source connectivity on sediment dynamics, and 3) perform a quantitative sediment hysteresis analysis on tile flowrate and separated hydrograph fractions to identify impacts of prevailing environmental factors.

## 4.2 Study Site and Materials

To meet the objectives of this study, we selected a site from the USDA-ARS Soil Drainage Research Unit edge-of-field monitoring network (Williams et al. 2016). The study site (0.16 km<sup>2</sup>) was a systematically drained field with a silty-clay-loam soil texture in Wood County, Ohio U.S.A. (Figure 4.1.a). Tile drains were implemented at depth of 0.9 m (3 ft) from the soil surface. Lateral spacing was 15.2 m (50 ft), and the laterals were routed to a 0.3 m (12 in) tile main with an outlet equipped with a drainage water management structure before flowing into a downstream ditch. The study site was selected because 1) study site characteristics were typical of prevailing agricultural management practices, soil texture, soil nutrient conditions, and runoff characteristics in the region (Williams et al., 2016); 2) The data collection efforts complement an extensive historic database and study record conducted by the USDA-ARS at the site including more than seven years of continuous precipitation, flowrate, and nutrient data with monitoring of both surface and subsurface pathways; 3) annual TP—DRP loading (a surrogate for PP loading) averaged 0.58 kg/ha and preferential flow constituted 48% of tile flow, both of which are typical of tile-drained fields in the region (King et al. 2015, Williams et al. 2016, see Chapters 2-3); 4) The producer manages the site under conservation tillage practices which are now widely adopted across row-cropping systems in the tile-drained Midwest (Djordjic et al., 2002; Cullum, 2009; Williams et al., 2016); and 5) the presence of a drainage water management flow control structure provided a secure structure to house sensing equipment.

Regarding management practices at the site, the typical crop rotation was corn-soybean-wheat. At the onset of our high-resolution monitoring (October 1, 2018), the

field contained soybean that was harvested on 10/17/2018, the field remained fallow until the following planting season and then wheat was planted on 10/11/2019 and remained for the duration of our monitoring efforts. The field was traditionally managed using conservation tillage practices. During our monitoring, no tillage operations were reported by the producer from 10/01/2018 to 9/2/2019 but disc tillage was performed on 09/02/2019, 09/21/2019 and 10/11/2019.

The surface and tile monitoring stations of the sites are depicted in Figure 4.1.a. A berm was installed at the edge of field to direct surface runoff to an H-flume. The tile-drain outlet at the edge-of-field was equipped with a drainage water management (DWM) structure. Historically, the DWM plates were opened prior to planting and harvesting and closed after planting and harvesting. However, the boards from the control structure were removed during our monitoring period from September 2018 to the end of December 2019 as part of a before-after-control-impact study conducted by the USDA-ARS SDRU.

Precipitation and flow sample collection was conducted by the USDA-ARS using well-accepted methods (Williams et al. 2016). We used over four years of data from 9/30/2015 to 12/30/2019 for our analysis. To measure rainfall duration, intensity and depth, tipping bucket rain gages were used. Surface monitoring stations were equipped with a bubbler meter which measures water depth and was used for calculating surface volumetric discharge using a calibrated stage-discharge curve specific to the flume. For calculation of subsurface discharge, tile mains were equipped with a weir insert (Thel-Mar, Brevard), an ISCO Bubbler Flow Meter (Teledyne Isco, Lincoln, Nebraska), and ISCO 2150 Area Velocity Sensor which measures velocity under submerged conditions.

Flow measurements were reported at 30-minute intervals for tiles and 10-minute intervals for surface runoff.

Both surface and subsurface sites included a Teledyne ISCO 6712 portable sampler and accessories to collect nutrient samples (Figure 4.1.b). Time compositing strategies were used for tile-drain samples. Generally, a 100-ml aliquot was collected every six hours for 48 hours and composited into a single sample bottle reflecting a two-day composite sample. Additionally, during events, samples were collected every 15 minutes and composited hourly. For surface water sample collection, a flow proportional sampling strategy was used, where samples were collected after a preset volume of water passes through the flume (Williams et al. 2015). All water samples were analyzed for dissolved reactive P (DRP) and Total P (TP), concentrations for the entire monitoring period. DRP concentrations were analyzed by vacuum filtration (0.45 $\mu$ m) and then analyzing for P using the ascorbic acid reduction method (Murphy and Riley, 1962). Concentrations of TP were determined on unfiltered samples following alkaline persulfate oxidation and subsequent analysis of DRP (Patton and Kryskalla, 2003). ISCO samples collected from 03/01/2019 to 12/30/2019 timeframe were subsampled and transported to the University of Kentucky for measurements of total suspended solid (TSS). Before TSS analysis, we used a newly calibrated YSI EXO3 Sonde to measure both turbidity and specific conductance of the sample in the lab since the ISCO samples were composite samples. The sample was then analyzed for TSS concentration by vacuum filtration through glass microfiber filters and dried at 104°C prior to weighing, consistent with EPA method 160.2 (U.S. EPA, 1983).

The tile-drain was equipped with a YSI EXO3 water quality sonde to measure *in situ* turbidity and specific conductance at 15-minute intervals from October 1, 2018 to December 31<sup>st</sup>, 2019 (Xylem Inc, Yellow Springs OH, USA). The sonde was located within a drainage water management structure (see Figure 4.1.c). The turbidity sensor is a non-ratiometric nephelometric turbidimeter, which uses a near-infrared light source and detects scattering at 90 degree of the incident beam (EXO User Manual). The conductivity/temperature sensor uses four internal, pure-nickel electrodes to measure solution conductance. Two of the electrodes are current driven, and two are used to measure the voltage drop (EXO User Manual). Maintenance was performed on the instrument approximately once per month based on recommendations of the manufacturer, which is consistent with other studies (Snyder et al., 2018). The turbidity sensor was calibrated using a three-point approach, in which turbidity values of 0 (Deionized water), 124 and 1010 FNU were used to calibrate the sensor. The sensor was rinsed between the second and third calibration points. Calibrations were performed using KorEXO software. For conductivity, a one-point calibration was used with a calibration standard with conductivity value of 1000  $\mu\text{s}/\text{cm}$ . Measurements were taken at a fifteen minute interval continuously during the monitoring period.

### **4.3 Analytical Methods**

#### **4.3.1 Sediment and Particulate Phosphorus Concentration and Loading Estimates**

To estimate continuous sediment concentrations from turbidity measurements, we developed a regression model for total suspended solids (TSS) as a function of turbidity. In total, 188 samples were used to develop the regression. A least squares linear

regression was performed on log transformed TSS and turbidity values, consistent with previously published approaches (Rasmussen et al., 2009). The calibrated curve was then used to estimate continuous sediment concentrations for the high-frequency continuous dataset.

We calculated continuous estimates of sediment flux using measured flowrate and TSS concentrations from the TSS-Turbidity calibration curve and integrated the sediment fluxes at event and daily timesteps to estimate event sediment loadings and daily flow-weighted mean concentrations. Suspended sediment flux ( $Q_{ss}$  in kg/s), was estimated as the product of sediment concentration and flowrate for a specified timeframe.

$$Q_{ss_t} = C_{TSS_t} \times Q_t$$

(1)

where,  $C_{TSS}$  ( $\text{kg m}^{-3}$ ) is the TSS concentration at time  $t$ ,  $Q_t$  ( $\text{m}^3 \text{s}^{-1}$ ) is tile discharge at time  $t$ . We estimated sediment yields for days, storm events, seasons, and annual timescales using the following numerical approximation of the integral of suspended sediment flux over a specified timeframe.

$$SY = \frac{\sum_{t=1}^n Q_{ss_t} \times \Delta t}{DA} \quad (2)$$

where,  $SY$  (kg/ha) is the suspended sediment yield for a given event ranging from 1 to 'n' number of timesteps,  $\Delta t$  (s) is length of the timestep, and  $DA$  (ha) is the drainage area of the subsurface drainage network. In addition to sediment loading, event TSS concentration (mg/l) for each event was calculated by dividing sediment load by event tile discharge volume. In total, 33 events were analyzed throughout our monitoring period from October 2018 to December 2019.



Surface and subsurface daily TP and DRP loadings were calculated using the approach of Williams et al. (2015). Briefly, we determined the midpoint of all sample time steps for each bottle. We then used linear interpolation between measured values at the midpoint to estimate the concentration for each interval when flow was measured. Loading was estimated as the product of interpolated concentrations and flow rate, analogous to the method for sediment loading. We calculated daily, event, seasonal and total subsurface TP minus DRP (TP—DRP) loading for the period that we performed high-resolution data collection as a surrogate for PP loading.

#### 4.3.2 Impact of flow pathway and water source connectivity on sediment loading

Hydrologic flow pathway and source connectivity dynamics for tile drainage was conducted using an approach that couples hydrograph recession analysis and specific conductance end-member unmixing (see Chapter 3). Hydrograph recession analysis was used to partition flow pathways into quickflow and slowflow drainage reservoirs. Quickflow ( $Q_{quick}$ ) represents the rapid flow pathway through subsurface soils via macropores, and slowflow ( $Q_{slow}$ ) represents water that percolates through the soil matrix before entering the tile drainage network. Quickflow and slowflow reservoirs can receive both ‘new-water’ ( $Q_{new}$ ) from precipitation and ‘old-water’ ( $Q_{old}$ ) that resides in the soil matrix prior to the event. We used SC data and followed previous published approaches of SC-member mixing analysis (SC-EMMA) to quantify new-water and old-water fractions (Smith et al., 2018; see Chapter 3). Based on these results, we applied the methodology described in chapter 3 to calculate pathway-connectivity hydrograph separations including quickflow of old ( $Q_{quick-old}$ ) and new ( $Q_{quick-new}$ ) water, and slowflow of old ( $Q_{slow-old}$ ) and new ( $Q_{slow-new}$ ) water for each event. The  $Q_{quick-old}$  is postulated to

represent matrix-macropore exchange. We build off results presented in Chapter 3 for this study. Briefly, quickflow and slowflow were found to account for 48.4 and 51.6% of subsurface discharge during events at the site. SC-EMMA results showed that new-water and old-water comprised 46.2 and 53.8% of total subsurface discharge, respectively. Results of the pathway-connectivity framework indicated all four hydrograph components had a significant, but variable contribution to tile hydrology.  $Q_{quick-old}$ ,  $Q_{quick-new}$ ,  $Q_{slow-old}$  and  $Q_{slow-new}$  contributed to 12%, 37%, 42% and 9% of total tile discharge for all the events.

To assess the relationship between pathway-connectivity and TSS concentrations we used a multiple linear regression (MLR) model. We calculated daily flow contribution and divided them by total tile discharge to calculate daily flow fractions ( $F$ ). We developed a mass balance equation in which daily flow-weighted mean TSS concentrations of tile discharge were dependent variables ( $TSS_{tile}$ ) and flow fractions ( $F_{quick-new}$ ,  $F_{quick-old}$ ,  $F_{slow}$ ), were independent variables. Based on visual observations from all events, we combined  $Q_{slow-old}$  and  $Q_{slow-new}$  since most of the sediment loading occurred during the quickflow portion of the hydrograph. The unknown beta coefficients for the MLR reflect average TSS concentrations for each flow fraction (e.g., see Chapter 3). The MLR model was performed in RStudio software (RStudio, inc, 2011). The coefficient of determination ( $R^2$ ) and standard error of the regressions ( $S$ ) were calculated to measure how much of the variation in outcome can be explained by the variation in the independent variables and to estimate goodness-of-fit measures. The  $F$ -statistic was used to test the null hypothesis that individual coefficients were not equal to zero and the null hypothesis that the overall MLR model provided a superior fit to a mean trend. We report

p-values for the overall model and coefficient values for  $p < 0.10$ ,  $p < 0.05$ ,  $p < 0.01$ , and  $p < 0.001$ .

#### 4.3.3 Tile sediment hysteresis analysis

Sediment hysteresis analysis was performed for both total tile discharge and separated pathway-connectivity hydrographs. We used both qualitative hysteresis plots and quantitative hysteresis indices to evaluate shape and magnitude of hysteresis loops (Lloyd et al., 2015; Zuecco et al., 2016). Regarding qualitative hysteresis plots, we first normalized flow and TSS concentration values.

$$\text{Normalized } Q_t = \frac{Q_t - Q_{min}}{Q_{max} - Q_{min}} \quad (3a)$$

$$\text{Normalized } C_{TSS_t} = \frac{C_{TSS_t} - C_{TSS_{min}}}{C_{TSS_{max}} - C_{TSS_{min}}} \quad (3b)$$

where,  $Q_{min}$  and  $C_{TSS_{min}}$  are minimum discharge and concentration values during an event,  $Q_{max}$  and  $C_{TSS_{max}}$  are maximum discharge and concentration values during a storm, and  $t$  is the given timestep during an event. Normalized values were plotted with concentrations on the y-axis and flowrates on the x-axis (see Supplemental Information S1).

A quantitative hysteresis index (Lloyd et al., 2015) was used to quantify strength and direction of hysteresis loops. The hysteresis index for each of the flow components were calculated using the normalized flow and sediment concentration data. The hysteresis index ( $HI$ ) was calculated every 5% of the discharge and averaged for the event. The index was estimated as follows.

$$HI = C_{TSS_{RL}} - C_{TSS_{FL}} \quad (4)$$

where,  $C_{TSS_{RL}}$  the sediment concentration on the rising limb at a given flow percentile, and  $C_{TSS_{FL}}$  is the sediment concentration value at the equivalent point in discharge on the falling limb. Hysteresis strength is indicated by the magnitude of the HI index, with values approaching ( $\pm$ ) 1 indicating stronger hysteretic behavior (Lloyd et al., 2016). The sign of the index illustrates the direction of the loop with positive denoting clockwise and negative denoting counterclockwise.

## 4.4 Results

### 4.4.1 Sediment and Particulate P Loadings

Findings from the total suspended solids (TSS) vs. turbidity regression analysis showed the reliability of turbidity as a surrogate measure for TSS in tile drainage (Figure 4.2). Results showed a strong correlation between TSS concentration and turbidity with an  $R^2$  of 0.92 with a P-value  $<0.001$  (Figure 4.2). Regression results spanned values of TSS ranging from 5.3-1163.8 mg/L and turbidity from 2.9-875.3 FNU, reflecting the range observed during our 15-month *in situ* monitoring period (Figure 4.3). While some uncertainty in the regression model existed, particularly at low concentrations, we anticipate the impacts on overall sediment load estimation is minimal, given that most of the sediment is transported at high concentration and flow conditions.

Results of continuous sediment concentration and sediment yield analysis showed significant differences between TSS concentrations and loadings at seasonal and event timescales (Figure 4.3; Tables 4.1 and 4.2). Total annual sediment yield for water year 2019 was 717.4 kg/ha (Table 4.1). The maximum sediment loading occurred in spring when precipitation was greatest, and the minimum sediment loading occurred in summer

(Table 4.1). Nevertheless, maximum tile discharge occurred in winter. The finding that sediment yields were greater in spring than winter reflects greater concentrations of suspended sediment during peak runoff periods in spring which is likely reflective of the high precipitation intensities (Figure 4.3). The event tile sediment yield varied significantly between events and had a weak positive correlation with event discharge ( $R^2 = 0.42$ ), suggesting high variability in sediment concentration dynamics during storm events both seasonally and between events (Table 4.2).

Results of PP loading showed similar seasonal and event-based dynamics to sediment loading results. Total annual particulate P for water year 2019 was found to be 1.212 kg/ha (Table 4.1). Like sediment loading, the maximum particulate P loading occurred in spring, and the minimum particulate P loading occurred in summer despite maximum tile discharge occurring in winter (Table 4.1). The event TP—DRP flow-weighted mean concentrations were lowest in winter and highest in spring. The event-based relationship between TP—DRP and sediment loading indicated a strong positive relationship with significant correlation (p-value <0.001 at  $\alpha=0.05$  and  $R^2 = 0.86$ ). These findings provide support that TP—DRP dynamics are strongly regulated by suspended sediment transport dynamics for the study site.

#### 4.4.2 Impact of Flow Pathway and Water Connectivity on Sediment Concentrations

The results showed temporal variability in fractions and time to peak of flow pathways, and impact of precipitation on macropore flow and matrix-macropore exchange. Average time-to-peak of  $Q_{quick-new}$  was 1027 minutes for fall and winter events but was 417 minutes for spring and summer events. We found that  $Q_{quick-new}$  for the 33

events had a significant positive linear relationship with event precipitation ( $R^2 = 0.4$ ,  $P < 0.001$  at  $\alpha = 0.05$ ), and a weak negative correlation with 10-day antecedent rainfall ( $R^2 = 0.12$ ,  $P = 0.079$  at  $\alpha = 0.05$ ). Similar to  $Q_{quick-new}$ , we found a positive linear relationship between  $Q_{quick-old}$  and precipitation magnitude ( $R^2 = 0.52$ ,  $P < 0.001$  at  $\alpha = 0.05$ ), and a weak negative relationship with 10-day antecedent rainfall ( $R^2 = 0.08$ ,  $P = 0.0164$  at  $\alpha = 0.05$ ). These results aligned with our prior study (Chapter 3) and highlight the importance of intrinsic event properties and seasonal controls on the magnitude of  $Q_{quick-new}$  and matrix-macropore exchange rather than soil moisture conditions.

Results of the multiple linear regression analysis of daily flow-weighted mean concentrations highlight the importance of quickflow of new water, limited importance of slow flow, and variable impact of the quick-old pathway. Daily flow weighted mean TSS concentrations were found to have a significant positive relationship with daily discharge ( $p < 0.001$ ;  $R^2 = 0.40$ ), 1-day antecedent rainfall ( $p = 0.04$ ;  $R^2 = 0.15$ ), and precipitation intensity ( $p = 0.01$ ;  $R^2 = 0.24$ ). Multiple linear regression (MLR) analysis suggests that TSS concentration prediction improved ( $p\text{-value} < 0.001$ ;  $R^2 = 0.73$ ) when including quickflow of new water ( $p\text{-value} < 0.001$ ) and slowflow ( $p\text{-value} < 0.001$ ) suggesting pathway-connectivity dynamics integrate many of the confounding environmental gradients impacting tile sediment concentrations (See Table 4.3). The coefficient for the matrix-macropore exchange ( $Q_{quick-old}$ ) was not significant ( $p = 0.187$ ), and the standard error for the coefficient (60.4 mg/L) was more than twice that of other pathways. The results of the model showed that  $Q_{quick-new}$  had the greatest impact on concentrations, with a beta coefficient equal to 336.5 mg/L.  $Q_{slow}$  had limited impact on sediment loads,

which is reflected by a beta coefficient of 29.6 mg/L, that was an order of magnitude less than  $Q_{quick-new}$ .

#### 4.4.3 Tile sediment hysteresis analysis

The hysteresis analysis showed that magnitude and directions of HI values differed between tile discharge and the separated hydrograph components (Table 4.2; Figure 4.4; Supplemental Figures S.4.1-S.4.4). For total tile discharge ( $Q_{Tile}$ ), 14 out of 31 events demonstrated clockwise hysteresis with an average HI value of -0.02 (Supplemental Figure S.4.1). For the quickflow pathway transporting pre-event, or old water ( $Q_{quick-old}$ ) hysteresis indices were negative in 29 out of 31 events with an average HI value of -0.35, indicating predominantly counter-clockwise hysteresis loops (Supplemental Figure S.4.2). Conversely, for the quickflow pathway transporting event, or new water ( $Q_{quick-new}$ ) hysteresis indices were positive in 21 out of 31 events demonstrating predominantly clockwise hysteresis with an average HI value of 0.07 (Supplemental Figure S.4.3). For the slow flow pathway ( $Q_{slow}$ ) hysteresis demonstrated clockwise patterns for 28 out of 31 events, with an average HI value of 0.31 (Supplemental Figure S.4.4).

Hysteresis index values were observed to vary seasonally for both  $Q_{Tile}$  and  $Q_{quick-old}$ , but not  $Q_{quick-new}$  (Figure 4.5). Average seasonal HI values oscillated between clockwise and counterclockwise hysteresis for  $Q_{Tile}$  with HI values averaging a minimum of -0.076 in spring and a maximum of 0.357 in summer. Average seasonal HI values showed limited variability for  $Q_{quick-new}$  ranging from a minimum of 0.073 in summer and a maximum of 0.163 in fall. Conversely, average HI values showed large ranges in variability for  $Q_{quick-old}$  from a minimum of -0.57 in spring and a maximum of 0.32 in

summer. The shift from counter clockwise in winter to clockwise in summer/fall reflects the shift in timing of the  $Q_{quick-new}$  peak in which  $Q_{quick-new}$  was found to occur much earlier in the events for warm periods (417 minutes) with average water temperature of 15.5 Celsius as compared to cold periods (1027 minutes) with average water temperature of 7.5 Celsius.

Regression of HI index values against environmental drivers including antecedent rainfall, precipitation intensity and precipitation magnitude were found to be insignificant for  $Q_{quick-old}$  and  $Q_{quick-new}$ , but variable significance for  $Q_{Tile}$  and  $Q_{slow}$ . For  $Q_{Tile}$ , significant positive linear relationships were observed between HI and event rainfall magnitude ( $p=0.037$ ;  $R^2=0.174$ ) and rainfall intensity ( $p<0.001$ ;  $R^2=0.507$ ). We found a significant negative relationship between  $HI_{slow}$  and 1-day antecedent rainfall conditions ( $p=0.002$ ;  $R^2 = 0.312$ ). All other HI values for the various pathway-connectivity fractions with precipitation intensity and magnitude and antecedent rainfall (1, 5 and 10-day antecedent rainfall) were non-significant.

## 4.5 DISCUSSION

### 4.5.1 Field-scale tile sediment loading

Our results indicated that turbidity is a reliable surrogate for field-scale suspended solids monitoring in tile-drained landscapes, likely reflecting the homogeneity of field conditions as compared to applications that are often conducted at the watershed-scale. The power relationship between TSS and turbidity had an  $R^2 = 0.92$ . Strong relationships between TSS and turbidity have been reported in other previous watershed-scale studies that estimated surface suspended solids concentrations (Downing, 2006; Line et al., 2013,



Snyder et al. 2018; Sherriff et al. 2018; Pickering and Ford, 2021). However, studies have highlighted that organic matter and sediment property variability impact regressions, and many studies report lower  $R^2$  values than found in our study (e.g., Lewis et al., 2002; Line et al., 2013; Landers et al., 2013; Snyder et al., 2018). In part, this reflects the fact that field-scale monitoring is reflective of relatively homogeneous zones of soil and landcover, contrasting objectives of many watershed-scale application studies which focus on quantifying source fate and transport dynamics in large, heterogenous systems (e.g. Coelho et al. 2012; Molder et al., 2015; Sherriff et al., 2018). Real-time monitoring of turbidity using high-frequency sensors enables detection of rapid changes in TSS concentrations during daily cycles or storm events. Thus, turbidity sensors in tile-drained landscapes have the potential to provide a deeper understanding of sediment source, fate and transport processes and accurate estimates of sediment loads.

Results of our continuous loading analysis highlight the importance of continuous monitoring for accurate sediment yield estimates. Our sediment yield estimates of 717.4 kg/ha in water year 2019 (Table 4.1) was on the same order of magnitude of other low-gradient systematically drained systems that measured year-round sediment loadings (e.g., Turunen et al., 2017), but were often an order of magnitude higher than values reported using infrequent and short duration sampling methods were used (Culley et al., 1983; Zhao et al., 2001; Stone et al., 2011; Coelho et al., 2012). This finding likely reflects that continuous monitoring is important for capturing infrequent, large events, which often disproportionately impact sediment loadings (Pickering and Ford, 2021). For example, the seven largest events (out of twenty-seven total events) in water year 19

constituted nearly 60% of the sediment load for the year. Cumulatively, this finding highlights the importance of long-term, high frequency monitoring.

Annual TP—DRP loads were strongly correlated with sediment loadings at event to seasonal timescales and were reflective of PP loads across the tile-drained Midwest, suggesting sediment loads from our site are likely reflective of the broader region. The relationship between TP-DRP and sediment loading was significant ( $P < 0.001$ ) in all seasons, but with stronger correlations during low-flow conditions. This variation can be an indication of changes in sources of sediment, erosion and transport processes during higher flow conditions. TP—DRP (a surrogate for PP) loads fell within typical values reported in the literature for fine-textured, tile-drained landscapes (e.g. Eastman et al., 2010; Christianson et al., 2016; Nazari et al., 2020). For example, the annual PP loading varied from 1.48 kg/ha/year in a clayey site to 0.65 kg/ha/year in a loamy site in the same region, in Ohio (see Chapter 2); and from an average of 0.33 to 0.88 kg/ha/year in nearly 1300 North American tile drained sites reported in MANAGE (Measured Annual Nutrient loads from AGricultural Environments) database (Christianson et al., 2016). Given the similarities in loading, agricultural management practices, soil type and land slope gradient of our study site to the broader midwestern US, the findings of this study may be generalizable to tile sediment processes occurring at broader spatial scales.

#### 4.5.2 Impact of pathway-connectivity and environmental drivers on tile sediment transport

Results suggest that preferential transport of low ionic strength water is the primary contributor to sediment loadings and are postulated to exhaust an easily erodible sediment source. Findings from the MLR analysis highlighted that the quickflow pathway

of new water had the highest flow-weighted mean daily sediment concentrations. Hysteresis results generally showed positive, clockwise hysteresis values for  $Q_{quick-new}$  (Figure 4.4; Table 4.2; Supplemental Figure S.4.3). Clockwise hysteresis loops often indicated the existence of proximal sediment sources, with subsequent exhaustion of sources on the rising limb of the event (Williams, 1989; Evans & Davies, 1998). New water has a low ionic strength which are more erosive than inflowing water with high ionic strength (Rousseau et al., 2004). Further, in between storm events, drying promotes development of a biocrust layer that is easily eroded in both surface soils and preferential flow paths by the low ionic strength water (Majdalani et al., 2007; Van den Bogaert et al., 2016; Wilson et al., 2018). Several previous watershed-scale studies have highlighted an initial flush of loose particles from the surface soils (Nouwakpo et al., 2010; Wilson et al., 2016) and laboratory studies have shown analogous processes in macropores (Jacobsen et al., 1997; Schelde et al., 2002; Michel et al., 2010). Based on the existing data, it is difficult to assess surface vs. subsurface sourcing of sediment. Future work should incorporate ambient source tracing methods (e.g., stable isotopes, elemental, and physical tracers) that are sensitive to vertical gradients in the soil profile.

Results for the  $Q_{quick-old}$  pathway suggest transport of matrix water through macropores did not significantly impact sediment delivery to tile, contrasting recent findings for dissolved reactive phosphorus (DRP). Maximum TSS concentrations typically occurred on the falling limb of  $Q_{quick-old}$  flow path although the HI values showed the highest variability as compared with other pathways (Figure 4.4). Similarly, MLR results showed the coefficient for the quick-old pathway was non-significant. These result contrasts recent findings in tile drainage that matrix-macropore exchange is

an important predictor of DRP since matrix-macropore exchange may be initiated in the root-zone (Klaus et al., 2013; Williams et al., 2016; Ford et al., 2018; see Chapter 3). While translocation or seeping of particles from the soil matrix to macropores (suffusion or illuviation) is hypothesized as one of the sources of sediment transported in macropores (Wilson et al., 2018), the role of matrix-macropore exchange on this translocation remains unclear. The high variability in this source may partially reflect the sensitivity of erosion and detachment processes under variable soil moisture conditions. More experimental studies are needed to address hydraulic non-equilibrium effects (e.g. seepage forces) on flow and particle detachment or particle illuviation (Wilson et al. 2018). Such processes may be particularly important for tile sediment dynamics in systems where matrix-macropore exchange comprises a larger percentage of the storm event hydrograph.

Our results showed that the slow flow pathway had limited impact on sediment delivery to tile-drainage. While hysteresis analysis showed inconsistent directions and magnitudes for total tile discharge, these characteristics were more consistent when using partitioned flow components. For example, strong and positive HI values of  $Q_{slow}$  hysteresis showed that the peak of  $Q_{slow}$  is significantly lagged after TSS peak (Figure 4.4, Supplemental Table S.4.1), and suggests that slowflow has limited impact on tile sediment loadings. As a result, the discretization of slow and quick-new hydrographs improved prediction of TSS concentration as compared with simple Q-based regression analysis, although concentrations of  $Q_{slow}$ , were an order of magnitude lower than  $Q_{quick-new}$  (further highlighting the limited importance of  $Q_{slow}$  on sediment loadings). This finding reflects the idea that slowflow pathways are important filters for sediment laden

waters. In this regard, previous studies suggested that particle sieving and retention can occur in subsurface pathways (van den Bogaert et al., 2016; Burkhardt et al., 2008; Turtola et al., 2007; Jarvis et al., 1999). Smaller particle sizes in clayey soil are less sensitive to filtration processes (Ulén, 2004). The process of retention and sieving processes have not been extensively studied practically, but Turunen et al., 2017 modelling study suggested that a large portion of the eroded sediment can stay in the field due to the retention and sieving processes. Cumulatively these results suggest converting  $Q_{quick-new}$  fluxes to  $Q_{quick-old}$  or  $Q_{slow}$  may significantly reduce sediment and PP delivery to tile drains.

Based on our results, we postulate that seasonal differences in flow pathway dynamics play a significant role in sediment loading dynamics to tiles. In regard to seasonal differences, our results show short hydrograph time to peaks in the growing season and longer time to peaks in winter and late fall. In addition, HI values for  $Q_{quick-new}$  were consistent, but variable for  $Q_{quick-old}$  and  $Q_{tile}$ , reflecting the variability in time to peaks. Previous studies in tile-drained landscapes showed that during the growing season, dry soil conditions promote desiccation crack expansion and rapid transport of event water to tiles via macropores (see Chapter 2). Under saturated and unsaturated conditions of winter, large infiltration can occur because a considerable portion of macropores remain air-filled (Stadler et al., 2000, Pittman et al., 2020; Mohammed et al., 2018 and 2020). However, in the winter freezing/thawing effects can result in freezing of preferential water and blockage of macropore path, delaying the hydrograph time to peak (Stadler et al., 1997; Watanabe and Kugisaki, 2017; Demand et al., 2019; Mohammed et al., 2020). The more tortuous macropore flow conditions in winter as compared to

summer and spring are one reason for the decreased sediment concentration and loadings we found in our study, despite greater flow volumes in winter.

A second environmental factor impacting dynamics were the contrasting precipitation patterns in growing vs. dormant seasons. Our results showed positive correlations between precipitation magnitude and  $Q_{quick-new}$ , and we observed that average precipitation intensity was almost twice as high in spring and summer as compared to winter and fall. While this, in part, impacts flow pathway dynamics, it may also impact source erosion dynamics. Previous studies have shown that hydraulic forces and splash erosion rates, which were the factors behind the sediment loss during the growing seasons, have direct positive relationship with rainfall intensity and magnitude (Warsta et al., 2013; Turunen et al., 2017). Collectively, these findings highlight the potential importance of both seasonality of flow pathway dynamics and precipitation dynamics for explaining temporal variability in tile sediment loading dynamics.

#### 4.5.3 Implications for Management

Despite the adoption of conservation tillage practices at the study site, subsurface tile loadings were high because of preferential flow of event water, suggesting management practices should target reductions in  $Q_{quick-new}$ . No-till is recognized to reduce time to peak of macropore flow (Verbee et al., 2010; Williams et al., 2016) resulting in less transit time for sediment retention and higher shear stresses in subsurface pathways. Based on our results we suggest that management practices that will combat the unintended impacts of no-till or reduced tillage has on subsurface pathways should be considered. For instance, hydrogels, which are water-absorbing polymers that are applied

in agricultural settings for their environmental benefits such as reduction of soil erosion and nutrient loss, enhanced soil permeability and infiltration rate, and increased water-holding capacity (Narjary et al. 2013; Hosseini et al., 2020; Bairwa et al., 2020) may be beneficial in reducing the intensity of preferential flow and increasing tortuosity of water, which consequently aids in remedying the preferential flow of new water and sediment loading. Further, practices such as controlled drainage may reduce preferential flows of new water, although flow pathway dynamics have not been robustly evaluated in these landscapes (Cook and Verma, 2012; Saadat et al., 2018; Shedekar et al., 2020). Further work should assess how other tile-drain best management practices may be coupled with conservation tillage practices to reduce subsurface sediment loadings.

In addition to the well-recognized environmental implications for P transport, sediment from tile-drains also have practical implications for edge-of-field treatment techniques such as denitrifying bioreactors. It is well-established that various water source compositions and quality can alter nitrate removal effectiveness of bioreactors and may require long-term maintenance (Addy et al., 2016). Water sources available for treatment in woodchip bioreactors in many agricultural landscapes is high which necessitates TSS calculations for investigation of bioreactors performance in removal of particulate P or TSS (Beauchemin et al., 1998; Vanni et al., 2001; Gentry et al., 2007). Assuming a typical reactor will have a volume of roughly 150 cubic yards / 50 acre of drainage, we would have a 120 cubic yard, or 92 m<sup>3</sup> reactor that would be required for our study site (Addy et al., 2016). Assuming a sediment density of 1500 kg /m<sup>3</sup>, 7.7 m<sup>3</sup> of sediment will pass through the bioreactor each year. The increased hydraulic residence time for these systems will decrease transport capacity and subsequently result

in sedimentation, highlighting the potential for high maintenance needs in these environments. As a result, it may be necessary to couple woodchips with other sediment filtration practices such as sedimentation basins or solid settling tanks in order to provide high-capacity and low-maintenance treatment of TSS (e.g., Choudhury et al., 2016).

#### **4.6 Conclusion**

We used a recently developed framework to evaluate the impact of flow pathways and source connectivity on sediment and particulate P delivery in tile-drained landscapes. Our results highlight the capability and successful application of high-resolution sensors in improving understanding of pathways and source connectivity dynamics for sediment loadings in tile-drainage. Subsurface water source connectivity and flow pathway dynamics, precipitation patterns, seasonal differences and subsurface erosion play a role in sediment and PP loadings to tile drains. We found that new-water that routes through quickflow and slowflow play a significant role in sediment delivery and matrix-macropore exchange impacts need more investigation in different soil textures. The estimation of event-based sediment concentrations has implications for the process of design and assessment of bio-reactors. High concentrations of sediment in our study suggest that the combined use of conservation tillage with other management practices such as hydrogels or drainage water management, which can increase tortuosity of water and decrease surface and subsurface soil erosion, is necessary for reduction of sediment delivery in tile-drained landscapes. Our inexpensive high-resolution estimation of sediment concentrations and loadings and pathway dynamics within the events can be used for evaluation of newly developed process-based models.



#### 4.7 Figures and Tables

Table 4.1 Seasonal and annual sediment yield, precipitation, and discharge for water year 2019

	<b>PRC (mm)</b>	<b>Discharge (mm)</b>	<b>Sediment Yield (kg/ha)</b>	<b>TP—DRP load (kg/ha)</b>
<b>WY 2019</b>	1213.5	517.75	717.38	1.212
Fall	234.62	127.03	148.19	0.2
Winter	219.01	211.26	258.90	0.445
Spring	414.67	170.03	283.27	0.547
Summer	345.20	9.44	27.02	0.019

Table 4.2 Summary of discharge, event-based sediment yield, and HI values for pathway-connectivity indicators for the 31 monitored events.

Event	Start Time	End Time	Discharge (mm)	Sediment Yield (kg/ha)	TP-DRP load (kg/ha)	HI Values			
						(Qtotal)	(Qq-o)	(Qq-n)	(Qs)
S1	11/1/2018 0:30	11/9/2018 10:00	33.21	21.46	0.022	0.02	-0.27	0.17	0.46
S2	11/9/2018 11:30	11/12/2018 23:30	3.96	0.21	0.004	-0.08	-0.3	0.04	0.33
S3	11/25/2018 19:30	11/30/2018 4:00	21.78	46.35	0.077	0.05	-0.54	0.16	0.36
S4	12/1/2018 0:00	12/5/2018 22:30	16.85	22.06	0.006	-0.24	-0.44	0.17	0.34
S5	12/20/2018 12:00	12/27/2018 4:00	16.37	25.76	0.033	-0.16	-0.67	0.01	0.49
S6	12/27/2018 4:30	12/31/2018 7:00	5.5	2.35	0.025	-0.15	-0.5	0.03	0.51
S7	12/31/2018 7:30	1/5/2019 23:30	21.87	58.68	0.081	-0.22	-0.44	0.05	0.36
S8	1/21/2019 18:00	1/31/2019 7:00	34.85	28.95	0.057	-0.17	-0.34	0.14	0.54
S9	2/12/2019 0:00	2/14/2019 12:00	5.72	2.12	0.006	-0.04	-0.16	0.11	0.14
S10	2/14/2019 12:30	2/19/2019 17:00	9.67	5.25	0.008	-0.1	-0.29	0.06	0.3
S11	2/20/2019 14:24	2/21/2019 10:04	4.37	2.46	0.007	0.15	-0.72	0.08	0.3
S12	2/23/2019 13:00	2/26/2019 3:30	12.64	24.04	0.026	0.06	-0.22	0.09	0.49
S13	3/9/2019 15:00	3/13/2019 8:00	12.4	30.77	0.031	0.1	-0.62	0.17	0.29
S14	3/13/2019 8:30	3/20/2019 9:00	25.03	47.08	0.077	-0.21	-0.5	0.03	0.16
S15	3/20/2019 17:00	3/26/2019 17:30	11.01	5.5	0.010	-0.08	-0.37	0.17	0.33
S16	3/28/2019 0:00	4/4/2019 3:30	27.23	50.47	0.066	0.06	-0.55	0.19	0.29
S17	4/18/2019 15:36	4/20/2019 4:04	16.11	48.45	0.087	0.42	-0.78	0.06	0.4
S18	4/20/2019 4:33	4/25/2019 7:26	23.19	52.63	0.076	-0.09	NA	0.04	0.1
S19	4/27/2019 15:00	4/29/2019 15:30	12.75	27.3	0.045	-0.02	-0.45	0.15	0.27
S20	4/30/2019 8:30	5/1/2019 13:30	4.44	6.94	0.027	-0.28	-0.77	0.14	0.38
S21	5/13/2019 6:00	5/16/2019 22:00	4.43	1.44	0.006	-0.31	-0.49	0.06	0.25
S22	5/28/2019 3:07	5/31/2019 12:28	10.14	45.13	0.066	-0.16	NA	0.11	0.24
S23	6/13/2019 16:00	6/14/2019 23:30	3.86	5.37	0.014	-0.32	-0.53	0.03	0.25
S24	6/15/2019 7:00	6/19/2019 13:30	11.62	9.06	0.032	0.02	-0.44	0.11	0.31
S25	7/6/2019 19:00	7/10/2019 9:30	0.62	0.2	0.000	0.46	0.51	0.06	0.63
S26	9/21/2019 15:00	9/22/2019 19:00	1.01	2.52	0.004	0.12	-0.09	0.02	0.45
S27	9/30/2019 1:30	9/30/2019 23:30	6.19	22.48	0.012	0.49	0.54	0.14	0.21
S28	10/26/2019 17:00	10/28/2019 23:30	2.99	0.64	0.002	0.08	-0.03	0.33	0.44
S29	10/30/2019 7:00	11/2/2019 23:30	26.33	8.32	0.020	0.03	-0.03	0.36	0.26
S30	12/9/2019 9:30	12/11/2019 23:30	3.25	0.49	0.001	0.2	-0.13	0.38	0.55
S31	12/29/2019 20:00	12/31/2019 23:30	9.45	38.7	0.055	-0.28	-0.53	0.09	0.28

Table 4.3 Results of the multiple linear regression analysis for daily flow-weighted mean TSS concentrations. Estimated coefficient column shows estimated TSS concentration (mg/L) associated with  $Q_{quick-new}$  and  $Q_{quick-old}$  and  $Q_{slow}$  fractions with standard error in parenthesis.

	<b>Estimated Coefficients</b>	<b>p-value of coefficient</b>	<b>p-value of overall model</b>
$TSS_{quick-old}$	80.1(60.4)	0.187	$<2.2e^{-16}$
$TSS_{quick-new}$	336.5 (28.4) <sup>***</sup>	$<2e^{-16}$	
$TSS_{slow}$	29.6 (8.3) <sup>***</sup>	0.00062	

·P=0.05, \*P=0.01, \*\*P=0.001, \*\*\*P=0.0001

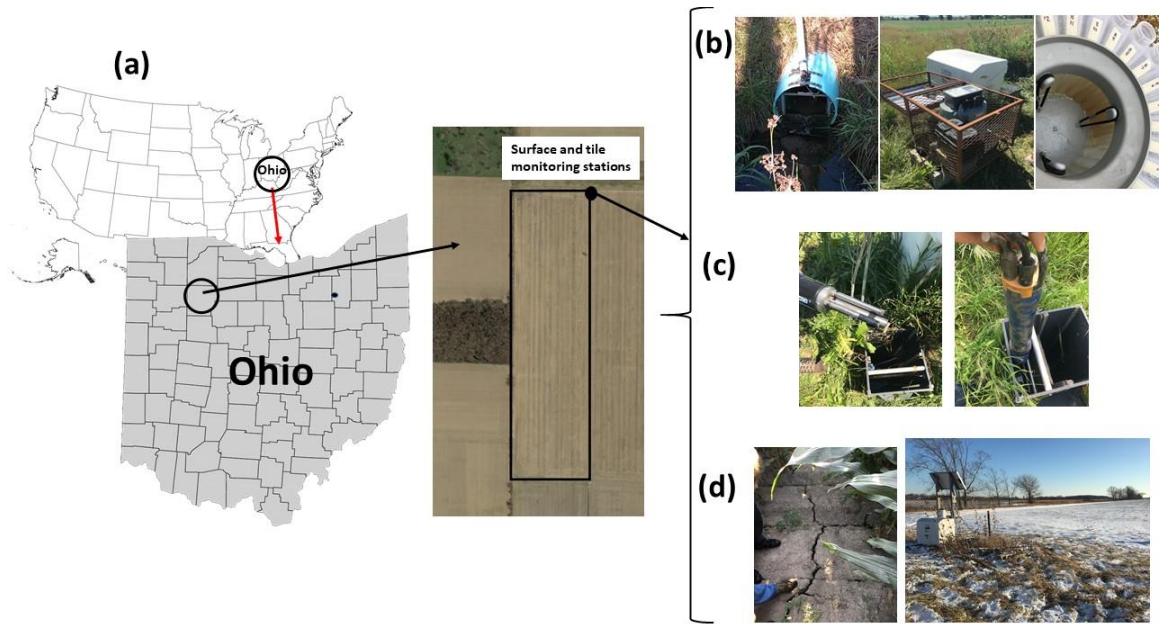


Figure 4.1 a) Study site sampling locations in Ohio, USA; b) Typical USDA-ARS edge-of-field monitoring platforms for surface and tile; (c) YSI EXO sonde (with turbidity and conductivity sensors) were installed in the drainage water management structure; (d) Environmental conditions: macropores and snow-covered field.

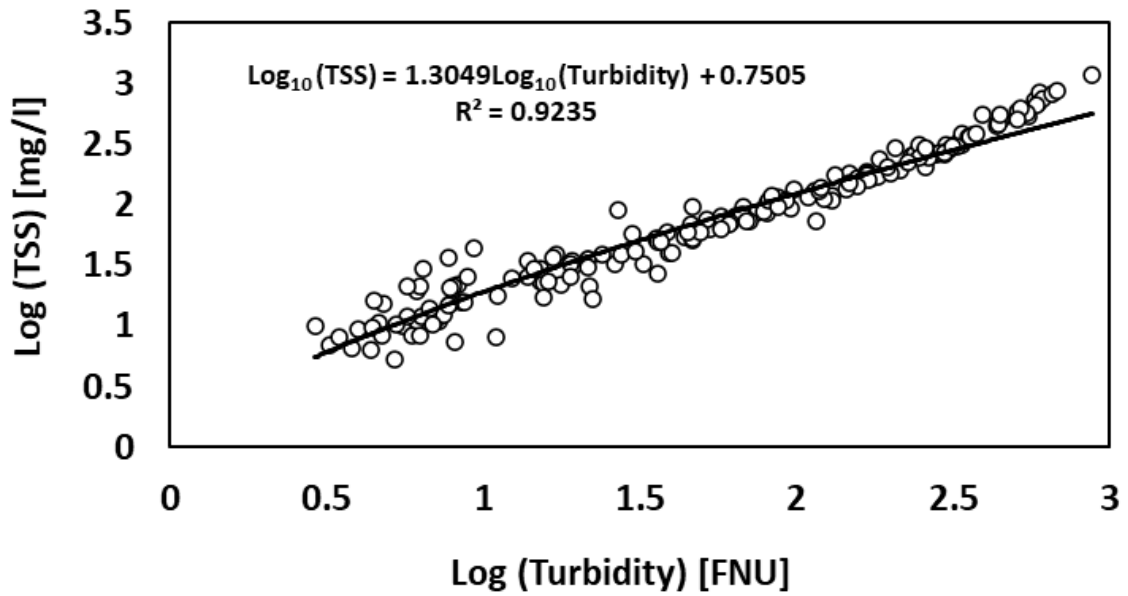


Figure 4.2 Regression of total suspended solids (TSS) and turbidity curve using log-transformed measures of TSS concentrations and turbidity values.

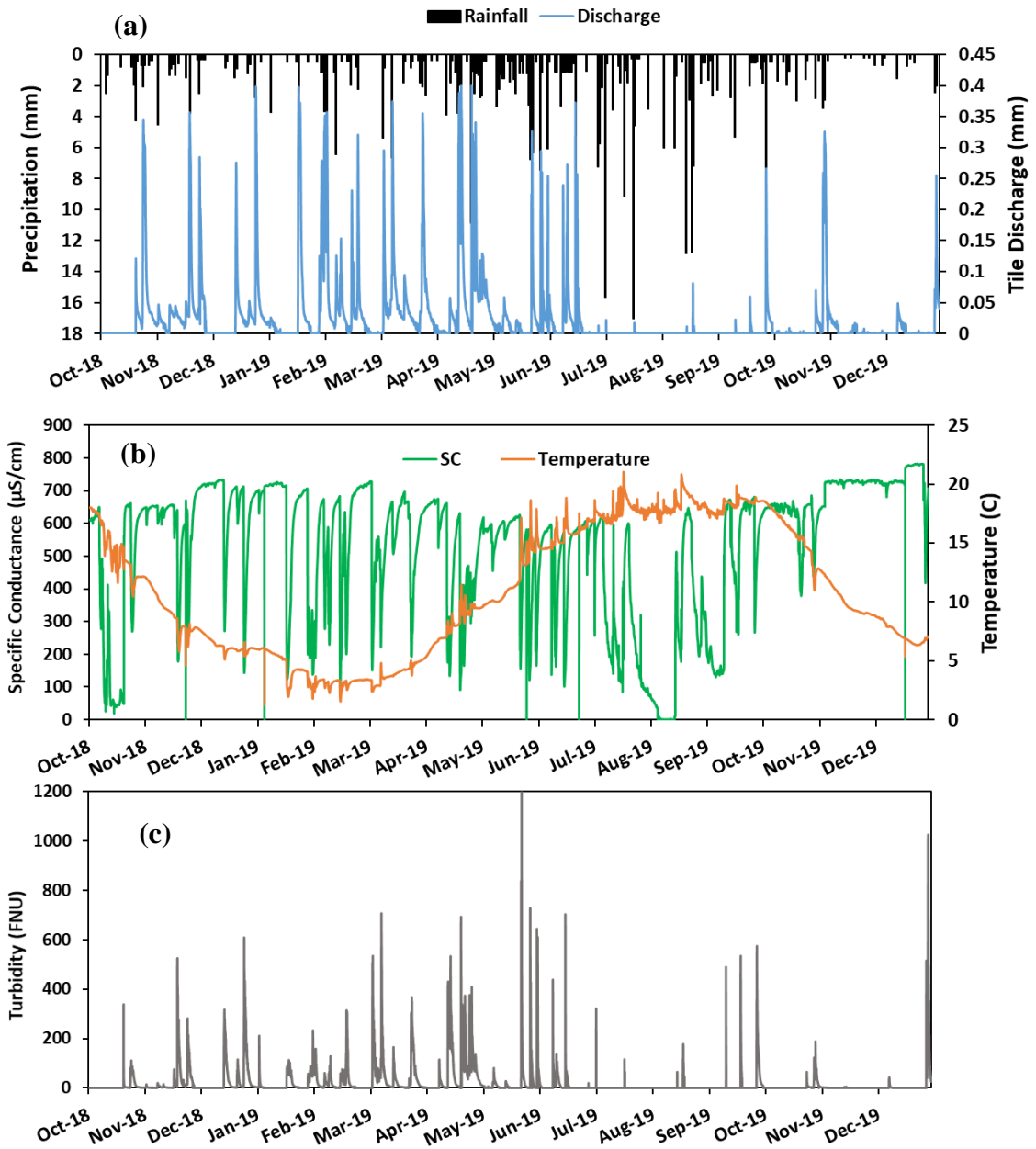


Figure 4.3 Continuous timeseries for a) precipitation and tile discharge, b) temperature and specific conductance, and c) turbidity

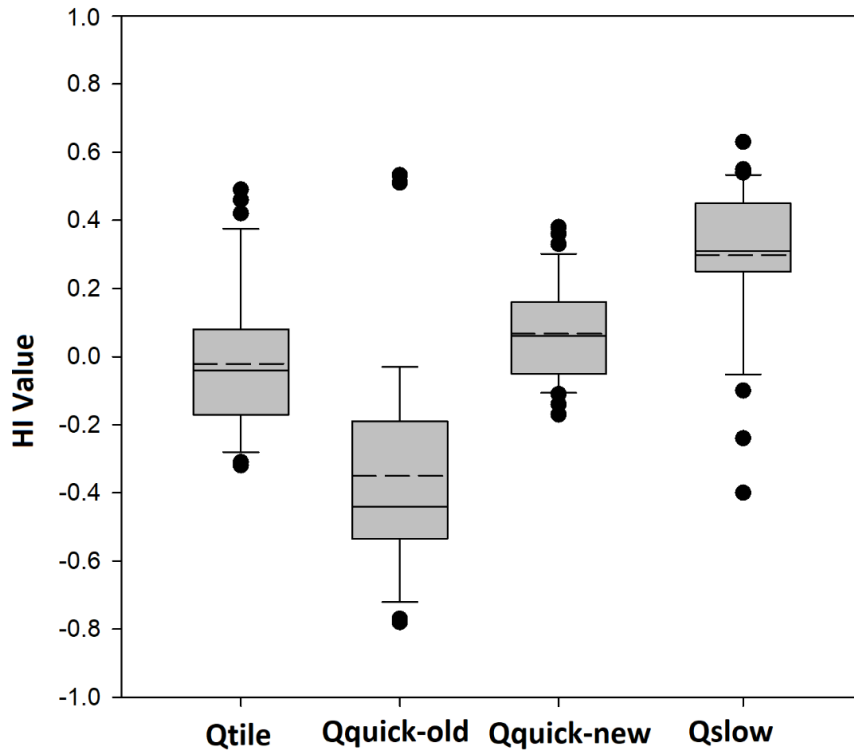


Figure 4.4 Box-and-Whisker plots of HI values of Qtile, Q<sub>quick-old</sub>, Q<sub>quick-new</sub>, Q<sub>quick</sub> and Q<sub>slow</sub> against TSS concentrations. The dash and solid line within each box show mean and median HI values, respectively.

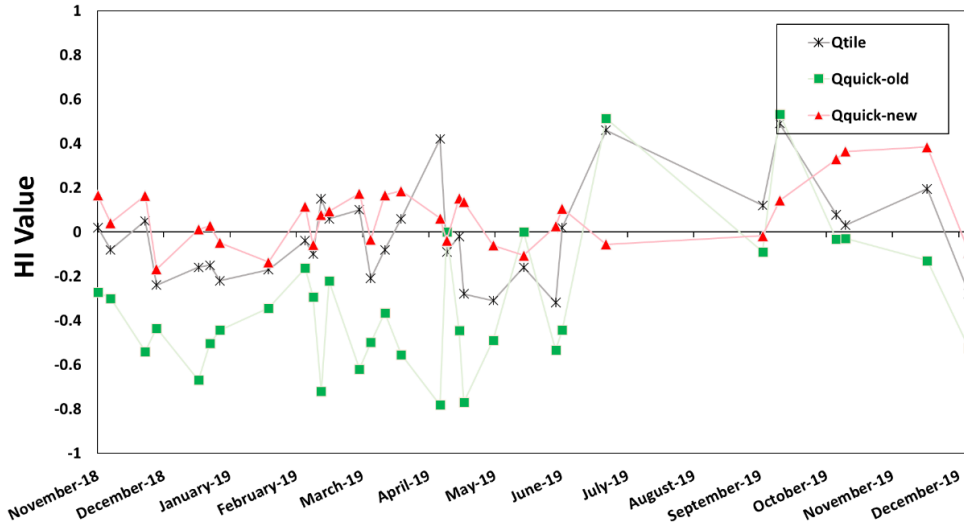


Figure 4.5 Box-and-Whisker plots of HI values of Qtile, Q<sub>quick-old</sub>, Q<sub>quick-new</sub>, Q<sub>quick</sub> and Q<sub>slow</sub> against TSS concentrations. The dash and solid line within each box show mean and median HI values, respectively. Hysteresis Index (HI value) is a quantitative assessment for direction and strength of hysteresis loops.



## CHAPTER 5. IMPACTS OF DRAINAGE WATER MANAGEMENT ON FLOW PATHWAY-CONNECTIVITY AND SEDIMENT PHOSPHORUS DYNAMICS IN A TILE-DRAINED AGROECOSYSTEM

### 5.1 Introduction

Subsurface tile drainage in fine-textured soils throughout the midwestern U.S has enhanced eutrophication and persistence of harmful and nuisance algal blooms in receiving waterbodies (Blann et al., 2009; Radcliffe et al., 2015; Smith et al., 2015; Williams et al., 2016). Sediment-bound phosphorus (P), or particulate P (PP) loadings from tile-drainage has been recognized to play a key role in eutrophication and is suggested to be governed by preferential flows (Macrae et al., 2007; and Eastman et al., 2010; Christianson et al., 2016). Widespread study of preferential flows in tile-drained landscapes has been conducted over the past 20 years (Kung et al., 2000; Paasonen-Kivekas and Koivusalo, 2006; Shilling and Helmers 2008; Radcliffe et al., 2015; King et al., 2015; Nazari et al., 2020). An area that has received less attention is the study of drainage water management impacts on preferential flow and PP loads (Cooke and Verma, 2012; Ross et al., 2016; Lavaire et al., 2017). Drainage water management (DWM) systems are a structural management practice commonly utilized in tile-drained landscapes to regulate the water table in order to enhance crop yields, reduce subsurface drainage fluxes, and improve water quality (Drury et al., 1999; Ghane et al., 2012). The practice has been cited in several studies for its positive impacts on subsurface drainage reductions, although water quality benefits remain uncertain (Fausey, 2005; Skaggs et al., 2012; Lavaire et al., 2017; Shedakar et al., 2020).

Although DWM has generally shown flow reductions that have resulted in decreases in both DRP and TP loadings, the impact on concentrations have been more variable

(Williams et al., 2015; Nash et al., 2015; Ross et al., 2016). Drainage water management has been found to increase evapotranspiration, surface runoff and lateral and vertical seepage, leading to decreases in volumetric flow reductions through tile drains (Singh et al., 2007; Cook et al., 2012; Williams et al., 2014; Liu et al., 2019). Studies have also emphasized the impact of climate, crop type, and management practices on DWM flow reduction (King et al., 2016; Ross et al., 2016). However, the impact of DWM on P concentration and loading is not well understood and inconsistent P loading and concentration results has hindered approval of DWM as a P mitigation strategy (Carstensen et al., 2019; Hoffmann et al., 2020). For example, several studies showed that DWM is effective to reduce both TP and DRP loading, but this reduction has been attributed to subsurface flow reduction; and P concentration often is insignificantly impacted (e.g. Evans et al., 1995; Feser et al., 2010; Williams et al., 2015, Ross et al., 2016). However, Nash et al. (2015) found that ortho-P load reduction was not solely attributed to tile water reduction, but partially was due to seasonality and plant uptake of P during dry seasons when water is held in the field. Nevertheless, studies have postulated high tendency toward higher TP and other P form losses when using DWM due to increased water level and change of redox conditions (e.g. Ross et al., 2016; Carstensen et al., 2019). Therefore, further investigation on evaluating the impact of DWM on PP delivery is needed.

Studies have used a variety of methodologies to assess the impact of DWM on hydrology and water quality. Previous studies have assessed DWM performance using before-and-after impact, before-after control-impact (BACI) study designs of paired controlled (CD) and free-drainage (FD) fields, and computer modeling (Youssef et al.,

2005; Fang et al., 2012; Williams et al., 2015; Salehi et al., 2017; Shedekar et al., 2017, 2020). BACI study designs are a common approach because they control for the temporal variability of external factors such as climate or crop type. The BACI study design requires two experimental fields with similar soil characteristics, drainage system design, and cropping practices (Clausen and Spooner, 1993). While these methodologies have been effective in understanding cumulative impacts of drainage water management, few studies have assessed how specific timescales (e.g., event, seasonal, or longer-term) are impacted, although it's perceived that numerous timescales will be impacted given the impacts on soil moisture, evapotranspiration, and surface runoff.

Comparison of hydrologic and water quality trends from time-series analysis can provide insight into specific processes impacting sediment and nutrient transport (Ford et al., 2015). Empirical Mode Decomposition (EMD) is a time series analysis methodology that has been effective in identifying event-based, seasonal, and longer-term trends in hydrologic and water quality parameters in subsurface drained agroecosystems, and the associated impact of agricultural management practices (Huang et al., 1998; Wu et al., 2007; Ford et al., 2018; 2019). In this study, we postulate that combination of BACI study design with EMD will provide deeper insight into the processes impacting hydrologic and PP fluxes under drainage water management.

Inconsistencies in our understanding of how CD impacts water quality in part reflects a limited understanding on how CD impacts flow pathway dynamics and water source connectivity (Cook et al., 2012; King et al., 2015; Ross et al., 2016). Regarding subsurface flow pathways, preferential flow is a function of soil matrix infiltration capacity, soil moisture, exchange between macropores and the soil matrix and

connectivity of macropores (Tsuboyama et al., 1994; Sidle et al., 2001; Klaus et al., 2013). DWM can alter soil moisture conditions, seepage, subsurface flow pathways, and consequently soil matrix and macropore interactions during high water table conditions (Skaggs et al., 2012; Saadat et al., 2018; Liu et al., 2019). Source water connectivity refers to origin of water in tile drainage and has traditionally been discretized into event water (e.g., precipitation or irrigation water), and pre-event water (e.g., water residing in the soil matrix prior to stormflows) (e.g. Vidon and Cuadra, 2010; Williams et al., 2016; Smith et al., 2018). Recent work in tile-drained landscapes has found that degree of soil saturation has significant impacts on source water connectivity in addition to flow pathway (see Chapter 3), and hence DWM is anticipated to alter pathway-connectivity dynamics. There is a pressing research need to evaluate pathway-connectivity dynamics in controlled drainage sites.

Water source connectivity and subsurface flow pathway dynamics have been found to significantly impact sediment transport dynamics in tile-drained landscapes (e.g. Michaud and Laverdiere, 2004; Wilson et al., 2018; Collins et al., 2019; Nazari et al., 2020). It is commonly assumed that sediment and PP delivery to tiles is through macropore flow and selective removal and transport of sediment from different parts of soil profile (Oygarden et al., 1997; Uusitalo et al., 2001; Stone and Krishnappan, 2002; Paasonen and Koivusali, 2006; Schilling and Helmers, 2008). Specifically, preferential transport of event water provides heightened connectivity to surface soils and has low ionic strength which enhances its potential to erode and transport fine sediments (Hendrick et al., 1993; Jacobsen et al., 1997; Schelde et al., 2002; Rousseau et al., 2004; Wilson et al., 2018). Conversely, matrix-macropore exchange has been found to be less

erosive because it has higher ionic strength and decreases the fraction of water connected to surface soil sources (see Chapter 4). We postulate that altering flow pathway, and water source connectivity dynamics will impact the delivery of sediment and PP to tile drains.

Tile-drainage source-connectivity and sediment transport dynamics can be quantified through coupling of high-frequency sensing with hydrograph separation and hysteresis analysis techniques. Hydrograph recession analysis is an empirically-based hydrograph separation approach that can be used in tile-drainage to partition the flow hydrograph into quick and slow-flow components at an event-scale (Schilling and Helmers, 2008, Ford et al. 2019, Husic et al. 2019, Nazari et al. 2020). Combination of hydrograph recession analysis with specific conductance end-member mixing analysis (e.g. Smith et al., 2018) can aid in separating tile hydrographs into permutations of water sources (i.e., new water/old water) and pathway connectivity (i.e., quick/slow) (see Chapter 3). Regarding sediment dynamics, studies have highlighted the ability of high-frequency turbidity sensor data to improve estimates of sediment fluxes and provide insight into sediment hysteresis dynamics in a variety of landscapes and spatial scales (Sherriff et al., 2016; Snyder et al., 2018). Performing hysteresis analyses with separated hydrograph source-connectivity fractions can inform prominent sediment source and transport mechanisms (see Chapter 4). Application of these techniques for assessing impacts of DWM on sediment erosion and transport dynamics is a novel application and current research need.

The overarching objective of this study is to investigate impacts of DWM on flow pathway-connectivity and sediment phosphorus dynamics in a tile-drained

agroecosystem. We collected and used data from a fine-textured paired field that was a part of USDA-ARS SDRU edge-of-field monitoring network (Williams et al., 2016). Specific objectives of this manuscript were to perform 1) hydrograph recession analysis of 4-year subsurface discharge to partition the tile hydrograph into quickflow and slowflow pathways in both paired fields, one with controlled-drained (CD) and one free-drained (FD) during treatment; 2) BACI analysis on flow, quickflow, slowflow, and TP—DRP loading in order to assess the annual impact of DWM treatment on flow pathways and PP loading; 3) Empirical Mode Decomposition (EMD) time-series analysis to investigate event-scale impacts of DWM on tile flow and TP—DRP loadings; and 4) Specific Conductance End-Member Mixing Analysis (SC-EMMA) to partition new-water and old-water, and perform TSS and flow-pathway hysteresis analysis to better understand the impacts of pathway-connectivity on sediment delivery dynamics between paired CD and FD sites.

## **5.2 Methodology**

### **5.2.1 Study Site**

To meet the objectives of this study, we selected a paired field site from the USDA-ARS Soil Drainage Research Unit edge-of-field monitoring network (Williams et al. 2016). The study site is a systematically drained field in Wood County, Ohio U.S.A. and is delineated into two fields with separate surface (F1 and F3) and subsurface (F2 and F4) outlets (Figure 5.1.a). The contributing area for the western and eastern fields are 0.154 km<sup>2</sup> and 0.158 km<sup>2</sup>, respectively. The average annual precipitation during the four years of monitoring was 1003.3mm. The site is classified as a silty-clay-loam soil texture

consisting of Nappanee (NpA) and Hoytville (HcA) soils (SSURGO soil data base, NRCS USDA, 2019). The study site was selected for the present study because: 1) study site characteristics were typical of prevailing agricultural management practices, soil texture, soil nutrient conditions, and runoff characteristics in the region; 2) the presence of drainage water management structures on both tile mains enabled a BACI study design and provided a secure structure to house sensing equipment; 3) the fields were managed by a single producer with analogous management practices outside of the drainage water management treatment; and 4) high-frequency water quality sensor data collection efforts complemented an extensive historic database conducted by the USDA-ARS including more than five years of continuous data from the monitoring site including precipitation, flowrate and water quality data from surface and subsurface pathways.

Regarding management practices, the typical crop rotation at the site was corn-soybean-wheat. The field was managed using conservation tillage practices (Table S.5.1). Historically, the DWM plates were opened prior to planting and harvesting and closed after planting and harvesting from 2015 through 2017. Starting in December 2017, DWM boards were removed at F2 through the remainder of the study, while F4 remained managed (Table 5.1). Water years were separated based on when F2 was managed with DWM (WY 2016-2017) and when F2 was under free drainage (WY 2018-2019). Thus, F4 served as the control site and F2 as the treatment site.

### 5.2.2 Data Collection and Analysis

Precipitation and flowrate timeseries were collected using well-accepted edge-of-field (EOF) methods (Williams et al; 2016; Figure 5.1.b). To measure rainfall duration, 10-

minute rainfall intensities and depths, tipping bucket rain gages were used. The subsurface outlet for each field was equipped with a weir insert (Thel-Mar, Brevard), and an ISCO 4230 Bubbler Flow Meter (Teledyne Isco, Lincoln, Nebraska). The tile outlet was also equipped with an ISCO 2150 Area Velocity sensor for 30-minute discharge measurements under submerged conditions. A berm was installed on the surface at the EOF to direct surface runoff to an H-flume. Surface monitoring stations were equipped with a bubbler meter which measures water depth and was used for calculating 10-minute volumetric discharge using a calibrated stage-discharge curve specific to the flume. The 30-minute subsurface and 10-minute surface discharges were collected for WYs 2016, 2017, 2018 and 2019 (10/01/2015 to 09/31/2019).

Surface and tile water samples were collected using a Teledyne ISCO 6712 portable sampler and accessories. Surface samples were collected using a flow proportional methodology; that is, a 100 mL aliquot was collected for every 1mm volumetric depth. Ten composited aliquots made up one sample. Due to periodic submergence, a time-proportional approach was used to collect water samples. A 100-ml aliquot was collected every six hours for 48 hours and composited into a single sample bottle reflecting a two-day composite sample. During rainfall events, additional high frequency samples (four samples collected every 15 minutes and composited hourly) were collected on the rising limb of the hydrograph to better capture initial flushes. Collected water samples were analyzed for dissolved reactive P (DRP) throughout the monitoring period by first vacuum filtration (0.45 $\mu$ m) and then analyzing for P using the ascorbic acid reduction method (Murphy and Riley, 1962). Concentrations of TP were determined on unfiltered samples following alkaline persulfate oxidation and subsequent analysis of DRP (Patton



and Kryskalla, 2003). Subsurface daily TP and DRP loadings were calculated using the approach of Williams et al. (2015). Briefly, we determined the midpoint of all sample time steps for each bottle, used linear interpolation between measured values at the midpoint to estimate the concentration for each interval when flow was measured, and estimated loading as the product of interpolated concentrations and flow rate. Particulate P loading was then estimated as the difference between TP and DRP loadings (Nazari et al., 2020).

A YSI EXO 3 sonde (Xylem/YSI Incorporation, 2020) was deployed for WY 2019 at both tile monitoring platforms to measure turbidity and specific conductance continuously (see Chapters 3-4). The sonde was placed on the upstream side of the DWM structure for both sites (see Figure 5.1.c). Maintenance and calibration were performed on the instruments approximately once per month based on recommendations of the manufacturer, which is consistent with other studies (Snyder et al., 2018). Measurements were obtained at a fifteen-minute interval continuously during water year 2019, i.e., October 1, 2018-September 30, 2019 (Figure 5.2.c-d). Data gaps occurred from 01/11/2019-02/22/2019 because of sensor malfunction at F4.

Sediment loads were estimated for high-frequency monitoring periods in WY 2019 using a TSS-turbidity calibration curve at each site. From 03/01/2019 to 12/30/2019, a sample split from the ISCO samples were collected and transported to the University of Kentucky for measurement of total suspended solids (TSS) and turbidity. Before TSS analysis, we used freshly calibrated sensors to measure turbidity and specific conductance of the sample in the lab since the ISCO samples were composite samples. The sample was then analyzed for TSS concentration by vacuum filtration through a 0.7  $\mu\text{m}$  glass

microfiber filter and dried at 104°C prior to weighing, consistent with EPA method 160.2 (U.S. EPA, 1983). To estimate continuous sediment concentrations from turbidity measurements, two separate regression models were developed for TSS as a function of turbidity for the two sites. In total, 188 and 211 samples were used to develop the regressions for F2 and F4, respectively. A simple least squares linear regression was performed on log transformed TSS and turbidity values, consistent with previously published approaches (Rasmussen et al., 2009). TSS-Turbidity curves showed a strong correlation between TSS concentration and Turbidity with an  $R^2$  of 0.92 and 0.87 for F2 and F4, respectively. We calculated estimates of sediment fluxes by multiplying sediment concentrations by measured flow rates. In total, we analyzed 47 events (27 at F2 and 20 at F4) throughout the 2019 water year.

### 5.2.3 Analytical Methodology

#### 5.2.3.1 Hydrograph Pathway Analysis

Hydrograph recessions from events throughout the monitoring period were compiled to perform master recession curve (MRC) analysis. This analysis has previously been performed for freely drained tile drained fields for soil textures characteristic of the region (see Chapters 2-3). In this study, we aimed to test applicability of the MRC method to sites with CD, hence, we only selected event recessions from the CD site if the DWM was closed. The MRCs were automatically created using a Genetic Algorithm (GA) incorporated in RC 4.0 software (HydroOffice; Gregor and Malik, 2012; Malik and Vojtkova, 2012). For our study, we generated MRCs using 4 years of tile hydrology data. We selected 35 recessions of FD period from F2 and 30 recessions of CD period from F4

to create a single MRC for each site using RC 4.0 software (HydroOffice; Gregor & Malik, 2012; Malik & Vojtkova, 2012). More recessions existed for each field, but they were not included in the analysis because they were either comprised of days with zero flow (i.e., associated with no flux or tile backwater) or had nonlinear recessions associated with disruption of initial recession with secondary flow peaks. We assumed two flow pathways reflecting reservoirs for matrix and macropore flow, consistent with previous studies (Schilling and Helmers 2008; Vidon and Cuadra 2010; Williams et al., 2016). As a result, we selected two linear reservoirs and fit recession curves so that the two recessions provided optimal fit to the data. The goodness-of-fit was tested using the Nash-Sutcliffe Efficiency (NSE) value (Moriassi et al., 2007).

Event-based hydrograph recession analysis was used to separate tile flow into quickflow and slowflow reservoirs for the continuous tile-drainage flowrate time-series (e.g., Husic et al., 2019; Ford et al., 2019; see Chapter 2). For each hydrologic event, we plotted the falling limb of the subsurface discharge hydrograph on a logarithmic scale and manually fit linear curves to distinct log-linear regions based on findings of two distinct reservoirs during our MRC analysis. Then, a linear increase in slow flow was assumed from the beginning of the rising limb of the hydrograph, which represents the start of quickflow ( $Q_{quick}$ ), to the determined inflection point on the falling limb from the previous step, which represents the end of quickflow (Husic et al., 2019). On an event basis, the area between the hydrograph and the slow flow curve represented  $Q_{quick}$  and the area underneath the slow flow reservoir curve represented  $Q_{slow}$ . We performed this analysis on data from 2015 to 2019 water year and calculated results for 30-minute flow

intervals. The analysis was performed on separated events from both sites. A total of 188 paired events (94 events per site) were analyzed.

#### 5.2.3.2 Before-After-Control-Impact Assessment

Before-after-control-impact (BACI) study design assumes that changes over time such as weather, crop and management (unrelated to the treatment) in the impact site are controlled for by these same changes over time in the control site. In this study, tile discharge, quickflow and slowflow, and TP—DRP loading were analyzed using BACI study design to assess the impact of DWM treatment at F4 (Smith, 2002). For water years 2016-2017, linear regressions were performed between tile flow, slowflow, quickflow and TP—DRP loading for the impacted site (F2) as a function of the control site (F4). We used the F statistic to test the null hypothesis that the linear regressions are significant at level of  $\alpha=0.05$ . Statistical tests were performed in the Sigmaplot 13. The regression equations were used to predict tile flow, quickflow, slowflow and TP—DRP loading of F2 using the control site (F4) data for 2018 and 2019. Annual percent change in tile discharge was calculated as explained by Clausen and Spooner, 1993. The change in tile discharge, quickflow, slowflow and TP—DRP loading was determined by summing the difference between observed F2 values without DWM and predicted F2 values from F4 with DWM.

#### 5.2.3.3 Time-series Analysis

Empirical mode decomposition (EMD) was applied to investigate event-scale impacts of controlled drainage on tile flow and TP—DRP loadings. The EMD method was selected because the method is purely empirical and can be applied to a wide class of non-stationary signals, overcoming limitations of Fourier and regression-based approaches (Wu et al., 2007; Ford et al., 2015). The EMD method decomposes the time-series into a series of intrinsic mode functions (IMFs) and a residual term. Among the IMF functions, the lowest frequency one serves as the base residual trend and the one with highest frequency is considered noise, which is generally true for well-sampled datasets (Wu et al., 2007). The EMD analysis to generate IMFs was performed in MATLAB using previously published code (Rato et al., 2008). We performed a statistical significance test to determine if IMFs were significantly different from white noise. Briefly, logarithmic confidence intervals were plotted based on base noise (based on the variance of the highest frequency IMF) and a log-log relationship of variance versus mean period was plotted for each IMF on the same graph (Wu et al., 2007). Then, the IMFs that plotted outside of the specified confidence interval were considered statistically different from white noise, reflecting a significant trend in the data (Wu et al., 2007). The EMD was applied to daily tile flow and TP—DRP loading for water years 16-19 to observe the change in pattern before and after periods when the treatment was applied.

#### 5.2.3.4 High-frequency Pathway Connectivity and Hysteresis Analysis

In addition to hydrograph recession analysis, SC-EMMA was employed to each storm event to partition the storm flow into new-water ( $Q_{new}$ ) and old-water ( $Q_{old}$ )

fractions (Smith et al., 2018; see Chapter 3). Once  $Q_{quick}$ ,  $Q_{slow}$ ,  $Q_{new}$ ,  $Q_{old}$  were calculated, the approach described in Chapter 3 was used to calculate the portion of old-water that drains to the quickflow reservoir ( $Q_{quick-old}$ ), portion of new-water that drains to the quickflow reservoir ( $Q_{quick-new}$ ), portion of new-water that drains through the slowflow reservoir ( $Q_{slow-new}$ ), and the portion of old-water that drains to the slowflow reservoir ( $Q_{slow-old}$ ). In deriving this framework, we assumed that 1) if quickflow exceeded new-water, all new-water was attributed to the quickflow pathway, and 2) if new-water exceeded quickflow, then all quickflow was attributed to new-water. We partitioned the tile flow into  $Q_{quick-new}$ ,  $Q_{quick-old}$ ,  $Q_{slow-new}$ , and  $Q_{slow-old}$  for the entire 2019 water year. For each selected event (27 events), we calculated total water volume and fractions for each partitioning.

We were interested in understanding dynamics regarding within-event TSS flow pathway-connectivity dynamics and differences between the two sites. Given sediment is predominantly transported through the quick-flow pathway, we performed sediment hysteresis analysis at the control site using total tile discharge ( $Q_{Tile}$ ), new water transported through quickflow ( $Q_{quick-new}$ ) and old water transported through quick flow ( $Q_{quick-old}$ ), and compared to results from the impact site, which was conducted in Chapter 4. We used both qualitative hysteresis plots and quantitative hysteresis indices to evaluate shape and magnitude of hysteresis loops. To assess hysteresis shape, we first generated hysteresis plots based on normalized flow and TSS concentration values (e.g. Mano et al., 2009; Landers and Strum, 2013; Lloyd et al., 2016). Next, we used a hysteresis index (Lloyd et al., 2015), which provides quantitative estimates of both direction and strength of the hysteresis. The hysteresis index for each hydrograph analyzed was calculated using

the normalized flow and sediment concentration data. The hysteresis index (*HI*) was calculated every 5% of discharge. Detailed descriptions of this methodology are provided in supplemental information. Box-and-whisker plots were used to visualize distributions of HI values for  $Q_{\text{tile}}$ ,  $Q_{\text{quick-new}}$  and  $Q_{\text{quick-old}}$  hysteresis and were generated in Sigmaplot 13.

During the treatment period (WY 19) we investigated the relationship between the flow pathway-connectivity dynamics, timing of hydrograph dynamics, sediment loading and event-mean concentrations, and sediment hysteresis dynamics at our two study sites. We separated events where both sites were freely drained, and when only the control site was freely drained. Average values from the events are reported.

## **5.3 Results**

### **5.3.1 Hydrology and Hydrograph Recession Analysis**

The two study sites displayed similar surface runoff patterns, but contrasting tile-drain hydrologic behavior, even during periods before the treatment was applied. Average annual (2016 to 2019 water years) precipitation for the monitoring period was 1003 mm with maximum precipitation in spring and summer. Precipitation was greatest in WY-2019 (1263 mm) and least in WY-2016 (729 mm). Annual surface discharge was within 3% for F1 and F3 for all years. Surface runoff was highest in WY-17 when corn was growing. Cumulatively, surface runoff constituted less than 15% of total field runoff. Despite similar surface discharges, total tile discharge over the four-year monitoring period was different between the two sites and was equal to 1457 mm and 917 mm for F2 and F4, respectively. Total tile discharge was greatest in WY-2019, equal to

522 and 301.4 mm for F2 and F4, and the lowest in WY-2017, equal to 215.2 and 135.1 mm for F2 and F4, respectively.

Master recession curve analysis at both sites resulted in two discernable reservoirs reflecting a quick and slow reservoir (Figure 5.3). Reservoir 1 (R1) reflected a steeply recessing quickflow pathway, while reservoir 2 (R2) was characteristic of a mildly recessing slowflow pathway. The recession coefficients for R1 were 0.8 and 1.1  $\text{d}^{-1}$  for F2 and F4, respectively. The recession coefficients for R2 were 0.2 and 0.35  $\text{d}^{-1}$  for F2 and F4, respectively (Figure 5.3). Nash Sutcliffe Efficiency values for the optimal fit were found to be 0.7 and 0.75 for F2 and F4, respectively. Given that the recession coefficients vary by greater than three-fold and have strong goodness-of-fit, denoted by NSE values, our findings provide evidence of two distinct flow pathways for both sites (Schilling and Helmers, 2008; Rimmer and Hartmann, 2012; Husic et al., 2019).

Results of the continuous hydrograph recession analysis showed significant contributions of quickflow and slowflow at both sites, with high inter-event variability (Table 5.2; Table S.5.2). Continuous hydrograph recession results show that quickflow transported 31% and 33% of total subsurface flow to tiles in F2 and F4, respectively. Regarding events, we found that quickflow reservoir transported 34% and 43% of event subsurface flow to tiles at F2 and F4, respectively, which highlights the increased importance of slowflow contributions to tile-discharge at F2, relative to F4. Regarding within-event variability, flow pathway dynamics were highly variable between events, with quickflow contributions to total tile discharge ranging from 6% to 77% and from 1% to 88% for F2 and F4, respectively (Table S.5.2). The differences between the mean values of quickflow fractions of the two sites is 6.7 and 11.7% for WYs 2016-2017 and



WYs 2018-2019, respectively. At the F2 site, average quickflow fractions were 26% and 38% when the outlet was closed and opened, respectively. At the F4 site, average quickflow fractions were 41% and 46% when outlet was closed and opened, respectively. In general, average quickflow fractions were lower when drains were closed as compared to when they were open.

### 5.3.2 Before-After-Control-Impact (BACI) Analysis

Results of the linear regression models showed good agreement for all parameters between the two sites and provide insights into tile-drainage differences prior to treatment (Table 5.3). Linear regression analysis between F2 and F4 during the pre-treatment period showed significant regressions for all four models ( $P < 0.001$ ). The linear regression models had  $R^2$  values ranging from 0.78-0.86. Slopes of the regression lines were greater than one for most parameters, which was expected given the results for hydrology in Table 5.2 ( $Q_{Tile}$ ,  $Q_{slow}$ , and TP-DRP). However, the slope for  $Q_{quick}$  was very close to one, suggesting that differences between tile drainage at the two sites prior to treatment was likely associated with the slowflow pathway.

Results of the BACI analysis suggest that drainage water management decreased total flow, quickflow, and slowflow at the study site; however, impacts on the quickflow pathway were more prominent than total flow and slow flow (Table 5.3). Annual estimated increase in tile flow when site was freely drained was 86.5 mm, resulting in a 19.7% increase (see Table 5.3). The quickflow increased by an average of 45 mm, reflecting a 27.4% increase over projected values. Slowflow increased by 48.4 mm, which was a 17.32% increase over projected values. The results illustrate that drainage

water management had the largest relative annual impact on quickflow, although slowflow was also impacted.

Results of our BACI analysis for TP—DRP loading showed percent increases during the treatment period that were greater than percent differences in tile hydrology (Table 5.3). Estimated increases in TP—DRP loading for the free drainage site was 0.27 kg/ha, which reflected an average increase of 27%. This percent increase was greater than the percent increase in tile flow (19.7%). The finding that percent increase in loading exceeded percent increase in flowrate suggests that CD also decreased the concentration of PP. Interestingly, the percent decrease in TP—DRP loading was comparable to percent decrease in the quickflow pathway (27.4%).

### 5.3.3 Empirical Mode Decomposition (EMD) Analysis

Results of the empirical mode decomposition (EMD) analysis on tile flow showed significant IMFs at event and annual timescales at both sites, but also longer-term trends at the free drainage (treatment) site. The EMD analysis on tile flow generated eight and seven IMFs for F2 and F4, respectively (Figure 5.4.c-d). We found that four out of eight and three out of seven IMFs were statistically significant at the F2 and F4 sites, respectively. Significant trends at multiple frequencies including monthly (frequency = 0.082 year), annual (frequency ~ 1 year) and long-term (Frequencies > 1 year) were found at F2. Conversely, the long-term IMF trend was not found to be significant for F4, but similar to F2, both monthly and annual trends were found for this site.

Comparison of the sum of significant IMFs to the event-scale dynamics for both sites highlights the importance of event-scale controls on variance in the data and the

impact of the long-term trend at the free-drainage site (Figure 5.4.a-b). Visual observation of significant IMFs showed that the sum of significant IMFs noticeably deviates between the two sites when DWM was managed differently. For pretreatment and control periods, the average IMF value changed from -1.04 to 1.84 for the treatment site, F2, but remained approximately the same (-0.12 to -0.15) for the control site, F4 (see dashed lines on the Figure 5.4.a). This finding reflects the differences in significance in long-term IMFs at the site and reflects the increases in flowrate found for the treatment site in our BACI analysis. Regarding event-based dynamics, we compared the significant IMFs with frequencies less than one month (Figure 5.4.b). As can be observed, much of the variability in the sum of significant IMFs can be explained by the variability in the event-scale (or monthly) IMFs. For the pre-treatment period, the monthly trends between the two sites are relatively similar, particularly during the fall-spring. During the treatment period, we found greater fluctuations for F2 as compared to F4 when the boards were closed at F4 and similar magnitude of fluctuations when the boards were open at F4 (Figure 5.4).

Results of the EMD analysis for TP—DRP loading differed from the statistical significance tests for tile discharge. The EMD analysis for TP—DRP loading generated eight IMFs for F2 and seven IMFs for F4. We found that four out of eight and two out of seven IMFs were statistically significant at the F2 and F4 sites, respectively. Significant trends at monthly (frequency  $<0.082$  year) and annual (frequency  $\sim 1$  year) timescales were found at F2. Conversely, only event-scale trends were significant at F4.

Visual observation of significant IMFs for TP—DRP loading (Figure 5.4.a) showed that sum of significant IMFs noticeably deviates between the two sites during

treatment period. For pretreatment and control periods, average sum of significant IMF values remained approximately the same at both sites (See figure 5.5.a). Similar to event-scale flow results, during the treatment period, we found greater fluctuations for F2 as compared to F4 when the boards were closed at F4 and similar magnitude of fluctuations when the boards were open at F4. These findings highlight the importance of event-scale impacts of DWM on flow and PP loading dynamics to tile which is further investigated in the following section.

#### 5.3.4 High-Frequency Pathway-Connectivity and Sediment Hysteresis Analysis

Results of the pathway-connectivity analysis suggest that differences in flow between field sites for the quickflow pathway are primarily associated with changes in the  $Q_{quick-new}$  hydrograph (Table 5.4-5.5). Events where only the treatment site (F2) was freely drained had event  $Q_{Tile}$  values that were 6.8 mm greater at F2 than F4, and events where both sites were freely drained had event  $Q_{Tile}$  values that were 3.3 mm greater at F2 than F4, on average. Events where only the treatment site (F2) was freely drained had event  $Q_{quick}$  values that were 2.9 mm greater at F2 than F4, and events where both sites were freely drained had event  $Q_{quick}$  values that were 0.3 mm greater at F2 than F4, on average. Similarly, events where only the treatment site (F2) was freely drained had event  $Q_{quick-new}$  values that were 2.5 mm greater at F2 than F4, and events where both sites were freely drained had event  $Q_{quick-new}$  values that were 0.6 mm greater at F2 than F4, on average.  $Q_{quick-old}$  values were low, particularly for the events where both drains were open, and average values for the events were within 0.4mm for both conditions. Cumulatively these results show that differences in event-based water fluxes were associated primarily with new water transported through the quickflow pathway.

The results also highlight impact of controlled drainage on time-to-peak of separated hydrograph components. Generally, time-to-peak of the hydrograph and its separated components are lower in spring and summer as compared to winter and fall at both sites. The average hydrograph time-to-peak was 14.8 hours in winter and fall and was 8.6 hours in spring and summer at F2. Similarly, the average hydrograph time-to-peak was 17.2 hours in winter and fall and was 11.4 hours in spring and summer at the F4 site. In general, time-to-peak of hydrograph components was greater at F4 site as compared to F2 site, but with varying differences depending on CD management (Table 5.5), especially for  $Q_{quick-new}$ . Events where only the treatment site (F2) was freely drained had average time-to-peak of  $Q_{quick-new}$  of 18.42 and 20 hours for F2 and F4 site, respectively, while these values were equal to 9.14 and 9.57 at the F2 and F4 site when both sites were freely drained. Similar results were observed for  $Q_{quick}$  and  $Q_{tile}$ , but not for  $Q_{quick-old}$ . Time-to-peak of  $Q_{quick-old}$  had the opposite effect and occurred sooner than anticipated for events where the sites were managed differently. This can be observed in Table 5.5 given both sites were within 0.3 hours when only treatment site was open, but were almost 2 hours different, when both sites were freely drained. Collectively, our findings suggest that CD can delay time-to-peak of  $Q_{tile}$ ,  $Q_{quick}$  and  $Q_{quick-new}$ , but may decrease the time-to-peak of  $Q_{quick-old}$ .

Results of the TSS analysis suggest that the difference in sediment loadings of the two sites is associated not only with flow reductions but also sediment concentration reductions (Table 5.4-5.5). Events where only the treatment site (F2) was freely drained had event TSS loading values that were 12.9 kg/ha greater at F2 than F4, and events where both sites were freely drained had event TSS loading values that were 7.6 kg/ha

greater at F2 than F4, on average. In regard to concentration differences, events where only the treatment site (F2) was freely drained had event TSS concentrations values that were 18.1 mg/l greater at F2 than F4, and events where both sites were freely drained had negligible differences in event TSS concentration values between F2 and F4, on average. This finding suggests that CD decreases the sediment concentration delivered to tile outlets in addition to reducing flow volumes.

The results of hysteresis analysis showed event-to-event differences in HI values and variable impacts of CD on different components of the separated hydrographs. In general, the areas of hysteresis plots were visually greater at the CD site for all flow components, and this difference was more evident when the sites were managed differently (Figures S.5.1.a to c). Events where only the treatment site (F2) was freely drained had event HI values that were 0.27 greater at F2 than F4, and events where both sites were freely drained had HI values that were only 0.02 greater at F2 than F4, on average (Figure 5.7.c). The average HI values of  $Q_{quick-new}$  is positive and close to zero with slight differences between the two sites, which indicates proximity of TSS peak to  $Q_{quick-new}$  peak at both sites for all events.  $Q_{quick-old}$  hysteresis results were similar to  $Q_{Tile}$  in that events where only the treatment site (F2) was freely drained, event HI values were 0.15 greater at F2 than F4, and events where both sites were freely drained had HI values that were 0.04 less at F2 than F4, on average (Table 5.5). This result suggests that pathway-connectivity dynamics in CD can alter sediment delivery to tiles.

## 5.4 Discussion

### 5.4.1 Impacts of DWM on Subsurface Flow Pathway and Water Source Connectivity

Results from the pathway-connectivity analysis suggested that DWM significantly reduced subsurface quickflow of new water. Results from the empirical mode decomposition analysis showed event-scale reductions in  $Q_{tile}$  during periods with controlled drainage was a significant reason for differences in flow between the two sites. Likewise, our results from the pathway-connectivity analysis highlighted that the differences in average  $Q_{Tile}$  between the two sites when the control site was freely drained were explained by the increase in  $Q_{quick}$ , and more specifically  $Q_{quick-new}$  (Figure 5.7). Cumulatively, the BACI results suggest the quickflow pathway was reduced by nearly 27% because of CD, which was substantially higher than that of slowflow and total tile flow. While previous studies have hypothesized that DWM can influence preferential flow path dynamics (Cooke and Verma, 2012; Williams et al., 2015; Saadat et al., 2018), this is one of the few studies to directly quantify impacts. Our study provides quantitative evidence that DWM reduces preferential transport of event water and highlights the efficacy of the pathway-connectivity approach for assessing these dynamics in other systems.

Contrary to anticipated results, surface runoff was negligible compared to tile discharge during the treatment period, despite higher than average precipitation in 2018-2019 (Table 5.2). Studies have often shown that reductions in subsurface drainage have increased surface runoff (e.g. Ale et al., 2008; Singh et al., 2007; Drury et al., 2009; Skaggs et al., 2010). In our study, this result may reflect the use of conservation tillage practices at the study site which are well recognized to promote establishment and

connectivity of macropore flow to tile drains (e.g. Jarvis, 2007; Cullum, 2009; Williams et al., 2015). In addition, soils without vegetation often enhance macropore flow (Simard et al., 2000) and our study site was fallow during most of the high-frequency data collection efforts during the treatment period. While more robust datasets that are collected throughout the extent of the BACI monitoring period are needed to control for other environmental drivers, our results suggest that DWM may be an effective method for cumulatively reducing quickflow from both overland and subsurface preferential pathways in similar fine-textured tile drained landscapes with conservation tillage practices.

In addition to altering magnitude of hydrologic pathways and water source connectivity, results also showed differences in time to peak. In general, DWM increased time-to-peak of  $Q_{Tile}$ ,  $Q_{quick}$ , and  $Q_{quick-new}$ , but decreased the time-to-peak for  $Q_{quick-old}$ . Several previous studies have suggested that elevated water tables associated with CD can dampen peak flow and increase time-to-peak of drainage discharge (Robinson and Rycroft 1999; Lahdou et al., 2018). Our results provide further insight and suggest that delayed time to peaks are associated with new water transported through preferential pathways. However, preferential transport of old water due to matrix-macropore exchange had an earlier peak than expected when sites were managed differently. The shorter time to peak differences associated with  $Q_{quick-old}$  for the controlled drainage events likely reflects the higher soil moisture conditions which promote more rapid exchange between the matrix and macropore domains. Previous studies have highlighted that CD increases soil moisture conditions (e.g. Singh et al., 2007; Ale et al., 2008). Furthermore, previous studies support that the greater saturation of soils results in greater



rates of matrix-macropore exchange (Nazari et al., 2020), and macropore–matrix interaction leads to an initiation of macropore flow after a moisture threshold is exceeded and is a significant driver of saturated macropore flow (Klaus et al., 2013; Tokunaga and Wan 1997; Cey and Rudolph 2009; Bishop et al., 2015; Callaghan et al., 2017). This finding, in part, may contribute to the variable impacts that DWM has on water quality, particularly in systems where matrix-macropore exchange comprises a significant portion of the subsurface preferential flow budget (Weiler and Naef, 2003; Klaus et al., 2013; Callaghan et al., 2017; see chapter 4). Further application of this approach across landscape gradients could advance our understanding of not only tile drain impacts on preferential flow, but more broadly the impact of water table dynamics on preferential flow in fine-textured soils.

Results of the study also suggest longer term impacts of DWM, particularly on the slowflow pathway, which likely reflects increased lateral seepage and evapotranspiration at the controlled drainage site. Given the event-scale impacts were primarily associated with reduction in quick flow, the slow flow reductions identified by the BACI analysis were likely associated with longer-term significant IMFs, found from the tile flowrate empirical mode decomposition analysis. Our EMD analysis showed long-term deviations of tile flow signals with a substantially higher sum of IMFs at F2 during the treatment period as compared with F4, despite similar mean IMF values during the control period (Figure 5.4.a). We postulate that these longer-term IMFs were associated with longer-term impacts of DWM on the soil water storage dynamics including lateral seepage and evapotranspiration, which have commonly been reported to increase as a result of controlled drainage (Thorp et al., 2008; Ale et al., 2008; Skaggs et al., 2010; Liu et al.,

2019; Shedekar et al. 2020). As will be discussed in the following section, these slowflow alterations had little impact on sediment or TP-DRP dynamics, although they could be important for biochemical processes that could alter soluble contaminant transport and should be considered as a potential driver in how controlled drainage impacts nutrient budgets holistically.

#### 5.4.2 Impacts of DWM on Sediment and PP Dynamics in Tile-Drainage

The findings of this study suggest that TP—DRP loadings were primarily associated with the quickflow pathway, highlighting the importance of preferential flows on PP delivery to tile drainage at the study site. Results from the BACI analysis that showed higher TP-DRP reductions as compared to tile flow suggest PP load reductions by DWM is only partly explained by volumetric flow reductions. Nevertheless, volumetric flow reductions in  $Q_{quick}$  were similar (on average) to the reductions for TP-DRP. Further, the long-term EMD analysis of PP loading highlighted the significance of event-scale IMFs for PP, analogous to observations in  $Q_{tile}$  that were associated with  $Q_{quick}$ , but lacked significant IMFs for longer-term dynamics that reflected alterations to the slowflow pathway. Our finding that much of the PP load is associated with macropore flow is consistent with descriptions provided by others that have studied sediment and PP delivery to tile (e.g. Oygarden et al., 1995; Unsitalo et al., 2001; Stone and Krishnappan, 2001; Paasonen and Koivusali, 2006; Schilling and Helmers, 2008; see Chapter 4). Nevertheless, few studies have directly quantified preferential flow dynamics for long-term assessments. Our results provide direct evidence of the importance of quick flow reductions for mitigating downstream particulate nutrient transport and similar analyses

could be easily implemented into existing BACI datasets given the utility of the hydrograph recession analysis methodology for the controlled drainage site.

Our pathway-connectivity results further suggest that PP load reductions under controlled drainage likely stemmed from both volumetric reductions of  $Q_{quick-new}$  and subsurface retention processes that decrease tile sediment concentrations. Generally, our findings suggested that sediment exhibited slightly clockwise hysteresis for the  $Q_{quick-new}$  pathway at both sites for all events and did not show differences in HI values for events where only the treatment site was open versus when both sites were open (Table 5.5). However, we did find a shift to more negative hysteresis for  $Q_{tile}$  and  $Q_{quick-old}$  for the CD site during the treatment period (Table 5.5). These findings suggest that the sediment is transported predominantly through the quick-new hydrograph even under controlled drainage, and that the peak occurs later in the hydrograph because of delayed  $Q_{quick-new}$  peaks. Further, results showed higher sediment concentrations at F2 than F4 during the treatment period as compared to the freely drained period. Previous studies in tile-drained fields have indicated that particle sieving and retention can occur when particles are transported to subsurface drains (Jarvis et al., 1999; Turtola et al., 2007; Burkhardt et al., 2008; van den Bogaert et al., 2016; Turunen et al., 2017). We postulate that the delayed  $Q_{quick-new}$  peak imposed by DWM increased the distance and time for particles to move from source to sink within subsurface paths, which consequently resulted in more filtration and sieving of particles and reduced TSS concentrations at the CD site. Retention and sieving processes have been rarely studied in the context of sediment balances and modeling, although studies have indicated that subsurface transport processes can have a major role in the sediment loads (e.g. Øygarden et al., 1997;

Uusitalo et al., 2001; Turtola et al., 2007; Bechmann, 2012; Warsta et al., 2013; Turunen et al., 2017). This finding underscores the importance of hydrologic pathway and source water connectivity dynamics for informing sediment and PP loading dynamics in tile-drained landscapes.

While our results illustrate subsurface retention, it is unclear based on existing data whether sediment composition changed during transport from source to sink. Larger particles can be retained in the soil and clog soil pores, resulting in transport of smaller size particles, similar to fluvial transport processes that generally result in downstream fining due to the preferential mobilization and transport of the small and less dense soil particles (Slattery and Burt, 1997; Di Stefano and Ferro, 2002; Asadi et al., 2011; Koiter et al., 2015; Guan et al., 2017). The source and particle size distribution of sediments will impact the elemental composition of P, and subsequently sediment loads (Michaud and Laverdiere, 2004; McDowell et al., 2001; Poirier et al., 2012; Perks et al., 2015; Collins et al., 2019; Jiang et al., 2020). Future studies should collect sediment datasets for their BACI studies that are sensitive to these changes such as stable isotopes (e.g. Glaser et al., 2005; Oerter et al., 2017; Upadhyay et al., 2017), P:N elemental ratios of sediments (Nazari et al., 2020), and particle size distributions (Ulen et al., 2004; Stone et al., 2011; Poirier et al., 2012; Wilson et al., 2020). Further understanding of how source composition changes in freely and controlled drained landscapes will aid management by informing agricultural water management models.

## **5.5 Conclusion**

This study investigated annual and event-scale impacts of Drainage Water Management (DWM) on water budget, subsurface flow pathways, sediment, and

particulate P loading and concentration dynamics in a tile-drained agroecosystem. Based on our analysis, we found that DWM did not change surface runoff but decreased total flow, slowflow and, more prominently, quickflow. DWM decreased both TP—DRP and TSS loadings due to both flow reductions and PP and sediment concentrations. Long-term time series analysis reflected intra-annual and event-scale importance of flow and TP—DRP loadings and deviation between flow and TP—DRP loading signals when the sites were managed differently. The results highlighted that the differences in flow between sites for the quickflow pathway are primarily associated with changes in the  $Q_{quick-new}$  hydrograph. We also found that DWM can delay time-to-peak of all flow components, and shortened time to peak of matrix-macropore flow. The findings of this study suggest that TP—DRP loadings were primarily associated with the quickflow pathway, highlighting the importance of preferential flows on PP delivery to tile drainage at the study site. The delayed  $Q_{quick-new}$  peak imposed by DWM increased the distance and time for particles to move from source to sink within subsurface paths, which consequently resulted in more filtration and sieving of particles and reduced TSS concentrations at the CD site.

## 5.6 Figures and Tables

Table 5.1 Control structure management periods for F2 and F4 in WY 16-19.

Date	Structure Status	
	F2	F4
9/30/2015-10/27/2015	Open	Open
10/27/2015-5/7/2016	Close	Close
5/7/2016-5/27/2016	Open	Open
5/27/2016-4/22/2017	Close	Close
4/22/2017-6/24/2017	Open	Open
6/24/2017-11/17/2017	Close	Close
11/17/2017-12/18/2017	Open	Open
12/18/2017-3/20/2018	Open	Close
3/20/2018-06/25/2018	Open	Open
06/25/2018-07/18/2018	Open	Close
07/18/2018-10/31/2018	Open	Open
10/31/2018-04/02/2019	Open	Close
04/02/2019-08/07/2019	Open	Open
08/07/2019-09/30/2019	Open	Close

Table 5.2 Summary four years of surface and tile discharge, quickflow and slowflow for subsurface drain sites F2 and F4.

	<b>Precip (mm)</b>	<b><math>Q_{surface}</math> (mm)</b>		<b><math>Q_{tile}</math> (mm)</b>		<b><math>Q_{quick}</math> (mm)</b>		<b><math>Q_{slow}</math> (mm)</b>	
		<b>F1</b>	<b>F3</b>	<b>F2</b>	<b>F4</b>	<b>F2</b>	<b>F4</b>	<b>F2</b>	<b>F4</b>
<b>2016</b>	728.94	11.6	11.3	346.0	249.7	66.3	60.4	279.7	187.6
<b>2017</b>	969.59	113.0	110.2	215.2	135.1	41.7	28.4	173.5	106.6
<b>2018</b>	1051.13	7.6	7.4	374.6	230.9	160.6	102.5	212.7	128.5
<b>2019</b>	1263.52	25.3	24.7	522.0	301.4	183.2	115.3	338.4	186.1
<b>Average</b>	1003.3	39.375	38.4	364.45	229.275	112.95	76.65	251.075	152.2

Table 5.3 Before-After-Control-Impact (BACI) results. Effect of DWM on annual tile flow, quickflow and slowflow. The values in the table are observed values of F2 without DWM and predicted F2 values with DWM using F4 observed values and generated regression equations using data from water year 2016 and 2017.

<b>Year</b>	<b>Predicted</b>	<b>Observed</b>	<b>Difference</b>	<b>Percent Increase</b>
<b>Tile Flow (mm)</b>				
2018	276.53	333.29	56.76	17.03
2019	405.82	522.03	116.21	22.26
<b>Avg</b>	341.17	427.66	86.48	19.65
<b>Quickflow (mm)</b>				
2018	106.04	143.07	37.03	25.88
2019	130.26	183.24	52.98	28.91
<b>Avg</b>	118.15	163.15	45.01	27.40
<b>Slowflow (mm)</b>				
2018	163.08	188.88	25.79	13.66
2019	267.46	338.50	71.04	20.99
<b>Avg</b>	215.27	263.69	48.42	17.32
<b>TP-DRP (kg/ha)</b>				
2018	0.52	0.66	0.14	20.94
2019	0.82	1.22	0.41	33.12
<b>Avg</b>	0.67	0.94	0.27	27.03

$$F2_{\text{Tileflow}} = 1.1778 \times F4_{\text{Tileflow}} + 0.0029 \quad R^2 = 0.86.$$

$$F2_{\text{Quickflow}} = 1.0389 \times F4_{\text{Quickflow}} + 0.0006 \quad R^2 = 0.82.$$

$$F2_{\text{Slowflow}} = 1.1921 \times F4_{\text{Slowflow}} + 0.0026 \quad R^2 = 0.78.$$

$$F2_{\text{TP-DRP}} = 1.2149 \times F4_{\text{TP-DRP}} + 0.003 \quad R^2 = 0.79.$$



Table 5.4 Event-to-event Pathway connectivity, sediment and TP-DRP loading and concentrations, and HI values.

	Start Time	End Time	Quick-new		Quick-old		TSS Load		Event TSS		TP-DRP load		Event TP-DRP		HI Values					
			(mm)		(mm)		(kg/ha)		(mg/l)		(kg/ha)		(mg/l)		$Q_{tile}$		$Q_{quick-new}$		$Q_{quick-old}$	
			F2	F4	F2	F4	F2	F4	F2	F4	F2	F4	F2	F4	F2	F4	F2	F4	F2	F4
S1	11/1/2018 0:30	11/9/2018 10:00	12.6	6.94	8.9	6.24	21.46	23.94	64.62	133.7	0.02	0.01	0.06	0.03	0.02	-0.1	0.17	0.2	-0.27	-0.4
S2	11/9/2018 11:30	11/12/2018 23:30	0.1	0.01	0.4	0.22	0.21	0.07	5.3	0.96	0.00	0.00	0.06	0.02	-0.1	-0.1	0.04	0	-0.3	-0.1
S3	11/25/2018 19:30	11/30/2018 4:00	11.4	5.63	2.2	1.22	46.35	26.94	212.8	236.3	0.08	0.04	0.19	0.17	0.05	-0.2	0.16	0.1	-0.54	-0.5
S4	12/1/2018 0:00	12/5/2018 22:30	6.7	3.74	1.2	1.38	22.06	12.51	130.9	129.7	0.01	0.01	0.03	0.10	-0.2	-0.4	-0.2	0.1	-0.44	-0.7
S5	12/20/2018 12:00	12/27/2018 4:00	5.2	3.82	2.7	2.71	25.76	14.51	157.4	154.6	0.03	0.02	0.12	0.09	-0.2	-0.3	0.01	0.1	-0.67	-0.6
S6	12/27/2018 4:30	12/31/2018 7:00	0.3	0.12	0.7	0.66	2.35	0.92	42.73	33.1	0.02	0.00	0.15	0.02	-0.2	-0.7	0.03	0.2	-0.5	-0.7
S7	12/31/2018 7:30	1/5/2019 23:30	10.9	6.14	1.8	1.45	58.68	29.83	268.3	237.7	0.08	0.02	0.25	0.12	-0.2	-0.4	-0.1	0.1	-0.44	-0.6
S8	1/21/2019 18:00	1/31/2019 7:00	23.1		3.8		28.95		83.07		0.06		0.11		-0.2		-0.1		-0.34	
S9	2/12/2019 0:00	2/14/2019 12:00	1.5		0.3		2.12		37.06		0.01		0.10		-0		0.11		-0.16	
S10	2/14/2019 12:30	2/19/2019 17:00	3.6		0.2		5.25		54.29		0.01		0.07		-0.1		-0.1		-0.29	
S11	2/20/2019 14:24	2/21/2019 10:04	2.5		0.2		2.46		56.29		0.01		0.10		0.15		0.08		-0.72	
S12	2/23/2019 13:00	2/26/2019 3:30	6.8	6.59	1.5	1.68	24.04	17.77	190.2	120.3	0.03	0.01	0.14	0.12	0.06	-0.1	0.09	0	-0.22	-0.4
S13	3/9/2019 15:00	3/13/2019 8:00	4.83	3.86	0.3	0.59	30.77	15.13	242	211.6	0.03	0.03	0.20	0.35	0.1	-0.3	0.17	0	-0.62	-0.5
S14	3/13/2019 8:30	3/20/2019 9:00	7.1	4.31	1.3	1.44	47.08	19.33	183.4	145.5	0.08	0.03	0.25	0.16	-0.2	-0.2	-0	0	-0.5	-0.4
S15	3/20/2019 17:00	3/26/2019 17:30	1.26	0.64	1.5	1.3	5.5	2.24	48.71	43.18	0.01	0.00	0.08	0.06	-0.1	-0.6	0.17	0.1	-0.37	-0.8
S16	3/28/2019 0:00	4/4/2019 3:30	11.3	6.05	2.5	1.45	50.47	23.15	180.8	153.5	0.07	0.03	0.15	0.12	0.06	-0.1	0.19	0	-0.55	-0.6
S17	4/18/2019 15:36	4/20/2019 4:04	6.08	7.28	0.4	1.07	48.45	30.04	293.3	222.6	0.09	0.06	0.36	0.29	0.42	0.41	0.06	0.1	-0.78	-0.8
S18	4/20/2019 4:33	4/25/2019 7:26	8.72	6.03	0	0.31	52.63	26.64	221.3	194.3	0.08	0.03	0.32	0.15	-0.1	-0.2	-0	0.1	NA	-0.4
S19	4/27/2019 15:00	4/29/2019 15:30	4.5	3.35	0.6	1.32	27.3	17.33	214.1	215.2	0.05	0.01	0.27	0.12	-0	-0.2	0.15	0.1	-0.45	-0.5
S20	4/30/2019 8:30	5/1/2019 13:30	0.4	0.31	0.2	0.36	6.94	3.75	156.3	116.3	0.03	0.01	0.35	0.23	-0.3	-0.3	0.14	0.2	-0.77	-0.6
S21	5/13/2019 6:00	5/16/2019 22:00	0.3	0.26	0.2	0.4	1.44	1.5	32.51	50.3	0.01	0.00	0.10	0.06	-0.3	-0.3	-0.1	0.1	-0.49	-0.4
S22	5/28/2019 3:07	5/31/2019 12:28	2.53		0		45.13		433.9		0.07		0.35		-0.2		-0.1		NA	
S23	6/13/2019 16:00	6/14/2019 23:30	1.06	0.97	0.3	0.37	5.37	7.36	135.7	209.7	0.01	0.01	0.37	0.34	-0.3	-0.3	0.03	0.1	-0.53	-2.6
S24	6/15/2019 7:00	6/19/2019 13:30	5.07	3.85	0.7	0.93	9.06	11.45	76.05	121	0.03	0.00	0.20	0.14	0.02	0.08	0.11	0.1	-0.44	-0.4
S25	7/6/2019 19:00	7/10/2019 9:30	0.03		0		0.2		31.48		0.00		0.06		0.46		-0.1		0.51	
S26	9/21/2019 15:00	9/22/2019 19:00	0.25		0.3		2.52		243.6		0.00		0.36		0.12		-0		-0.09	
S27	9/30/2019 1:30	9/30/2019 23:30	1.97	0.68	1.2	0.52	22.48	4.3	354	244.3	0.01	0.01	0.18	0.30	0.49	-0.6	0.14	0.2	0.53	-0.7

Table 5.5 Average values of flow pathway-connectivity, timing of peaks, sediment load and concentration, and HI values for different pathways for events where both sites were freely drained, and only the treatment site (F2) was freely drained.

	<b>Only treatment site open</b>		<b>Both Open</b>
<b><math>Q_{Tile}</math> (mm)</b>	F2	16.62	11.11
	F4	9.86	7.78
<b><math>Q_{quick}</math> (mm)</b>	F2	8.19	4.10
	F4	5.34	3.83
<b><math>Q_{quick-new}</math> (mm)</b>	F2	6.19	3.73
	F4	3.73	3.15
<b><math>Q_{quick-old}</math> (mm)</b>	F2	2.02	0.35
	F4	1.60	0.68
<b><math>Q_{Tile}</math> peak timing (hrs)</b>	F2	16.31	7.64
	F4	18.00	8.21
<b><math>Q_{quick}</math> peak timing (hrs)</b>	F2	18.79	8.79
	F4	20.19	9.14
<b><math>Q_{quick-new}</math> peak timing (hrs)</b>	F2	18.42	9.57
	F4	20.04	9.86
<b><math>Q_{quick-old}</math> peak timing (hrs)</b>	F2	13.31	4.86
	F4	13.65	6.57
<b>TSS Load (kg/ha)</b>	F2	27.48	21.60
	F4	14.66	14.01
<b>TSS Mean Concentration (mg/l)</b>	F2	160.09	161.33
	F4	141.89	161.33
<b>HI Value (<math>Q_{Tile}</math>)</b>	F2	-0.03	-0.08
	F4	-0.30	-0.10
<b>HI Value (<math>Q_{quick-new}</math>)</b>	F2	0.07	0.06
	F4	0.09	0.11
<b>HI Value (<math>Q_{quick-old}</math>)</b>	F2	-0.38	-0.59
	F4	-0.53	-0.55

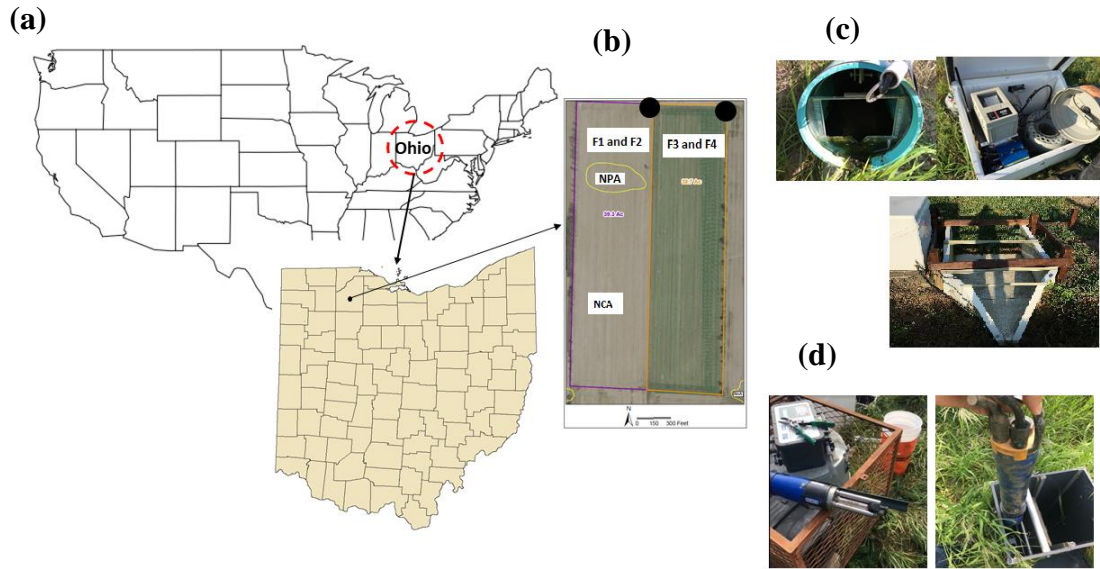


Figure 5.1 a) Study site sampling locations in Ohio, USA; b) study site delineation with location of monitoring platforms, c) typical USDA-ARS edge-of-field monitoring platforms for surface and tile drain monitoring; and d) YSI EXO3 sonde.

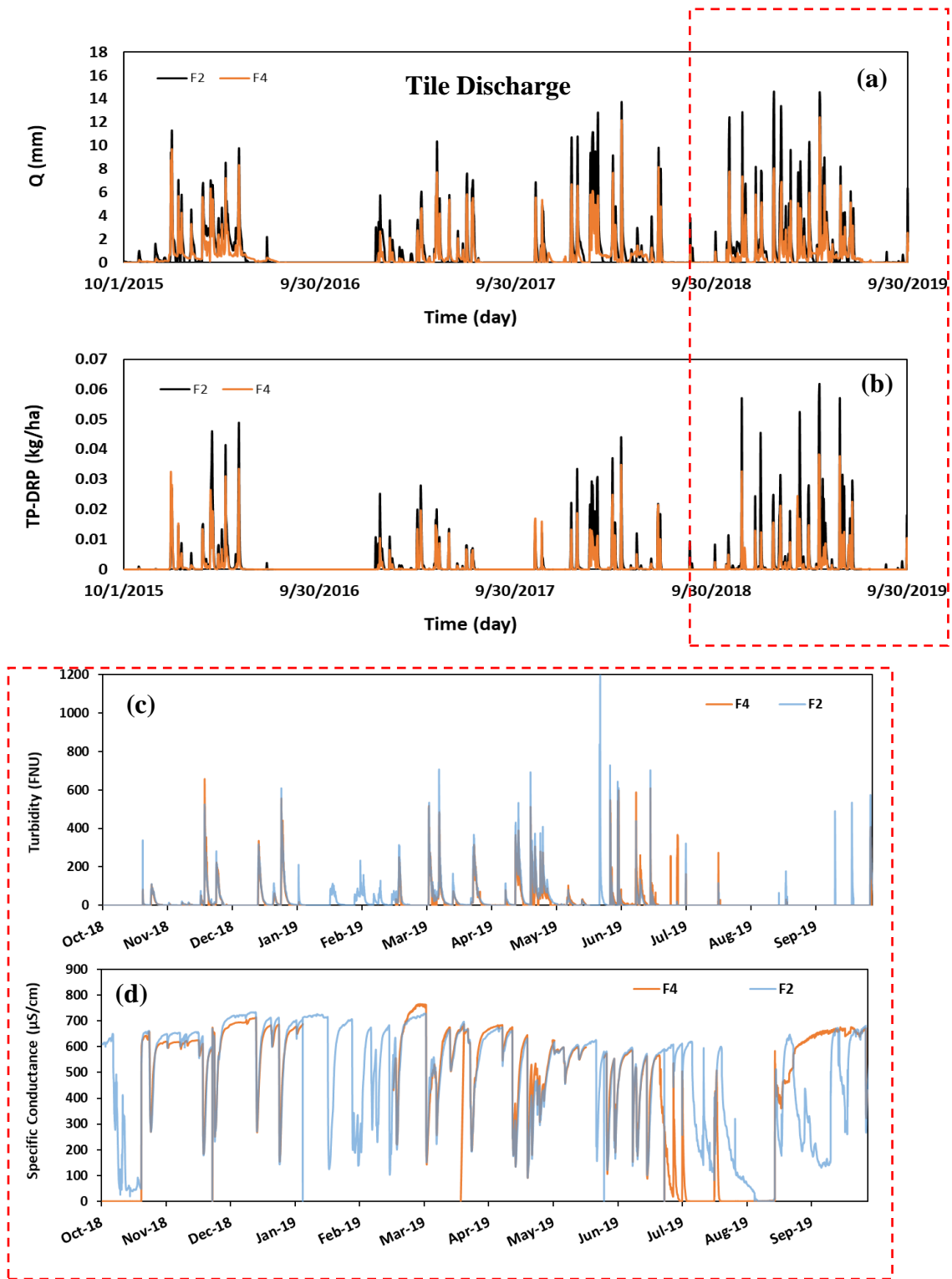


Figure 5.2 Time series of a) daily tile discharge, b) daily TP-DRP loading for 4 years; c) turbidity and d) specific conductance for WY 2019

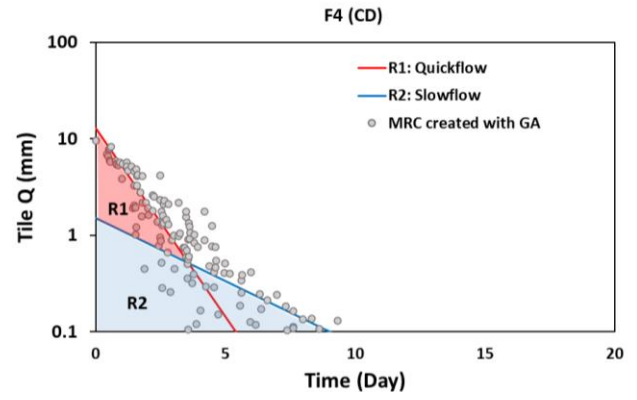
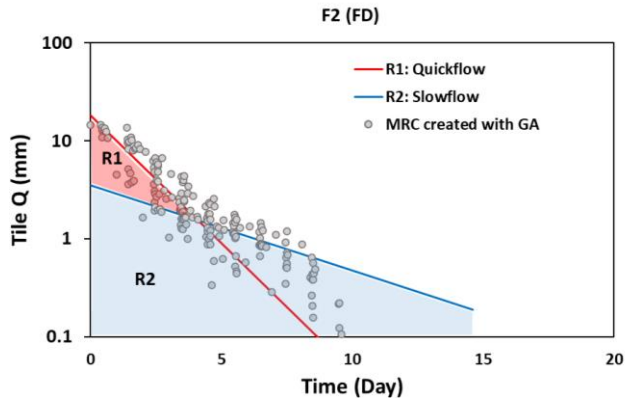


Figure 5.3 Master recession curve for a) F2 and b) F4 constructed subsurface flow recessions for water year 2019.

(a)

(b)

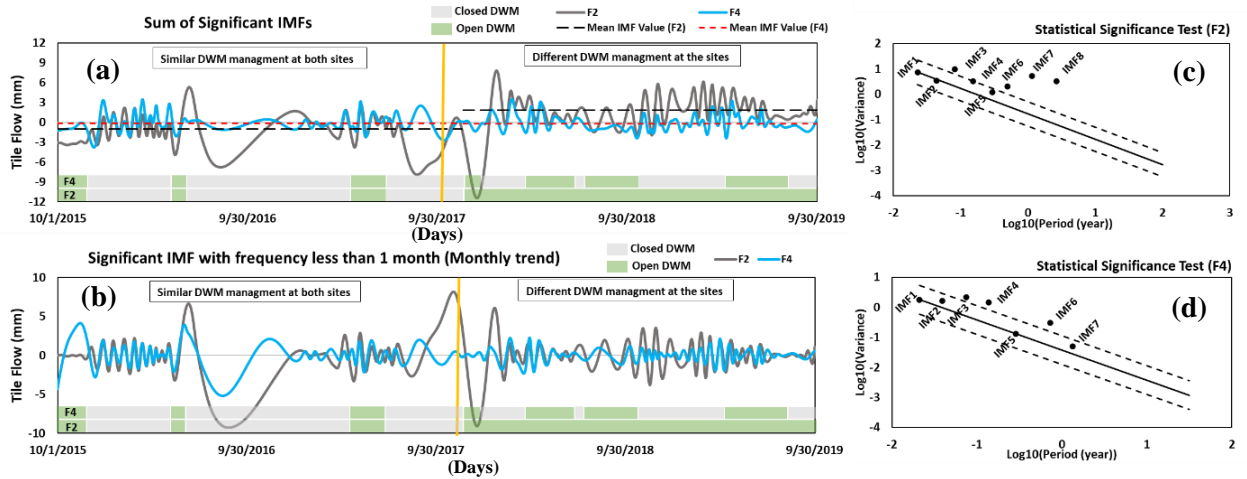


Figure 5.4 Four-year time series analysis of tile flow including a) sum of significant IMFs of tile for both sites; b) significant trends with frequencies less than one month; c) statistical significance test on IMFs of tile flow for F2, and d) Statistical significance test on IMFs of tile flow, slowflow and quickflow, respectively for F4.

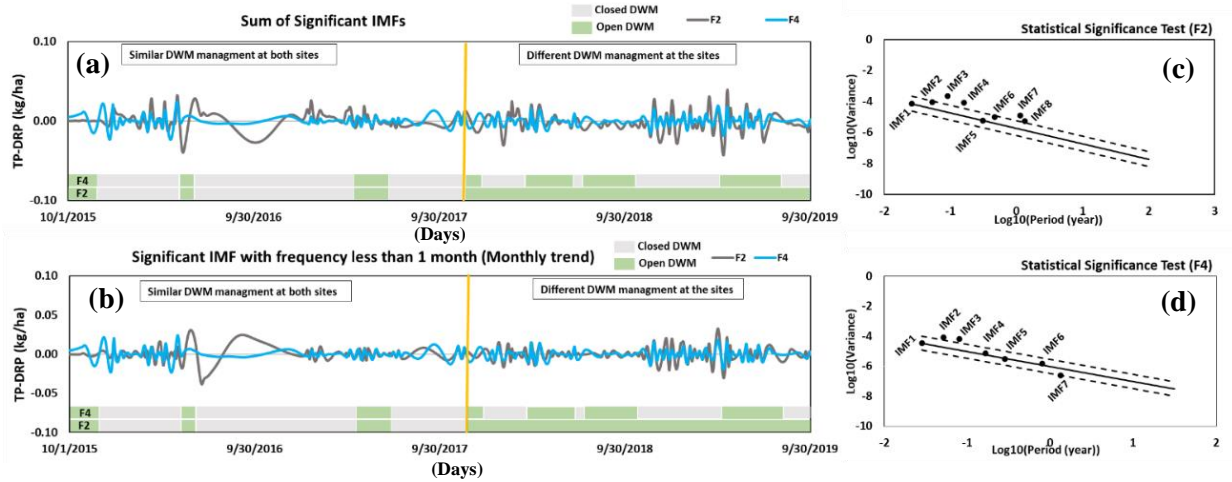


Figure 5.5 Four-year time series analysis of TP—DRP concentration a) sum of significant IMFs for F2 and F4, b) Monthly trends for F2 and F4 c) Statistical significance test on IMFs for F2, d) Statistical significance test on IMFs for F4.

## CHAPTER 6. SUMMARY

In this dissertation four main studies were conducted to understand impacts of preferential flow, source water connectivity, and agricultural management practices on dynamics of sediment and particulate phosphorus (PP) in tile-drained landscapes. The novel contributions of each study are summarized below:

### The first study:

- The use of hydrograph recession analysis for separation of tile hydrographs into quickflow and slowflow pathways was successfully tested, and we found that macropore flow plays a significant role in PP delivery at both clay and loam sites.
- The capability of Empirical Mode Decomposition (EMD) long-term time series analysis was successfully tested in tile-drained landscapes, and the results showed that PP delivery is significantly affected by environmental conditions and management practices.
- The efficacy of P/N ratio as a tracer for characterizing sediment delivery mechanisms in tiles was tested, and the results showed that that P/N atomic ratios can be used for sediment fingerprinting and unmixing models to quantify sediment source provenance in tile-drained studies.

### The second study:

- A new framework that couples hydrograph recession and SC-EMMA methods was developed to partition tile hydrograph into four pathway and water source connectivity components ( $Q_{quick-new}$ ,  $Q_{quick-old}$  (matrix-macropore exchange),  $Q_{slow-new}$  and  $Q_{slow-old}$ ).
- Using these four flow partitions improved prediction of DRP concentration as compared to only using tile flow.



- Noticeable differences in the magnitude and timing of the quick flow and new water fractions were shown with the new framework, challenging the traditional assumption that new-water is equivalent to preferential flow.
- Quickflow of new-water ( $Q_{quick-new}$ ) plays the most significant role in DRP delivery in tiles and it can be activated throughout the year under dry and saturated conditions, and is impacted by seasonal differences and precipitation patterns.
- Matrix-macropore exchange was found to have a significant role in activation of preferential flow which impacts on DRP delivery.

The third study:

- Hydrograph partitioning can improve prediction of sediment concentration, and the hysteresis analysis and multiple linear regression (MLR) results showed that  $Q_{quick-new}$  is the main pathway of sediment and PP delivery in tiles.
- Sediment concentrations were different in dry season with promoted macropores as compared to cold season with higher soil moisture and freezing and thawing effects.
- The results highlighted that seasonal differences and soil condition can impact on macropore routes and time-to-peak of preferential flow.

The fourth study:

- DWM has event-scale impacts on preferential flow and longer term impacts on slowflow.
- Tile discharge, preferential flow and sediment P are significantly impacted by DWM at the event timescale.

- DWM results in delayed  $Q_{quick}$ ,  $Q_{quick-new}$  and hydrograph time-to-peaks, but decreased time-to-peak of matrix-macropore exchange due to imposition of higher soil moisture conditions.
- DWM was found to decrease sediment and PP concentration and loadings at the study site through enhancement of subsurface filtration and decreases in preferential transport of new water.
- The differences between sediment and TP—DRP concentration reductions showed that DWM can impact on source composition of sediment, but further investigations are needed.

## CHAPTER 7. FUTURE WORK

### 7.1 Preliminary Findings

One of the major limitations of this research was the inability to quantitatively differentiate surface and subsurface derived sediment sources. Future studies should consider using more robust tracers in addition to high-frequency sensors for advancing understanding of subsurface erosion and sediment transport dynamics in tile drained landscapes, which will aid in informing agricultural water management models. In this chapter we further elaborate on the potential utility of P:N ratio of sediments and particle size distribution as a sensitive tracer of subsurface erosion and filtering processes.

In regard to sediment transport processes, few studies have assessed subsurface erosion and transport processes in tile-drained landscapes, although laboratory studies of preferential flow through undisturbed soil cores have shown that subsurface flow, ionic strength of water, matrix-macropore interaction, and subsurface filtering play key roles in subsurface sediment transport processes and thus are perceived to impact tile sediment loadings (Hendrick et al., 1993; Jacobsen et al., 1997; Schelde et al., 2002; Rousseau et al., 2004; Wilson et al., 2018). Our results and several previous studies have also indicated that eroded particles may be retained within the soil matrix due to subsurface filtering (van den Bogaert et al., 2016; Burkhardt et al., 2008; Turtola et al., 2007; Jarvis et al., 1999). Sediment retention can be due to physical ‘straining’ in pore necks, physicochemical attraction to the soil matrix, gravitational settling, and immobilization within micropores or dead-end pores (Jarvie et al., 1999). Vertical sieving may also be important. Several studies on subsurface pipeflows have illustrated an initially high sediment concentration at the beginning of leaching soil experiments with larger particle

sizes that decrease to a lower concentration sediment with finer size particles as the event proceeds (Jacobsen et al., 1997; Nouwakpo et al., 2010; Michel et al., 2010; Wilson et al., 2020). This, in part, has been attributed to mechanical entrapment of the larger particles in the active layer of macropore walls as saturation and mixing advances during events (Turtola et al., 2007; Burkhardt et al., 2008; van den Bogaert et al., 2016).

In regard to sediment source compositions, studies have traditionally attributed fine sediments in tile-drains to erosion from surface soils during storm events that are transported to tile drains *via* preferential flowpaths, thus partially bypassing the filtration capacity of the soil matrix (Michaud and Laverdiere, 2004; Turunen et al., 2017; Collins et al., 2019). The findings of this dissertation highlighted that sediment transported in tile drains are anticipated to originate from both surface and subsurface erosion sources (Nazari et al., 2020), and DWM may change sediment source compositions. Subsurface sources may reflect contributions from macropore walls, which contain a thin erodible surface layer that has temporally dynamic erodibility (Majdalani et al., 2007; Wilson et al., 2018). Alternatively, subsurface sources may reflect seepage from the matrix to preferential flow paths (i.e., matrix-macropore exchange) that can result in translocation of sediment from the soil matrix to preferential flowpaths (Wilson et al., 2018). These subsurface sources are often excluded from consideration in field-scale transport models that simulate sediment and particulate P delivery to tile (e.g., Turunen et al., 2017; Sadhukhan et al., 2018). Improved understanding of the relative importance of subsurface processes and sediment source composition are important for advancement of agroecosystem management models.

Regarding partitioning surface and subsurface sources, physical and chemical properties of transported sediments can provide insights into source and fate processes. As previously discussed, elemental P:N ratios of sediments can provide insights into sediment source provenance because P:N ratios of surface soils often deviate from the relatively stable P:N ratios of organic matter deeper in the soil profile of cultivated agroecosystems (Cleveland and Liptzin, 2007; Frossard et al., 2016; Nazari et al., 2020). However, particle size distribution of tile sediments may reflect the filtering of coarser particles during transport from surface to tile sources, as well as preferential erosion and transport of fine particles (Stone et al., 2011; Wilson et al., 2018). Such processes could alter the P:N composition. Combining P:N measures with particle size distribution may help inform the prominence of subsurface erosion/filtering processes in tile-drained landscapes.

We further analyzed long-term ambient data, (including TP, TN, DRP, and DIN) from surface and subsurface pathways for the study site in chapter 4. Long-term daily TP—DRP loading (kg/ha) were plotted against daily TN—DIN (kg/ha) loading for surface and subsurface pathways from 09/30/2016-10/01/2019. A linear regression was performed for both pathways, and hypothetical lines reflecting typical P:N ratios of organic matter were used to infer forms of PP delivered to tile, analogous to the approach detailed in Nazari et al. (2020). A subsample from ISCO samples that were used for TSS analysis in Chapter 4 were analyzed using a Laser Diffraction Particle Size Analyzer (LISST-Portable|XR) to obtain particle size distribution of sediment in water samples. Particle size distribution data between surface and subsurface pathways were compared by calculation of average, maximum and minimum  $d_{50}$  values for surface and subsurface

samples. We plotted P:N ratio versus  $d_{50}$  for surface and subsurface samples, separately and fit a power regression relationship between P:N ratio and PSD data.

The slopes of the regression line between TP—DRP and TN—DIN loadings suggested variable surface and subsurface sediment sources, as well as alterations of the surface source during transport (Figure 7.1). Results of the regression analysis suggested a surface P:N ratio of 0.18 and a subsurface P:N ratio of 0.10 at the site, both of which exceeded the range of P:N ratios for organic matter reported in agroecosystems (0.034-0.083).

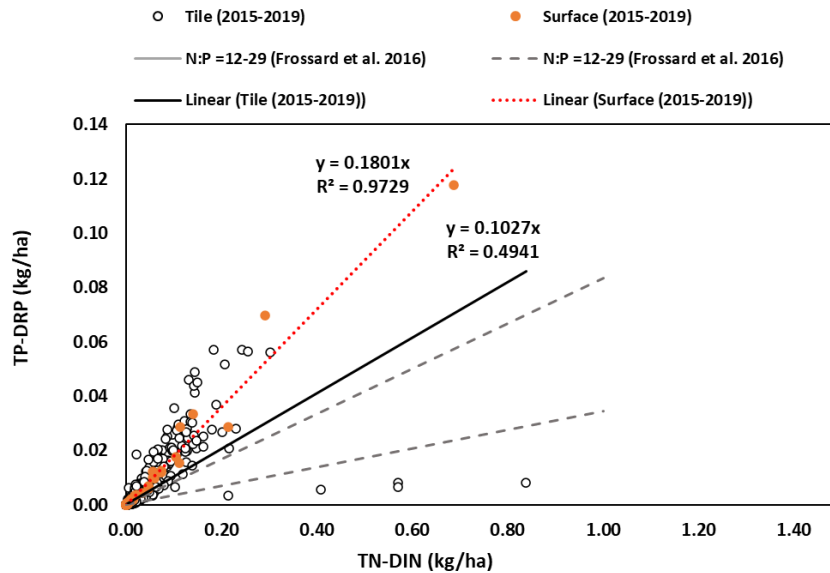


Figure 7.1 Comparison of daily flow-weighted mean concentration of total P (TP) – dissolved reactive P (DRP) and total N (TN) – dissolved inorganic N (DIN) from surface and tile runoff at the site.

The correlation between PSD and P:N ratio for surface and subsurface data were significantly different (Figure 7.2). Weak correlation ( $R^2=0.22$ ) was found between P:N ratio and  $d_{50}$  of all subsurface samples (Figure 7.2), although the model was statistically significant ( $P=0.003$ ). The relationship between P:N ratio and  $d_{50}$  of all surface samples (Figure 7.2) revealed a stronger correlation ( $R^2=0.4$ ;  $P=0.001$ ) although the number of

surface samples (n=13) were small compared to subsurface samples (n=61). The average  $d_{50}$  of subsurface and surface samples were 18.2 (min=10.1 and max=33 microns) and 21 microns (min=5.7 and max=132 microns), respectively, although Mann-Whitney rank sum test showed that there was not a significant difference (P value= 0.315) between the median values of D50 for surface and subsurface samples at 95% confidence interval.

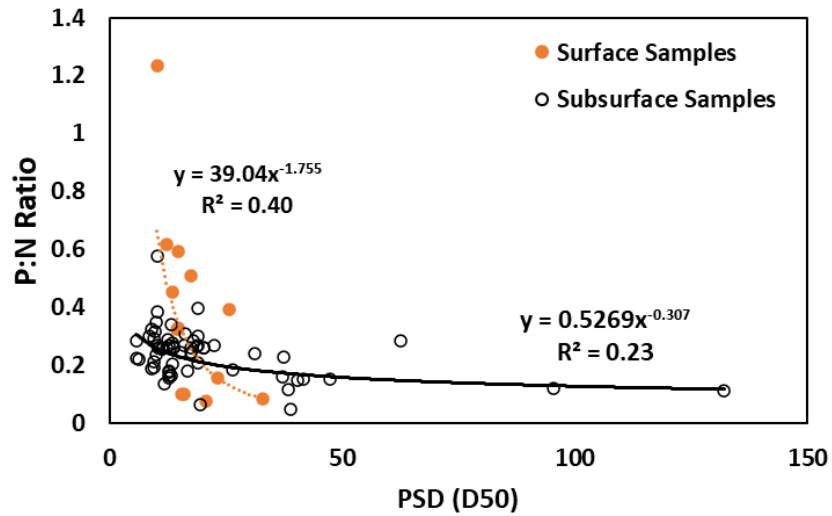


Figure 7.2 P:N ratio versus  $D_{50}$  of transported sediment for surface and subsurface samples

Results of the P:N and particle size distribution analysis suggests that tile sediments reflect variable contributions of surface and subsurface sediment sources, but also suggest removal of coarser sediment during subsurface transport, particularly at high loading conditions. Mean trendline results (Figure 7.1) showed a P:N ratio closer to a signal of soil organic matter than surface sediment samples and showed high heterogeneity for tile P:N ( $R^2 = 0.49$ ) as compared to the surface P:N ( $R^2=0.97$ ). This finding suggests tile sediments reflect a heterogenous mixture of surface and subsurface sediment sources, which agrees with findings from both clay and loam soil end-members reported in previous studies in Ohio (Williams et al., 2016; Nazari et al., 2020). Nevertheless, we

found a significant portion of samples with high TP—DRP loading that had P:N ratios far exceeding P:N of the surface source. This finding can be explained by results of our particle size distribution analysis which show that average  $d_{50}$  of tile sediments was less than surface sediments and P:N ratio increased with decreasing particle size (Figure 7.2). It is well recognized that sediment chemical properties vary as a function of size class. With regard to P:N, finer sediments have relatively higher P sorption index and lower potential P due to higher surface area as a P sorption proxy, so finer sediments should have higher P:N ratio (Stone and Mudroch, 1989; Mcdowell et al., 2001). These findings suggest that coarser sediments are removed during transport of surface sediments through preferential flow paths to tile drainage, resulting in preferential transport of P-rich fine sediments during high loading conditions. Particle filtering, or sedimentation is generally recognized to occur in subsurface sediment transport (Turtola et al., 2007; Burkhardt et al., 2008; Bogaert et al., 2016; Wilson et al., 2018). Our results highlight that coupling P:N and particle size distribution results may be useful to quantify the prominence of this process at the field-scale and should be broadly assessed across environmental gradients.

The findings that subsurface pathways may serve as both a source and sink of sediments to tile drain sediment loading at the field-scale suggests a need to revise existing agroecosystem management models to consider dynamic sediment transport processes. Processes such as subsurface erosion and subsurface sieving have not been investigated, nor incorporated to recent modeling works that have focused on sediment or particulate P detachment and delivery in subsurface drained soils and are an important area for future work (Jarvis and Larsbo 2012; Wastra et al., 2013; Turunen et al., 2017). Contrasting soil and management practices from the study sites focused upon in this



dissertation will strongly impact the composition and loading of sediment to tile drainage, hence models need to be developed generally, and evaluated over broad environmental and management gradients. Incorporating the flow pathways and processes identified in this study into existing continuous simulation numerical models (e.g., APEX, DRAINMOD, SWAT, and RZWQM2) will be critical for improving estimates of particulate-bound contaminants in tile-drained landscapes.

## APPENDICES

### APPENDIX 1. Supplemental Materials of Chapter 4

Supplemental Table S.4.1. Summary of event discharges and flow partitioning results (updated from chapter 3 to include data from Oct 2019-Dec 2019).

	Discharge (mm)	Qquick (mm)	Qslow (mm)	Qnew (mm)	Qold (mm)	Qquick-old (mm)	Qquick-new (mm)	Qslow-old (mm)	Qslow-new (mm)
<b>S1</b>	33.2	21.5	11.7	13.1	20.1	8.9	12.6	11.2	0.5
<b>S2</b>	4.0	0.5	3.5	0.1	3.9	0.4	0.1	3.5	0.0
<b>S3</b>	21.8	13.5	8.2	12.3	9.5	2.2	11.4	7.4	0.9
<b>S4</b>	16.9	7.9	9.0	7.7	9.2	1.2	6.7	8.0	1.0
<b>S5</b>	16.4	7.8	8.5	6.2	10.2	2.7	5.2	7.5	1.0
<b>S6</b>	5.5	0.9	4.6	0.4	5.2	0.7	0.3	4.5	0.1
<b>S7</b>	21.9	12.7	9.2	12.1	9.8	1.8	10.9	8.0	1.2
<b>S8</b>	34.8	26.8	8.0	24.2	10.7	3.8	23.1	6.9	1.1
<b>S9</b>	5.7	1.8	3.9	2.3	3.4	0.3	1.5	3.2	0.7
<b>S10</b>	9.7	3.9	5.8	4.4	5.3	0.2	3.6	5.1	0.7
<b>S11</b>	4.4	2.7	1.7	3.6	0.8	0.2	2.5	0.6	1.1
<b>S12</b>	12.6	8.3	4.4	7.2	5.4	1.5	6.8	4.0	0.4
<b>S13</b>	12.4	5.0	7.4	8.0	4.4	0.3	4.8	4.1	3.2
<b>S14</b>	25.0	8.2	16.8	9.7	15.3	1.2	7.1	14.2	2.6
<b>S15</b>	11.0	2.7	8.3	1.8	9.2	1.4	1.3	7.8	0.5
<b>S16</b>	27.2	13.4	13.8	13.8	13.5	2.2	11.2	11.2	2.6
<b>S17</b>	16.1	6.3	9.8	11.2	4.9	0.4	6.0	4.5	5.3
<b>S18</b>	23.2	8.5	14.7	13.7	9.5	0.0	8.5	9.5	5.2
<b>S19</b>	12.7	5.2	7.6	5.3	7.4	0.6	4.5	6.8	0.8
<b>S20</b>	4.4	0.6	3.8	0.7	3.8	0.2	0.4	3.5	0.3
<b>S21</b>	4.4	0.5	4.0	0.5	3.9	0.2	0.3	3.7	0.3
<b>S22</b>	10.1	2.5	7.7	5.3	4.9	0.0	2.5	4.9	2.8
<b>S23</b>	3.9	1.4	2.5	2.1	1.8	0.3	1.0	1.4	1.1
<b>S24</b>	11.6	5.6	6.0	6.1	5.5	0.6	5.0	4.9	1.1
<b>S25</b>	0.6	0.1	0.6	0.0	0.6	0.0	0.0	0.6	0.0
<b>S26</b>	1.0	0.5	0.5	0.3	0.7	0.3	0.3	0.5	0.0
<b>S27</b>	6.2	3.1	3.1	3.5	2.7	1.2	1.9	1.6	1.5
<b>S28</b>	2.99	0.75	2.24	0.05	2.94	0.72	0.04	2.23	0.01
<b>S29</b>	26.33	16.62	9.71	6.04	20.29	11.30	5.33	8.99	0.72
<b>S30</b>	3.25	0.69	2.56	0.07	3.18	0.63	0.06	2.55	0.02
<b>S31</b>	9.45	3.14	6.30	2.42	7.26	1.32	1.83	5.71	0.60

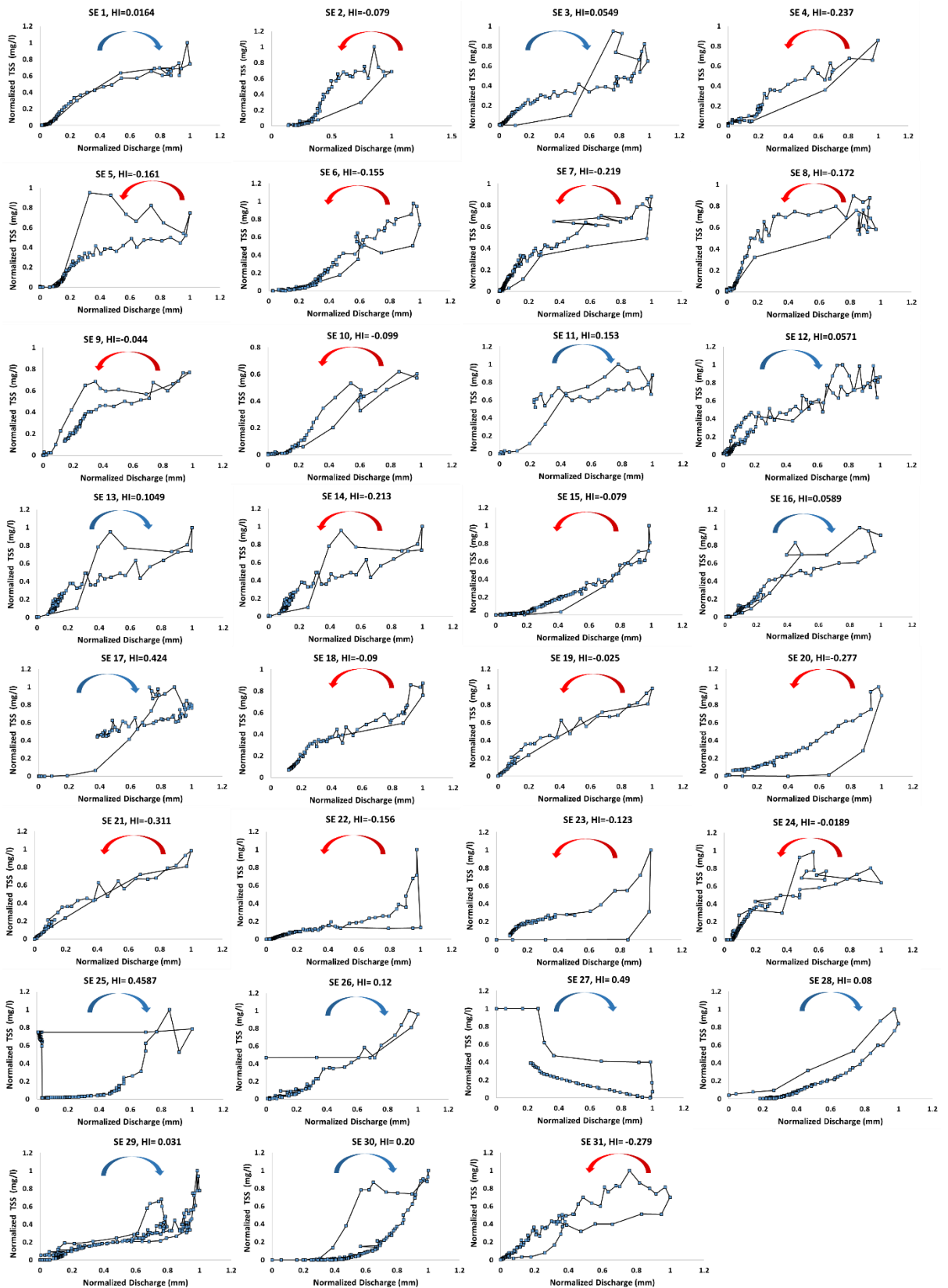


Figure S.4.1. Hysteresis plots of normalized TSS and total discharge for each event

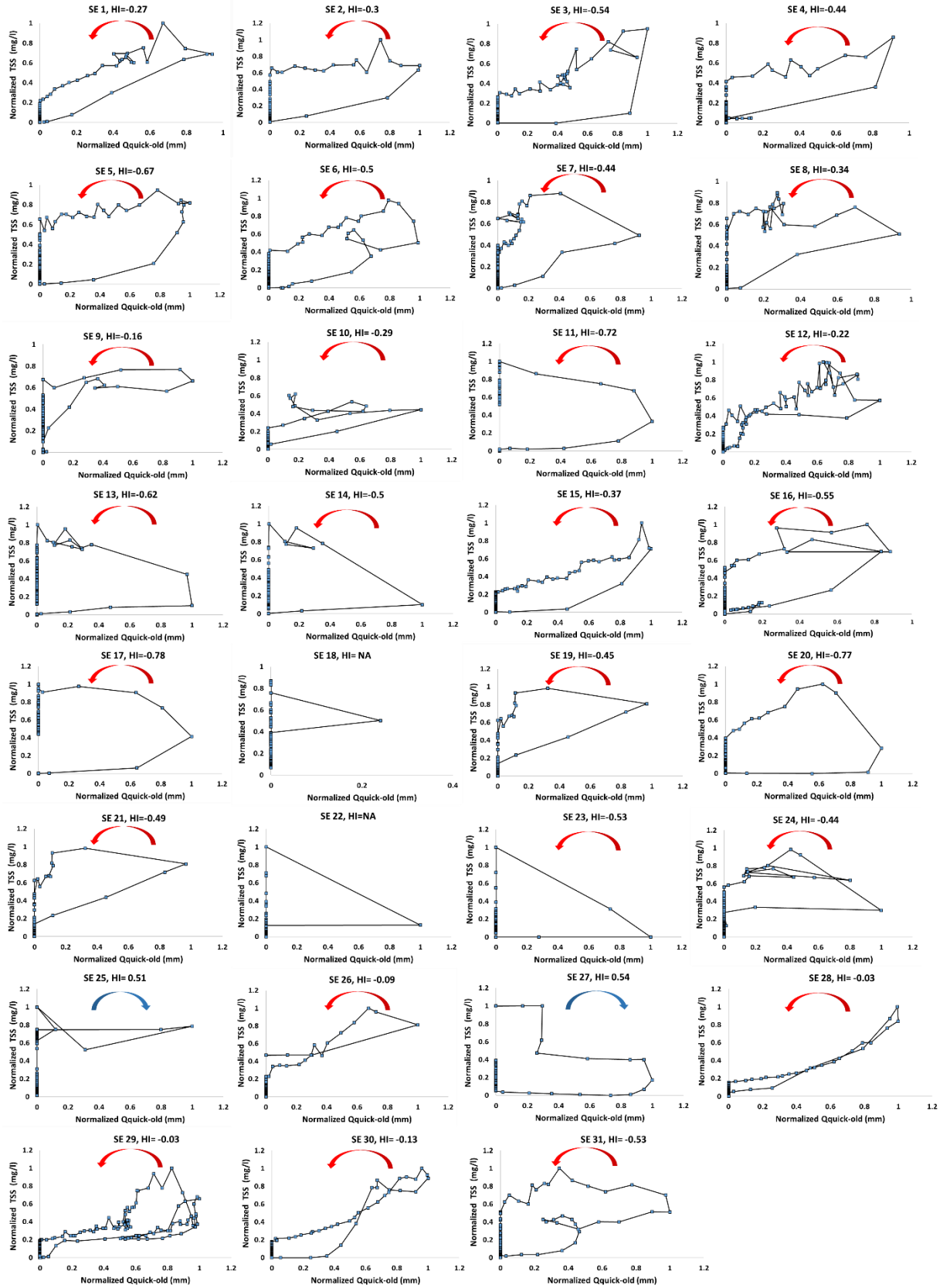


Figure S.4.2. Hysteresis plots of normalized TSS and  $Q_{\text{quick-old}}$  for each event

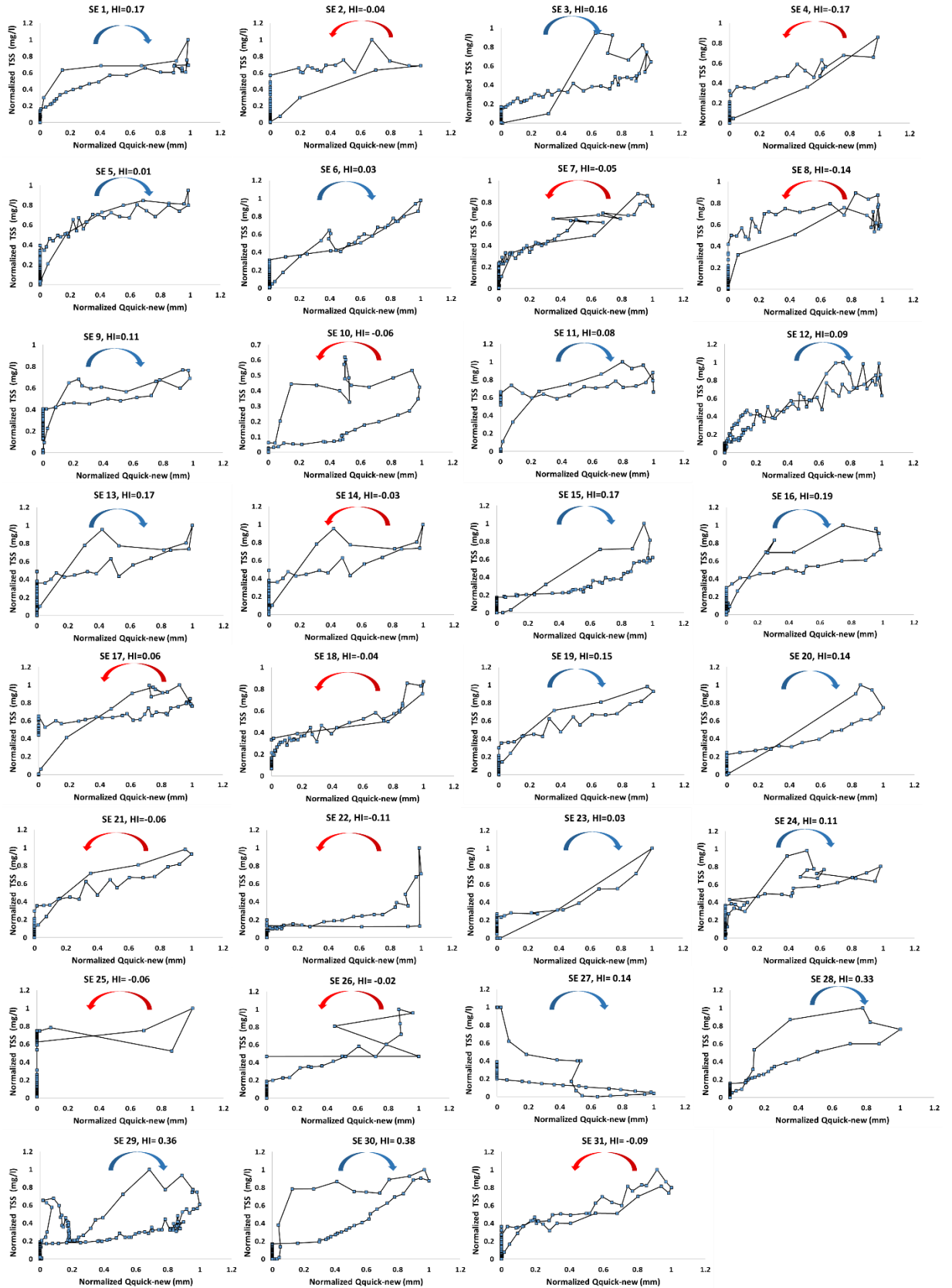


Figure S.4.3. Hysteresis plots of normalized TSS and  $Q_{\text{Quick-new}}$  for each event

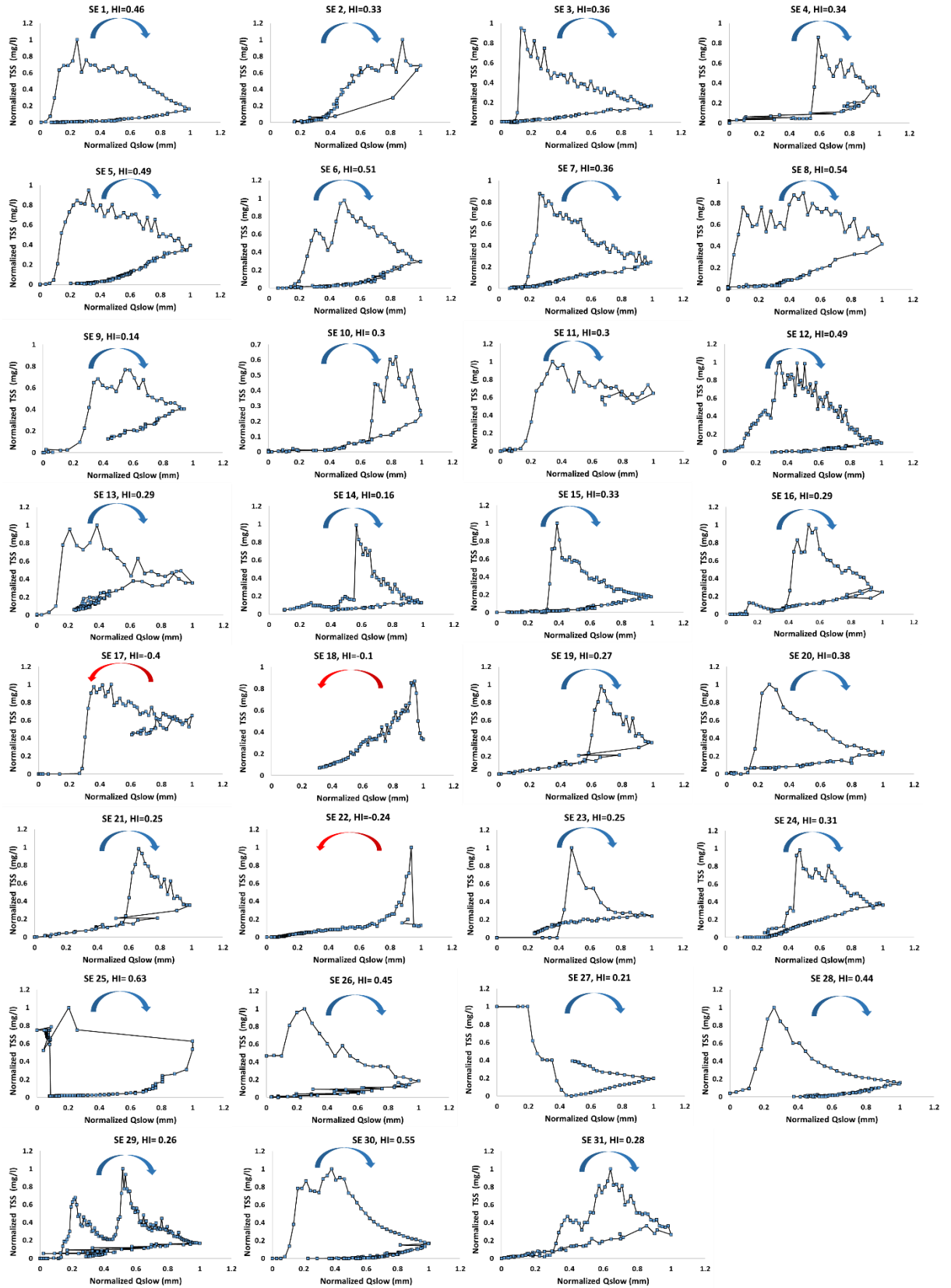


Figure S.4.4. Hysteresis plots of TSS and normalized TSS and Q<sub>slow</sub> for each event

## APPENDIX 2. Supplemental Materials of Chapter 5

Table S.5.1. Management practices and timings for F2 and F4 sites

F1/F2				F3/F4			
Date	Crop	Management Practice	Details	Date	Crop	Management Practice	Details
10/17/2015	corn	harvest	146 bu/acre	10/17/2015	corn	harvest	146 bu/acre
10/28/2015	cover	plant	56 lb/acre- Cereal rye (Broadcasted)	10/28/2015	cover	plant	56 lb/acre- Cereal rye (Broadcasted)
5/27/2016	beans	plant		5/27/2016	beans	plant	
10/11/2016	beans	harvest	46 bu/acre	10/11/2016	beans	harvest	46bu/acre
10/12/2016	cover	plant	60 lb/acre-broadcast rye	10/12/2016	cover	plant	60lbs/acre- broadcast rye
10/13/2016	cover	tillage	harrow (incorporate rye)	10/13/2016	cover	tillage	harrow (incorporate rye)
5/24/2017	corn	plant		5/24/2017	corn	plant	
5/24/2017	corn	fertilizer application	9 gal/acre (10.34.0)*	5/24/2017	corn	fertilizer application	9 gal/acre (10.34.0)
5/24/2017	corn	fertilizer application	30 gal/acre (10.0.4)	5/24/2017	corn	fertilizer application	30 gal/acre (10.0.4)
6/1/2017	corn	plant	replanted corn	6/1/2017	corn	plant	replanted corn
6/27/2017	corn	fertilizer application	200 lbs/acre (46.0.0)	6/27/2017	corn	fertilizer application	200 lbs/acre (46.0.0)
6/27/2017	corn	fertilizer application	100 lbs/acre (21.0.0)	6/27/2017	corn	fertilizer application	100 lbs/acre (21.0.0)
11/20/2017	corn	harvest	66 bu/acre	11/20/2017	corn	harvest	66 bu/acre
5/27/2018		tillage	field cultivator (tilled drive lane only)	11/20/2017	cover	plant	broadcast rye
5/29/2018		tillage	cultimulcher (tilled drive lane only)	5/27/2018		tillage	field cultivator (tilled drive lane only)
5/29/2018	soybeans	plant	150000 seeds/acre (15 inches row)	5/29/2018		tillage	cultimulcher (tilled drive lane only)
10/17/2018	soybeans	harvest	48 bu/acre	5/29/2018	soybeans	plant	150000 seeds/acre (15 inches row)
9/2/2019		tillage	disc- 3 in	10/17/2018	soybeans	harvest	59.5 bu/acre
9/21/2019		tillage	field finisher -3 in	9/2/2019		tillage	disc- 3 in
10/10/2019		tillage	5 bar harrow to level and size	9/21/2019		tillage	field finisher -3 in
10/11/2019	wheat	plant	135 lbs/acre	10/10/2019		tillage	5 bar harrow to level and size
10/11/2019	wheat	fertilizer application	250 lb/acre (20.21.20.6s)	10/11/2019	wheat	plant	135 lbs/acre
				10/11/2019	wheat	fertilizer application	250 lb/acre (20.21.20.6s)

\*The first, second and third number represent %N, % P, % K, respectively

Table S.5.2. Quickflow fractions associated with events from water years 2016 to 2019.

Event	Start Date	End Date	F2- Quickflow		F4- Quickflow	
			Fraction (%)	DWM	Fraction (%)	DWM
WY16-1	12/26/15 0:00	12/28/15 6:30	37.13%	close	15.69%	close
WY16-2	12/28/15 7:00	1/3/16 10:30	40.56%	close	46.88%	close
WY16-3	1/10/16 0:00	1/12/16 11:00	39.53%	close	57.44%	close
WY16-4	1/15/16 0:00	1/20/16 0:00	46.37%	close	52.13%	close
WY16-5	2/1/16 0:00	2/9/16 23:30	13.54%	close	24.63%	close
WY16-6	2/24/16 0:00	2/29/16 23:30	30.59%	close	38.53%	close
WY16-7	3/1/16 0:00	3/4/16 0:00	13.55%	close	39.97%	close
WY16-8	3/9/16 0:00	3/12/16 23:30	27.69%	close	47.06%	close
WY16-9	3/13/16 0:00	3/14/16 15:00	10.98%	close	17.71%	close
WY16-10	3/14/16 15:30	3/22/16 0:00	9.45%	close	14.92%	close
WY16-11	3/24/16 0:00	3/27/16 0:00	26.66%	close	31.76%	close
WY16-12	3/31/16 0:00	4/4/16 23:30	15.03%	close	33.05%	close
WY16-13	4/6/16 10:00	4/8/16 16:30	32.12%	close	48.39%	close
WY16-14	4/9/16 10:00	4/10/16 10:00	9.38%	close	15.76%	close
WY16-15	4/10/16 10:30	4/14/16 9:00	5.69%	close	7.79%	close
WY16-16	4/26/16 0:00	4/28/16 4:00	14.40%	close	22.12%	close
WY16-17	5/1/16 22:00	5/4/16 7:00	32.69%	close	42.55%	close
WY17-1	1/12/17 6:30	1/15/17 23:30	28.04%	close		close
WY17-2	1/17/17 0:00	1/19/17 11:30	31.82%	close	63.88%	close
WY17-3	1/20/17 0:00	1/23/17 4:30	27.79%	close	58.44%	close
WY17-4	1/23/17 7:00	1/28/17 23:30	8.32%	close	36.41%	close
WY17-5	2/7/17 4:30	2/10/17 5:30	42.99%	close	45.68%	close
WY17-6	2/11/17 14:00	2/13/17 13:00	17.32%	close	27.43%	close
WY17-7	2/24/17 12:00	2/27/17 5:00	19.85%	close	32.09%	close
WY17-8	3/1/17 0:00	3/4/17 23:30	9.67%	close	0.01%	close
WY17-9	3/18/17 0:00	3/20/17 0:00	25.29%	close	0.03%	close
WY17-10	3/30/17 0:00	4/2/17 4:30	49.18%	close	44.05%	close
WY17-11	5/5/17 19:30	5/10/17 23:30	21.72%	open	41.27%	open
WY17-12	5/11/17 0:00	5/15/17 23:30	49.66%	open	55.06%	open
WY17-13	5/28/17 0:00	5/31/17 23:30	51.90%	open	53.21%	open
WY17-14	6/13/17 0:00	6/17/17 23:30	45.02%	open	38.00%	open
WY17-15	6/30/17 14:00	7/3/17 23:30	39.08%	close	20.74%	close
WY18-1	11/4/17 0:00	11/9/17 23:00	71.11%	close	67.92%	close
WY18-2	11/15/17 0:00	11/16/17 23:30	15.30%	close	12.53%	close
WY18-3	1/19/18 0:00	2/7/18 23:31	36.29%	open	58.79%	close
WY18-4	2/14/18 0:00	2/18/18 23:30	60.17%	open	67.52%	close
WY18-5	2/19/18 0:00	2/23/18 23:30	42.81%	open	42.10%	close
WY18-6	2/24/18 19:30	2/28/18 10:00	27.17%	open	31.64%	close
WY18-7	3/1/18 3:00	3/14/18 23:30	48.50%	open	47.54%	close
WY18-8	3/26/18 15:00	4/2/18 23:30	46.47%	open	46.98%	open



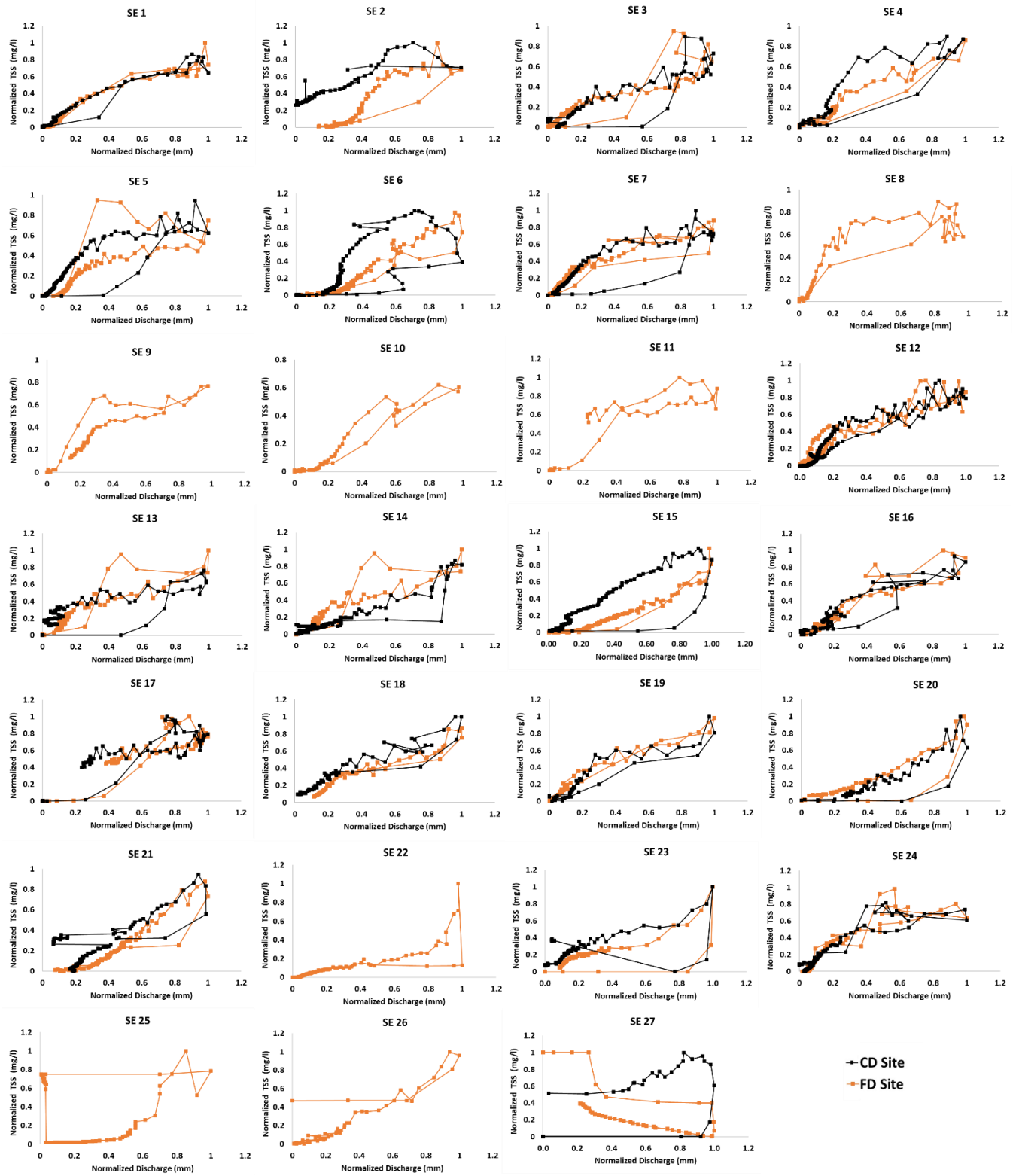
Table S.5.2. (Continued). Quickflow fractions associated with events from water years 2016 to 2019.

<b>Event</b>	<b>Start Date</b>	<b>End Date</b>	<b>F2- Quickflow Fraction (%)</b>	<b>DWM</b>	<b>F4- Quickflow Fraction (%)</b>	<b>DWM</b>
WY18-9	4/3/18 0:00	4/12/18 23:30	37.47%	open	72.69%	open
WY18-10	4/15/18 0:00	4/23/18 23:31	47.76%	open	70.15%	open
WY18-11	5/3/18 8:30	5/5/18 22:00	18.78%	open	6.54%	open
WY18-12	5/13/18 15:00	5/20/18 23:30	14.48%	open	16.66%	open
WY18-13	5/21/18 16:30	5/25/18 5:30	13.90%	open	8.34%	open
WY18-14	6/9/18 11:30	6/13/18 6:30	34.08%	open	23.64%	open
WY18-15	6/22/18 12:00	6/24/18 23:30	66.79%	open	86.29%	open
WY18-16	6/27/18 0:00	6/30/18 23:30	50.91%	open	64.49%	Close
WY18-17	8/21/18 0:30	8/23/18 23:30	42.97%	open	58.46%	open
WY18-18	8/25/18 0:28	8/28/18 23:31	34.05%	open		open
WY19-1	10/6/18 0:00	10/9/18 8:30	22.22%	open	69.29%	open
WY19-2	10/6/18 0:00	10/9/18 8:30	22.22%	open	85.80%	open
WY19-3	10/28/18 12:00	10/31/18 13:00	18.42%	open	54.21%	open
WY19-4	11/1/18 0:30	11/9/18 11:00	64.61%	open	73.64%	close
WY19-5	11/9/18 11:30	11/12/18 23:30	11.92%	open	24.73%	close
WY19-6	11/18/18 7:30	11/23/18 23:30	8.72%	open		close
WY19-7	11/24/18 0:00	11/25/18 19:00	13.45%	open		close
WY19-8	11/25/18 19:30	11/30/18 5:00	62.01%	open	66.88%	close
WY19-9	12/1/18 0:00	12/5/18 22:00	46.59%	open	53.12%	close
WY19-10	12/20/18 12:00	12/27/18 4:00	47.85%	open	69.36%	close
WY19-11	12/27/18 4:30	12/31/18 7:00	16.89%	open	27.88%	close
WY19-12	12/31/18 7:30	1/5/19 23:30	58.13%	open	60.27%	close
WY19-13	1/21/19 18:00	1/30/19 16:00	76.95%	open	87.58%	close
WY19-14	2/7/19 11:00	2/11/19 23:30	34.81%	open	22.45%	close
WY19-15	2/12/19 0:00	2/14/19 12:00	31.40%	open	55.22%	close
WY19-16	2/14/19 12:30	2/19/19 17:00	39.90%	open	54.22%	close
WY19-17	2/20/19 14:24	2/21/19 9:36	61.57%	open	55.52%	close
WY19-18	2/21/19 10:00	2/23/19 12:30	19.38%	open	20.87%	close
WY19-19	2/23/19 13:00	2/26/19 3:30	59.88%	open	18.56%	close
WY19-20	3/9/19 15:00	3/13/19 8:00	40.59%	open	62.18%	close
WY19-21	3/13/19 8:30	3/20/19 9:00	32.90%	open	43.34%	close
WY19-22	3/20/19 17:00	3/27/19 10:00	25.86%	open	37.56%	close
WY19-23	3/28/19 0:00	4/4/19 23:30	49.31%	open	49.68%	close
WY19-24	4/14/19 6:30	4/18/19 4:00	14.50%	open		close
WY19-25	4/18/19 15:36	4/20/19 4:04	39.23%	open	61.84%	open
WY19-26	4/20/19 4:33	4/25/19 8:24	36.78%	open	46.00%	open
WY19-27	4/27/19 15:00	4/29/19 15:30	40.64%	open	58.03%	open
WY19-28	4/30/19 8:30	5/1/19 13:30	14.58%	open	20.79%	open
WY19-29	5/13/19 6:00	5/16/19 22:00	10.61%	open	22.21%	open

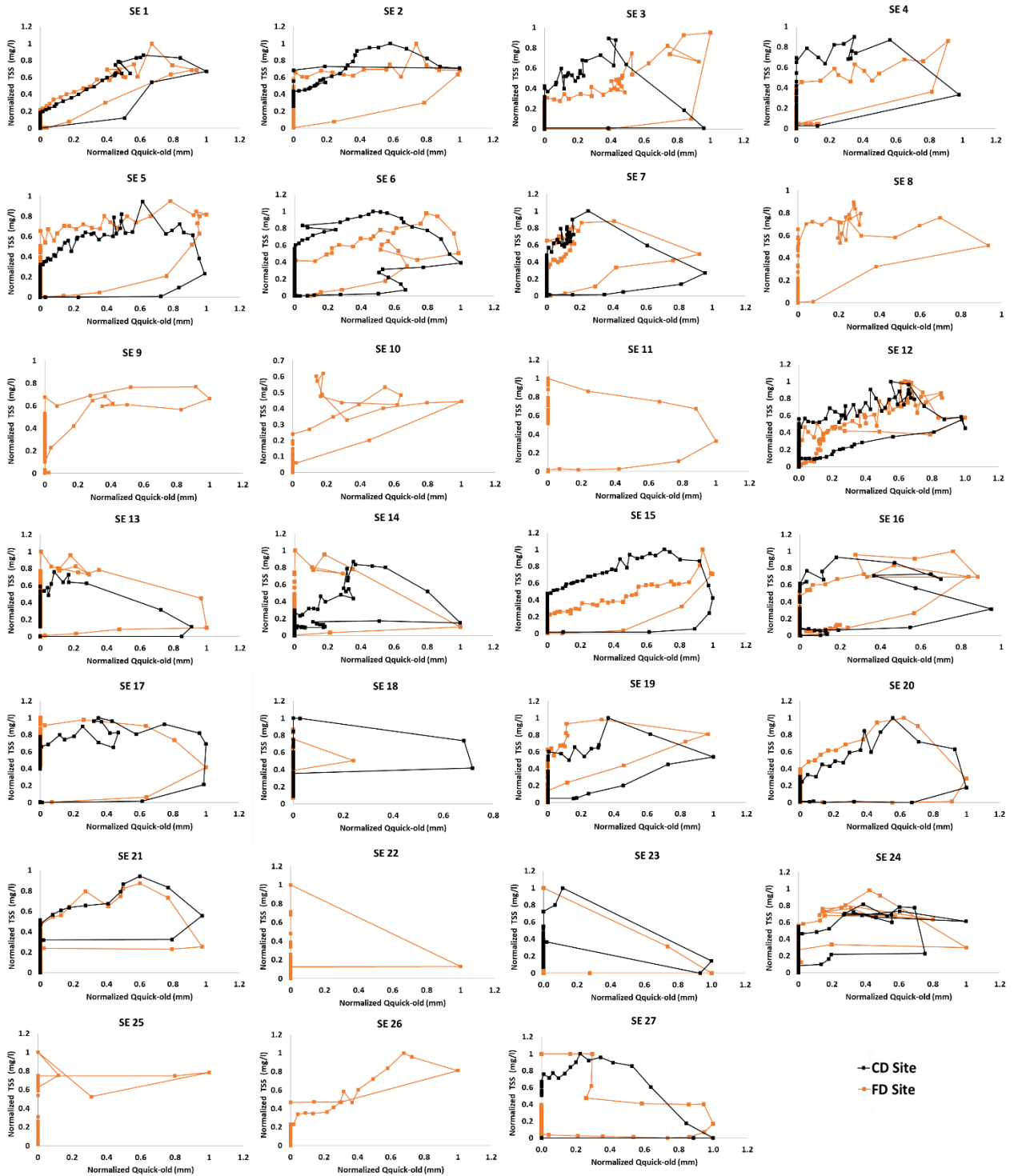
Table S.5.2. (Continued). Quickflow fractions associated with events from water years 2016 to 2019.

<b>Event</b>	<b>Start Date</b>	<b>End Date</b>	<b>F2- Quickflow Fraction (%)</b>	<b>DW M</b>	<b>F4- Quickflow Fraction (%)</b>	<b>DWM</b>
WY19- 30	5/28/19 3:00	5/31/19 12:30	24.45%	open	33.55%	open
WY19- 31	6/13/19 16:00	6/14/19 23:30	39.26%	open	38.01%	open
WY19- 32	6/15/19 7:00	6/19/19 14:30	48.11%	open	50.40%	open
WY19- 33	7/2/19 13:00	7/6/19 8:30		open	28.50%	open
WY19- 34	7/2/19 13:00	7/6/19 8:30		open	42.13%	open
WY19- 35	9/21/19 15:00	9/22/19 19:00	50.15%	open		close
WY19- 36	9/30/19 1:30	9/30/19 23:30	50.44%	open		close

a)



b)



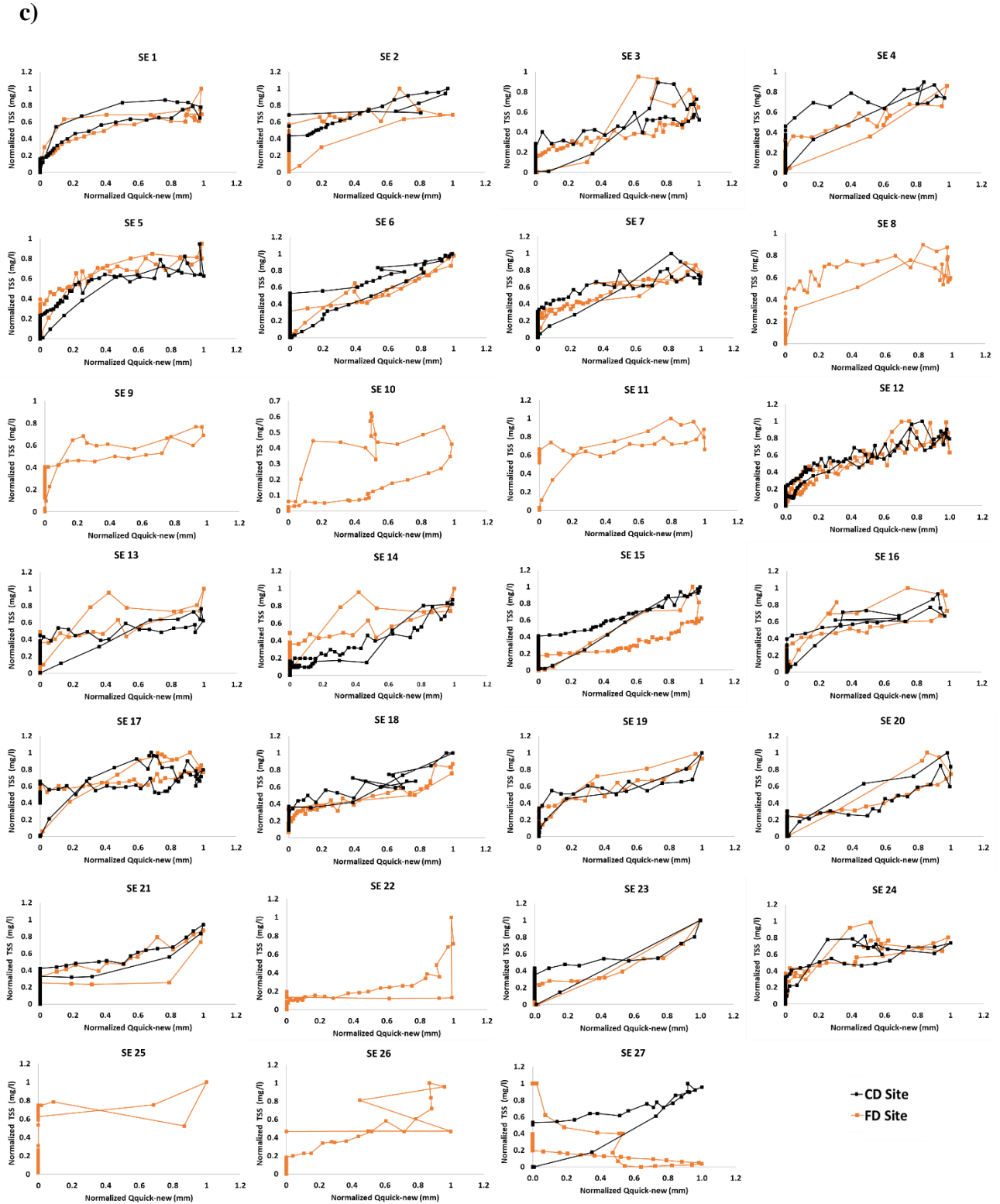


Figure S.5.1. Hysteresis plots of normalized TSS Vs a) normalized discharge b) normalized Quick-old and c) normalized Quick-old for each event for FD and CD site

## REFERENCES

- Addy, K., Gold, A. J., Christianson, L. E., David, M. B., Schipper, L. A., & Ratigan, N. A. (2016). Denitrifying bioreactors for nitrate removal: A meta-analysis. *Journal of Environmental Quality*, 45(3), 873-881.
- Akay, O., Fox, G.A., 2007. Experimental investigation of direct connectivity between macropores and subsurface drains during infiltration. *Soil Sci. Soc. Am. J.* 71 (5), 1600–1606.
- Ale, S., Bowling, L. C., Brouder, S. M., Frankenberger, J. R., & Youssef, M. A. (2009). Simulated effect of drainage water management operational strategy on hydrology and crop yield for Drummer soil in the Midwestern United States. *Agricultural Water Management*, 96(4), 653-665.
- Al-Kaisi, Mahdi M., Xinhua Yin, and Mark A. Licht. "Soil carbon and nitrogen changes as influenced by tillage and cropping systems in some Iowa soils." *Agriculture, Ecosystems & Environment* 105.4 (2005): 635-647.
- Asadi, H., Moussavi, A., Ghadiri, H., Rose, C., 2011. Flow-driven soil erosion processes and the size selectivity of sediment. *J. Hydrol.* 406, 73–81.
- Askar, M. H., Youssef, M. A., Chescheir, G. M., Negm, L. M., King, K. W., Hesterberg, D. L., & Skaggs, R. W. (2020). DRAINMOD Simulation of macropore flow at subsurface drained agricultural fields: Model modification and field testing. *Agricultural Water Management*, 242, 106401.
- Algoazany, A. S., Kalita, P. K., Czapar, G. F., & Mitchell, J. K. (2007). Phosphorus transport through subsurface drainage and surface runoff from a flat watershed in east central Illinois, USA. *Journal of environmental quality*, 36(3), 681-693.
- Bairwa, D. D., Prajapat, B. S., & Kadam, S. S. Hydrogel: The Best Option for Saving Irrigation Water.
- Beauchemin, S., R.R. Simard, and D. Cluis. 1998. Forms and concentrations of phosphorus in drainage water of twenty-seven tile-drained soils. *J. Environ. Qual.* 27:721–728.
- Bechmann, M., 2012. Effect of tillage on sediment and phosphorus losses from a field and a catchment in south eastern Norway. *Acta Agric. Scand. B* 62, 206–216.
- Beczek M, Ryzak M, Sochan A, Mazur R, Bieganowski A. 2019. The mass ratio of splashed particles during raindrop splash phenomenon on soil surface. *Geoderma* 347: 40–48.
- Bernatek-Jakiel A, Bruthans J, Vojtíšek J, Stolarczyk M, Zaleski T. 2020. Sediment detachment in piping-prone soils: cohesion sources and potential weakening mechanisms. *Earth Surface Processes and Landforms* (this issue).

- Beuselinck, L., Hairsine, P.B., Govers, G., Poesen, J., 2002. Evaluating a single-class net deposition equation in overland flow conditions. *Water Resour. Res.* 38, 15-1–15-10.
- Beven, K. and P. Germann (2013). Macropores and water flow in soils revisited. *Water Resources Research* 49(6): 3071-3092.
- Bishop, J. M., Callaghan, M. V., Cey, E. E., & Bentley, L. R. (2015). Measurement and simulation of subsurface tracer migration to tile drains in low permeability, macroporous soil. *Water Resources Research*, 51(6), 3956-3981.
- Blann, K. L., Anderson, J. L., Sands, G. R., & Vondracek, B. (2009). Effects of agricultural drainage on aquatic ecosystems: a review. *Critical reviews in environmental science and technology*, 39(11), 909-1001.
- Bottcher, A. B., Monke, E. J., & Huggins, L. F. (1981). Nutrient and sediment loadings from a subsurface drainage system. *Transactions of the ASAE*, 24(5), 1221-1226.
- Brauer, C. C., Teuling, A. J., Torfs, P. J. J. F., & Uijlenhoet, R. (2014). The Wageningen Lowland Runoff Simulator (WALRUS): a lumped rainfall–runoff model for catchments with shallow groundwater. *Geoscientific Model Development*, 7(5), 2313-2332.
- Brennan, R. B., Scott, J. T., Sharpley, A. N., Lally, H. T., Jarvie, H. P., Bowes, M. J., ... & Gbur, E. (2017). Linking soil erosion to instream dissolved phosphorus cycling and periphyton growth. *JAWRA Journal of the American Water Resources Association*, 53(4), 809-821.
- Burkhardt, M., Kasteel, R., Vanderborght, J., Vereecken, H., 2008. Field study on colloid transport using fluorescent microspheres. *Eur. J. Soil Sci.* 59, 82–93.
- Callaghan, M. V., Head, F. A., Cey, E. E., & Bentley, L. R. (2017). Salt leaching in fine-grained, macroporous soil: negative effects of excessive matrix saturation. *Agricultural Water Management*, 181, 73-84.
- Carstensen, M. V., Børgesen, C. D., Ovesen, N. B., Poulsen, J. R., Hvid, S. K., & Kronvang, B. (2019). Controlled drainage as a targeted mitigation measure for nitrogen and phosphorus. *Journal of environmental quality*, 48(3), 677-685.
- Casillas-Ituarte, N. N., Sawyer, A. H., Danner, K. M., King, K. W., & Covault, A. J. (2019). Internal Phosphorus Storage in Two Headwater Agricultural Streams in the Lake Erie Basin. *Environmental science & technology*, 54(1), 176-183.
- Cey, E. E., & Rudolph, D. L. (2009). Field study of macropore flow processes using tension infiltration of a dye tracer in partially saturated soils. *Hydrological Processes: An International Journal*, 23(12), 1768-1779.
- Chen, D., Shen, H., Hu, M., Wang, J., Zhang, Y., & Dahlgren, R. A. (2018). Legacy nutrient dynamics at the watershed scale: principles, modeling, and implications. *Advances in agronomy*, 149, 237-313.

- Choudhury, T., Robertson, W. D., & Finnigan, D. S. (2016). Suspended sediment and phosphorus removal in a woodchip filter system treating agricultural wash water. *Journal of environmental quality*, 45(3), 796-802.
- Christianson, L. E., Harmel, R. D., Smith, D., Williams, M. R., & King, K. (2016). Assessment and synthesis of 50 years of published drainage phosphorus losses. *Journal of Environmental Quality*, 45(5), 1467–1477.
- Clausen, J. C., & Spooner, J. (1993). *Paired watershed study design* (No. PB-94-154820/XAB; EPA-841/F-93/009). Environmental Protection Agency, Washington, DC (United States). Office of Wetlands, Oceans and Watersheds.
- Cleveland, C. C. and D. Liptzin (2007). C: N: P stoichiometry in soil: is there a “Redfield ratio” for the microbial biomass?. *Biogeochemistry* 85(3): 235-252.
- Coelho, B. B., Murray, R., Lapen, D., Topp, E., & Bruin, A. (2012). Phosphorus and sediment loading to surface waters from liquid swine manure application under different drainage and tillage practices. *Agricultural Water Management*, 104, 51-61.
- Collins AL, Burak E, Harris P, Pulley S, Cardenas L, Tang Q. (2019). Field scale temporal and spatial variability of  $\delta^{13}\text{C}$ ,  $\delta^{15}\text{N}$ , TC and TN soil properties: implications for sediment source tracing. *Geoderma* 333:108–122.
- Cooke, R., & Verma, S. (2012). Performance of drainage water management systems in Illinois, United States. *Journal of Soil and Water Conservation*, 67(6), 453-464.
- Culley, J. L. B., Bolton, E. F., & Bernyk, V. (1983). *Suspended solids and phosphorus loads from a clay soil: I. Plot studies* (Vol. 12, No. 4, pp. 493-498). American Society of Agronomy, Crop Science Society of America, and Soil Science Society of America.
- Cullum, R. F. (2009). Macropore flow estimations under no-till and till systems. *Catena*, 78(1), 87-91.
- Cullum, R. F., Locke, M. A., & Knight, S. S. (2009). Water Quality Assessment of a Conservation Reserve Program near an Oxbow Lake in the Mississippi Delta: Case Study of Beasley Watershed. In *2009 Reno, Nevada, June 21-June 24, 2009* (p. 1). American Society of Agricultural and Biological Engineers.
- Cuthbert, M. O., Mackay, R., & Nimmo, J. R. (2013). Linking soil moisture balance and source-responsive models to estimate diffuse and preferential components of groundwater recharge. *Hydrology and Earth System Sciences*, 17(3), 1003-1019.
- Davis, C. M., & Fox, J. F. (2009). Sediment fingerprinting: review of the method and future improvements for allocating nonpoint source pollution. *Journal of Environmental Engineering*, 135(7), 490-504.
- Dayton, E. A., Whitacre, S., & Holloman, C. (2017). Comparison of three persulfate digestion methods for total phosphorus analysis and estimation of suspended sediments. *Applied geochemistry*, 78, 357-362.



- Demand, D., Selker, J. S., & Weiler, M. (2019). Influences of macropores on infiltration into seasonally frozen soil. *Vadose Zone Journal*, 18(1), 1-14.
- Deurer, M., Grinev, D., Young, I., Clothier, B. E., & Müller, K. (2009). The impact of soil carbon management on soil macropore structure: a comparison of two apple orchard systems in New Zealand. *European Journal of Soil Science*, 60(6), 945-955.
- Di Prima, S., Rodrigo-Comino, J., Novara, A., Iovino, M., Pirastru, M., Keesstra, S., and Cerdà, A. 2018. Soil physical quality of citrus orchards under tillage, herbicide, and organic managements. *Pedosphere*, 28(3): 463–477.
- Di Stefano, C., Ferro, V., 2002. Soil and water: linking clay enrichment and sediment delivery processes. *Biosyst. Eng.* 81, 465–479.
- Djabekhir, K., Lauvernet, C., Kraft, P., & Carlier, N. (2017). Development of a dual permeability model within a hydrological catchment modeling framework: 1D application. *Science of the Total Environment*, 575, 1429-1437.
- Djordjic, F., Bergström, L., & Ulén, B. (2002). Phosphorus losses from a structured clay soil in relation to tillage practices. *Soil Use and Management*, 18(2), 79-83.
- Downing, J. A., Prairie, Y. T., Cole, J. J., Duarte, C. M., Tranvik, L. J., Striegl, R. G., ... & Middelburg, J. J. (2006). The global abundance and size distribution of lakes, ponds, and impoundments. *Limnology and Oceanography*, 51(5), 2388-2397.
- Drury, C. F., Tan, C. S., Reynolds, W. D., Welacky, T. W., Oloya, T. O., & Gaynor, J. D. (2009). Managing tile drainage, subirrigation, and nitrogen fertilization to enhance crop yields and reduce nitrate loss. *Journal of Environmental Quality*, 38(3), 1193-1204.
- Duffy, Michael, and Michael Hanthorn. *Returns to corn and soybean tillage practices*. No. 508. US Department of Agriculture, Economic Research Service, 1984.
- Duncan, E. W., King, K. W., Williams, M. R., LaBarge, G., Pease, L. A., Smith, D. R., & Fausey, N. R. (2017). Linking soil phosphorus to dissolved phosphorus losses in the Midwest. *Agricultural & Environmental Letters*, 2(1), 170004.
- Duvert, C., Gratiot, N., Evrard, O., Navratil, O., Némery, J., Prat, C., & Esteves, M. (2010). Drivers of erosion and suspended sediment transport in three headwater catchments of the Mexican Central Highlands. *Geomorphology*, 123(3-4), 243-256.
- Eastman, M., Gollamudi, A., Stämpfli, N., Madramootoo, C.A., Sarangi, A., 2010. Comparative evaluation of phosphorus losses from subsurface and naturally drained agricultural fields in the Pike River watershed of Quebec, Canada. *Agric. Water Manage.* 97, 596–604.
- Eckhardt, K. (2005). How to construct recursive digital filters for baseflow separation. *Hydrological Processes: An International Journal*, 19(2), 507-515.
- Enright, P. and C. A. Madramootoo (2004). Phosphorus losses in surface runoff and subsurface drainage waters on two agricultural fields in Quebec. *Drainage VIII*, 21-24 March 2004, American Society of Agricultural and Biological Engineers.

- Evans, R.O., R.W. Skaggs, and J.W. Gilliam. (1995). Controlled versus conventional drainage effects on water quality. *J. Irrig. Drain. Eng.* 121:271–276.
- Evans, C., & Davies, T. D. (1998). Causes of concentration/discharge hysteresis and its potential as a tool for analysis of episode hydrochemistry. *Water Resources Research*, 34(1), 129-137.
- Fang, Q.X., Malone, R.W., Ma, L., Jaynes, D.B., Thorp, K.R., Green, T.R., Ahuja, L.R., 2012. Modeling the effects of controlled drainage, N rate and weather on nitrate loss to subsurface drainage. *Agric. Water Manag.* 103, 150–161.
- Fausey, N. R. (2005). Drainage management for humid regions. *International Agricultural Engineering Journal*, 14(4), 209-214.
- Feser, S.E., Strock, J.S., Sands, G.R., Birr, A.S., 2010. Controlled drainage to improve edge-of-field water quality in southwest Minnesota. In: USA.XVII Th World Congress of the International Commission of Agricultural and Biosystems Engineering. 13–17 June 2010, Quebec City, Quebec, Canada.
- Flury, M., Flühler, H., Jury, W. A., & Leuenberger, J. (1994). Susceptibility of soils to preferential flow of water: A field study. *Water Resources Research*, 30(7), 1945-1954.
- Ford, W., King, K., Williams, M., Williams, J., & Fausey, N. (2015). Sensitivity analysis of the Agricultural Policy/Environmental eXtender (APEX) for phosphorus loads in tile-drained landscapes. *Journal of environmental quality*, 44(4), 1099-1110.
- Ford, W. I., King, K. W., Williams, M. R., & Confesor Jr, R. B. (2017). Modified APEX model for simulating macropore phosphorus contributions to tile drains. *Journal of Environmental Quality*, 46(6), 1413-1423.
- Ford, W. I., King, K., & Williams, M. R. (2018). Upland and in-stream controls on baseflow nutrient dynamics in tile-drained agroecosystem watersheds. *Journal of Hydrology*, 556, 800-812.
- Ford, W., Williams, M. R., Young, M. B., King, K. W., & Fischer, E. (2018). Assessing intra-event phosphorus dynamics in drainage water using phosphate stable oxygen isotopes. *Transactions of the ASABE*, 61(4), 1379-1392.
- Ford, W. I., Husic, A., Fogle, A., & Taraba, J. (2019). Long-term assessment of nutrient flow pathway dynamics and in-stream fate in a temperate karst agroecosystem watershed. *Hydrological Processes*, 33(11), 1610-1628.
- Frey, S. K., Rudolph, D. L., & Conant Jr, B. (2012). Bromide and chloride tracer movement in macroporous tile-drained agricultural soil during an annual climatic cycle. *Journal of Hydrology*, 460, 77-89.
- Frey, S. K., Hwang, H. T., Park, Y. J., Hussain, S. I., Gottschall, N., Edwards, M., & Lapen, D. R. (2016). Dual permeability modeling of tile drain management influences on hydrologic and nutrient transport characteristics in macroporous soil. *Journal of Hydrology*, 535, 392-406.

- Frossard, E., Buchmann, N., Bünemann, E. K., Kiba, D. I., Lompo, F., Oberson, A., ... & Traoré, O. Y. (2016). Soil properties and not inputs control carbon: nitrogen: phosphorus ratios in cropped soils in the long term. *Soil*, 2(1), 83-99.
- Gentry, L.E., M.B. David, T.V. Royer, C.A. Mitchell, and K.M. Starks. 2007. Phosphorus transport pathways to streams in tile-drained agricultural watersheds. *J. Environ. Qual.* 36:408–415.
- Gerke, H. H., & Van Genuchten, M. T. (1993). A dual-porosity model for simulating the preferential movement of water and solutes in structured porous media. *Water resources research*, 29(2), 305-319.
- Gerke, H. H., Dusek, J., Vogel, T., & Köhne, J. M. (2007). Two-dimensional dual-permeability analyses of a bromide tracer experiment on a tile-drained field. *Vadose Zone Journal*, 6(3), 651-667.
- Gerke, H. H., Dusek, J., & Vogel, T. (2013). Solute mass transfer effects in two-dimensional dual-permeability modeling of bromide leaching from a tile-drained field. *Vadose Zone Journal*, 12(2), vzt2012-0091.
- Ghane, E., Fausey, N. R., Shedekar, V. S., Piepho, H. P., Shang, Y., & Brown, L. C. (2012). Crop yield evaluation under controlled drainage in Ohio, United States. *Journal of Soil and Water Conservation*, 67(6), 465-473.
- Glaser, B. (2005). Compound-specific stable-isotope ( $\delta^{13}\text{C}$ ) analysis in soil science. *Journal of Plant Nutrition and Soil Science*, 168(5), 633-648.
- Graham, C. B., & Lin, H. S. (2011). Controls and frequency of preferential flow occurrence: A 175-event analysis. *Vadose Zone Journal*, 10(3), 816-831.
- Granger, R. J., Gray, D. M., & Dyck, G. E. (1984). Snowmelt infiltration to frozen prairie soils. *Canadian Journal of Earth Sciences*, 21, 669– 677.
- Grangeon, T., Ceriani, V., Evrard, O., Grison, A., Vandromme, R., Gaillot, A., ... & Salvador-Blanes, S. (2021). Quantifying hydro-sedimentary transfers in a lowland tile-drained agricultural catchment. *Catena*, 198, 105033.
- Grant, K. N., Macrae, M. L., & Ali, G. A. (2019). Differences in preferential flow with antecedent moisture conditions and soil texture: Implications for subsurface P transport. *Hydrological Processes*, 33(15), 2068-2079.
- Gregor, M., & Malik, P. (2012). *RC 4.0 user's manual, HydroOffice software package for water science*. Retrieved from <https://hydrooffice.org>.
- Guan, Z., Tang, X. Y., Yang, J. E., Ok, Y. S., Xu, Z., Nishimura, T., & Reid, B. J. (2017). A review of source tracking techniques for fine sediment within a catchment. *Environmental geochemistry and health*, 39(6), 1221-1243

- Harmel, R. D., King, K., Busch, D., Smith, D., Birgand, F., & Haggard, B. (2018). Measuring edge-of-field water quality: Where we have been and the path forward. *Journal of Soil and Water Conservation*, 73(1), 86-96.
- Heathwaite, A. L., & Dils, R. M. (2000). Characterizing phosphorus loss in surface and subsurface hydrological pathways. *Science of the Total Environment*, 251, 523-538.
- Hendricks, S. P. (1993). Microbial ecology of the hyporheic zone: a perspective integrating hydrology and biology. *Journal of the North American Benthological Society*, 12(1), 70-78.
- Heppell, C. M., & Chapman, A. S. (2006). Analysis of a two-component hydrograph separation model to predict herbicide runoff in drained soils. *Agricultural Water Management*, 79(2), 177-207.
- Hoffmann, C. C., Zak, D., Kronvang, B., Kjaergaard, C., Carstensen, M. V., & Audet, J. (2020). An overview of nutrient transport mitigation measures for improvement of water quality in Denmark. *Ecological Engineering*, 155, 105863.
- Hosseini, S. H., Niyungeko, C., Khan, S., & Liang, X. (2021). Effects of superabsorbent polyacrylamide hydrogel and gypsum applications on colloidal phosphorus release from agricultural soils. *Journal of Soils and Sediments*, 21(2), 925-935.
- Huang, N. E., Shen, Z., Long, S. R., Wu, M. C., Shih, H. H., Zheng, Q., ... & Liu, H. H. (1998). The empirical mode decomposition and the Hilbert spectrum for nonlinear and non-stationary time series analysis. *Proceedings of the Royal Society of London. Series A: mathematical, physical and engineering sciences*, 454(1971), 903-995.
- Husic, A. (2018). Numerical modeling and isotope tracers to investigate karst biogeochemistry and transport processes. PhD Dissertation. University of Kentucky. Lexington, Kentucky.
- Husic, A., Fox, J., Adams, E., Ford, W., Agouridis, C., Currens, J., & Backus, J. (2019). Nitrate pathways, processes, and timing in an agricultural karst system: Development and application of a numerical model. *Water Resources Research*, 55(3), 2079-2103.
- Jacobsen OH, Moldrup P, Larson C, Konnerup L, Petersen LW. 1997. Particle transport in macropores of undisturbed soil columns. *Journal of Hydrology* 196: 185–203.
- Jarvie, H. P., Sharpley, A. N., Brahana, V., Simmons, T., Price, A., Neal, C., ... & Haggard, B. E. (2014). Phosphorus retention and remobilization along hydrological pathways in karst terrain. *Environmental science & technology*, 48(9), 4860-4868.
- Jarvie, H. P., Johnson, L. T., Sharpley, A. N., Smith, D. R., Baker, D. B., Bruulsema, T. W., & Confesor, R. (2017). Increased soluble phosphorus loads to Lake Erie: Unintended consequences of conservation practices?. *Journal of Environmental Quality*, 46(1), 123-132.
- Jarvis, N.J., Villholth, K.G., Ulén, B., 1999. Modelling particle mobilization and leaching in macroporous soil. *Eur. J. Soil Sci.* 50, 621–632.

- Jarvis, N. J. (2007). A review of non-equilibrium water flow and solute transport in soil macropores: principles, controlling factors and consequences for water quality. *European Journal of Soil Science*, 58(3): 523-546.
- Jarvis, N., & Larsbo, M. (2012). MACRO (v5. 2): Model use, calibration, and validation. *Transactions of the ASABE*, 55(4), 1413-1423.
- Jiang, X., Livi, K. J., Arenberg, M. R., Chen, A., Chen, K. Y., Gentry, L., & Arai, Y. (2021). High flow event induced the subsurface transport of particulate phosphorus and its speciation in agricultural tile drainage system. *Chemosphere*, 263, 128147.
- Kaplan, D. I., Bertsch, P. M., Adriano, D. C., & Miller, W. P. (1993). Soil-borne mobile colloids as influenced by water flow and organic carbon. *Environmental Science & Technology*, 27(6), 1193-1200.
- Keesstra, S.D., Bruijnzeel, L.A., and Van Huissteden, J. 2009. Constructing a sediment budget in a meso-scale catchment using a variety of methods: the Dragonja catchment, SW Slovenia. *Earth Surf. Processes Landf.* 32(1): 49–65.
- Kienzler, P. M., & Naef, F. (2008). Subsurface storm flow formation at different hillslopes and implications for the ‘old water paradox’. *Hydrological Processes: An International Journal*, 22(1), 104-116.
- King, K. W., Fausey, N. R., & Williams, M. R. (2014). Effect of subsurface drainage on streamflow in an agricultural headwater watershed. *Journal of Hydrology*, 519, 438-445.
- King, K. W., Williams, M. R., Macrae, M. L., Fausey, N. R., Frankenberger, J., Smith, D. R., ... & Brown, L. C. (2015). Phosphorus transport in agricultural subsurface drainage: A review. *Journal of environmental quality*, 44(2), 467-485.
- Kladivko, E. J., Van Scoyoc, G. E., Monke, E. J., Oates, K. M., & Pask, W. (1991). *Pesticide and nutrient movement into subsurface tile drains on a silt loam soil in Indiana* (Vol. 20, No. 1, pp. 264-270). American Society of Agronomy, Crop Science Society of America, and Soil Science Society of America.
- Klaus, J. and J. McDonnell (2013). Hydrograph separation using stable isotopes: Review and evaluation. *Journal of Hydrology* 505: 47-64.
- Klaus, J., Zehe, E., Elsner, M., Külls, C., & McDonnell, J. J. (2013). Macropore flow of old water revisited: experimental insights from a tile-drained hillslope. *Hydrology and Earth System Sciences*, 17(1), 103-118.
- Kleinman, P. J., & Sharpley, A. N. (2002). Estimating soil phosphorus sorption saturation from Mehlich-3 data. *Communications in Soil Science and Plant Analysis*, 33(11-12), 1825-1839.
- Kleinman, P. J., Sharpley, A. N., Withers, P. J., Bergström, L., Johnson, L. T., & Doody, D. G. (2015). Implementing agricultural phosphorus science and management to combat eutrophication. *Ambio*, 44(2), 297-310.

- Köhne, S., Lennartz, B., Köhne, J. M., & Šimůnek, J. (2006). Bromide transport at a tile-drained field site: Experiment, and one-and two-dimensional equilibrium and non-equilibrium numerical modeling. *Journal of Hydrology*, 321(1-4), 390-408.
- Kokulan, V., Macrae, M. L., Lobb, D. A., & Ali, G. A. (2019). Contribution of Overland and Tile Flow to Runoff and Nutrient Losses from Vertisols in Manitoba, Canada. *Journal of Environmental Quality*.
- Koroleff, J. (1983). Determination of total phosphorus by alkaline persulphate oxidation. *Methods of Seawater Analysis*. Verlag Chemie, Weinheim: 136-138.
- Koiter, A.J., Owens, P.N., Petticrew, E.L., Lobb, D.A., 2015. The role of gravel channel beds on the particle size and organic matter selectivity of transported fine-grained sediment: implications for sediment fingerprinting and biogeochemical flux research. *J. Soils Sediments* 15, 2174–2188.
- Kronholm, S. C., & Capel, P. D. (2015). A comparison of high-resolution specific conductance-based end-member mixing analysis and a graphical method for baseflow separation of four streams in hydrologically challenging agricultural watersheds. *Hydrological Processes*, 29(11), 2521-2533.
- Kruskal, W. H. and W. A. Wallis (1952). Use of ranks in one-criterion variance analysis. *Journal of the American statistical Association* 47(260): 583-621.
- Lahdou, G. B., Bowling, L., Frankenberger, J., & Kladvko, E. (2019). Hydrologic controls of controlled and free draining subsurface drainage systems. *Agricultural Water Management*, 213, 605-615.
- Landers, M. N., & Sturm, T. W. (2013). Hysteresis in suspended sediment to turbidity relations due to changing particle size distributions. *Water Resources Research*, 49(9), 5487-5500.
- Lavaire, T., Gentry, L. E., David, M. B., & Cooke, R. A. (2017). Fate of water and nitrate using drainage water management on tile systems in east-central Illinois. *Agricultural Water Management*, 191, 218-228.
- Lee, L. J. E., Lawrence, D. S. L., & Price, M. (2006). Analysis of water-level response to rainfall and implications for recharge pathways in the Chalk aquifer, SE England. *Journal of Hydrology*, 330(3-4), 604-620.
- Lewis, J. (2003). Turbidity-controlled sampling for suspended. *Erosion and sediment transport measurement in rivers: Technological and methodological advances*, 13.
- Line, D. E., Hall, K. R., & Blackwell, J. D. (2013). Estimating suspended solids from turbidity in the Robeson Creek, NC Watershed. *JAWRA Journal of the American Water Resources Association*, 49(6), 1412-1420.
- Lloyd, C. E. M., Freer, J. E., Johnes, P. J., & Collins, A. L. (2015). Testing an improved index for analyzing storm nutrient hysteresis. *Hydrology and Earth System Sciences Discussions*, 12(8), 7875-7892.

- Lloyd, C. E., Freer, J. E., Johnes, P. J., & Collins, A. L. (2016). Testing an improved index for analysing storm discharge–concentration hysteresis. *Hydrology and Earth System Sciences*, 20(2), 625-632.
- Liu, Y., Youssef, M. A., Chescheir, G. M., Appelboom, T. W., Poole, C. A., Arellano, C., & Skaggs, R. W. (2019). Effect of controlled drainage on nitrogen fate and transport for a subsurface drained grass field receiving liquid swine lagoon effluent. *Agricultural Water Management*, 217, 440-451.
- Lyne, V., & Hollick, M. (1979). Stochastic time-variable rainfall-runoff modelling. In *Institute of Engineers Australia National Conference, 1979*, 89-93.
- Macrae, M. L., English, M. C., Schiff, S. L., & Stone, M. (2007). Intra-annual variability in the contribution of tile drains to basin discharge and phosphorus export in a first-order agricultural catchment. *Agricultural Water Management*, 92(3), 171-182.
- Macrae, M. L., Ali, G. A., King, K. W., Plach, J. M., Puer, W. T., Williams, M., ... & Tang, W. (2019). Evaluating hydrologic response in tile-drained landscapes: Implications for phosphorus transport. *Journal of environmental quality*, 48(5), 1347-1355.
- Majdalani, S., Michel, E., Di Pietro, L., Angulo-Jaramillo, R., & Rousseau, M. (2007). Mobilization and preferential transport of soil particles during infiltration: A core-scale modeling approach. *Water resources research*, 43(5).
- Malík, P. and S. Vojtková (2012). Use of recession-curve analysis for estimation of karstification degree and its application in assessing overflow/underflow conditions in closely spaced karstic springs. *Environmental Earth Sciences* 65(8): 2245-2257.
- Mano, V., Nemery, J., Belleudy, P., & Poirel, A. (2009). Assessment of suspended sediment transport in four alpine watersheds (France): influence of the climatic regime. *Hydrological Processes: An International Journal*, 23(5), 777-792.
- Mapa, R. B., Green, R. E., & Santo, L. (1986). Temporal Variability of Soil Hydraulic Properties with Wetting and Drying Subsequent to Tillage 1. *Soil Science Society of America Journal*, 50(5), 1133-1138.
- McDowell, R. W., & Sharpley, A. N. (2001). Approximating phosphorus release from soils to surface runoff and subsurface drainage. *Journal of environmental quality*, 30(2), 508-520.
- Mellander, P. E., Jordan, P., Melland, A. R., Murphy, P. N., Wall, D. P., Mehan, S., & Shortle, G. (2013). Quantification of phosphorus transport from a karstic agricultural watershed to emerging spring water. *Environmental Science & Technology*, 47(12), 6111-6119.
- Messing, I., & Jarvis, N. J. (1993). Temporal variation in the hydraulic conductivity of a tilled clay soil as measured by tension infiltrometers. *Journal of Soil Science*, 44(1), 11-24.

Michaud, A. and M. Laverdière (2004). Cropping, soil type and manure application effects on phosphorus export and bioavailability. *Canadian journal of soil science* 84(3): 295-305.

Michel E, Majdalani S, Di-Pietro L. 2010. How differential capillary stresses promote particle mobilization in macroporous soils: a novel conceptual model. *Vadose Zone Journal* 9: 307–316.

Michel, E., Majdalani, S., & Di-Pietro, L. (2014). A novel conceptual framework for long-term leaching of autochthonous soil particles during transient flow. *European journal of soil science*, 65(3), 336-347.

Mirus, B. B. and J. R. Nimmo (2013). Balancing practicality and hydrologic realism: A parsimonious approach for simulating rapid groundwater recharge via unsaturated-zone preferential flow. *Water Resources Research* 49(3): 1458-1465.

Miyazaki, T. 1993, 'Water flow in soils,' Marcel Dekker, New York.

Mohammed, A. A., Kurylyk, B. L., Cey, E. E., & Hayashi, M. (2018). Snowmelt infiltration and macropore flow in frozen soils: Overview, knowledge gaps, and a conceptual framework. *Vadose Zone Journal*, 17(1), 1-15.

Mohammed, A. A., Cey, E. E., Hayashi, M., Callaghan, M. V., Park, Y. J., Miller, K. L., & Frey, S. K. (2021). Dual-permeability modeling of preferential flow and snowmelt partitioning in frozen soils. *Vadose Zone Journal*, 20(2), e20101.

Molder, B., Cockburn, J., Berg, A., Lindsay, J., & Woodrow, K. (2015). Sediment-assisted nutrient transfer from a small, no-till, tile drained watershed in Southwestern Ontario, Canada. *Agricultural Water Management*, 152, 31-40.

Moriassi, D. N., Arnold, J. G., Van Liew, M. W., Bingner, R. L., Harmel, R. D., & Veith, T. L. (2007). Model evaluation guidelines for systematic quantification of accuracy in watershed simulations. *Transactions of the ASABE*, 50(3), 885-900.

Murphy, J., and J.P. Riley. 1962. A modified single solution method for the determination of phosphate in natural waters. *Analytica Chimica Acta* 27:31-36.

Nash, P. R., Nelson, K. A., Motavalli, P. P., Nathan, M., & Dudenhoefter, C. (2015). Reducing phosphorus loss in tile water with managed drainage in a claypan soil. *Journal of environmental quality*, 44(2), 585-593.

Narjary, B., Aggarwal, P., Kumar, S., & Meena, M. D. (2013, January). Significance of hydrogel and its application in agriculture. ICAR.

Nazari, S., Ford, W. I., & King, K. W. (2020). Impacts of preferential flow and agroecosystem management on subsurface particulate phosphorus loadings in tile-drained landscapes, *Journal of Environmental Quality*, 49(5), 1370-1383.  
<https://doi.org/10.1002/jeq2.20116>.



- Nazari, S, Ford, WI, & King, KW. Quantifying hydrologic pathway and source connectivity dynamics in tile drainage: Implications for phosphorus concentrations. *Vadose Zone J.* 2021;e20154. <https://doi.org/10.1002/vzj2.20154>.
- Nimmo, J. R. (2012). Preferential flow occurs in unsaturated conditions. *Hydrological Processes* 26(5): 786-789.
- Nouwakpo SK, Huang CH, Bowling L, Owens P. 2010. Impact of vertical hydraulic gradient on rill erodibility and critical shear stress. *Soil Science Society of America Journal* 74(6): 1914–1921.
- Oerter, E. J., Perelet, A., Pardyjak, E., & Bowen, G. (2017). Membrane inlet laser spectroscopy to measure H and O stable isotope compositions of soil and sediment pore water with high sample throughput. *Rapid Communications in Mass Spectrometry*, 31(1), 75-84.
- Ortega-Pieck, A., Norby, J., Brooks, E. S., Strawn, D., Crump, A. R., & Huggins, D. R. (2020). Sources and subsurface transport of dissolved reactive phosphorus in a semiarid, no-till catchment with complex topography, *Journal of Environmental Quality*, 49(5) 1286-1297.
- Osterholz, W. R., Hanrahan, B. R., & King, K. W. (2020). *Legacy phosphorus concentration–discharge relationships in surface runoff and tile drainage from Ohio crop fields* (Vol. 49, No. 3, pp. 675-687).
- Øygarden, L., Kværner, J., & Jenssen, P. D. (1997). Soil erosion via preferential flow to drainage systems in clay soils. *Geoderma*, 76(1-2), 65-86.
- Paasonen-Kivekäs, M. and H. Koivusalo (2006). Losses of sediment and phosphorus through subsurface drains in a clayey field in southern Finland. Transport and retention of pollutants from different production systems: NJF seminar 373, Nordic Association of Agricultural Scientists.
- Patton, C. J. and J. R. Kryskalla (2003). Methods of analysis by the U.S. Geological Survey National Water Quality Laboratory : evaluation of alkaline persulfate digestion as an alternative to Kjeldahl digestion for determination of total and dissolved nitrogen and phosphorus in water. Water-Resources Investigations Report 03-4174. US Geological Survey, Denver, Colorado.
- Pease, L.A., Fausey, N.R., Martin, J.F. and Brown, L.C., 2017. Projected climate change effects on subsurface drainage and the performance of controlled drainage in the Western Lake Erie Basin. *Journal of Soil and Water Conservation*, 72(3), pp.240-250.
- Pease, L. A., King, K. W., Williams, M. R., LaBarge, G. A., Duncan, E. W., & Fausey, N. R. (2018). Phosphorus export from artificially drained fields across the Eastern Corn Belt. *Journal of Great Lakes Research*, 44(1), 43-53.
- Perks, M. T., Owen, G. J., Benskin, C. M. H., Jonczyk, J., Deasy, C., Burke, S., ... & Haygarth, P. M. (2015). Dominant mechanisms for the delivery of fine sediment and

phosphorus to fluvial networks draining grassland dominated headwater catchments. *Science of the Total Environment*, 523, 178-190.

Pilgrim, D. H. and D. D. Huff (1983). Suspended sediment in rapid subsurface stormflow on a large field plot. *Earth Surface Processes and Landforms* 8(5): 451-463.

Pittman, F., Mohammed, A., & Cey, E. (2020). Effects of antecedent moisture and macroporosity on infiltration and water flow in frozen soil. *Hydrological Processes*, 34, 795–809.

Pferdmenges, J., Breuer, L., Julich, S., & Kraft, P. (2020). Review of soil phosphorus routines in ecosystem models. *Environmental Modelling & Software*, 126, 104639.

Pluer, W. T., Macrae, M., Buckley, A., & Reid, K. (2020). Contribution of preferential flow to tile drainage varies spatially and temporally. *Vadose Zone Journal*, 19(1), e20043.

Poirier, S. C., Whalen, J. K., & Michaud, A. R. (2012). Bioavailable phosphorus in fine-sized sediments transported from agricultural fields. *Soil Science Society of America Journal*, 76(1), 258-267.

Radcliffe, D. E., Reid, D. K., Blombäck, K., Bolster, C. H., Collick, A. S., Easton, Z. M., ... & Smith, D. R. (2015). Applicability of models to predict phosphorus losses in drained fields: A review. *Journal of environmental quality*, 44(2), 614-628.

Rasmussen, P. P., Gray, J. R., Glysson, G. D., & Ziegler, A. C. (2009). Guidelines and procedures for computing time-series suspended-sediment concentrations and loads from in-stream turbidity-sensor and streamflow data. *US geological survey techniques and methods, book, 3*, 52.

Rato, R., et al. (2008). On the HHT, its problems, and some solutions. *Mechanical systems and signal processing* 22(6): 1374-1394.

Rato, R. T., Ortigueira, M. D., & Batista, A. G. (2008). On the HHT, its problems, and some solutions. *Mechanical systems and signal processing*, 22(6), 1374-1394.

Rhoton, F. E., Shipitalo, M. J., & Lindbo, D. L. (2002). Runoff and soil loss from midwestern and southeastern US silt loam soils as affected by tillage practice and soil organic matter content.

Rimmer, A., & Hartmann, A. (2012). Simplified conceptual structures and analytical solutions for groundwater discharge using reservoir equations. *Water Resources Management and Modeling*, 2, 217-238.

Robinson, M., Rycroft, D., Skaggs, R., Schilfgaard, Jv., et al., 1999. The impact of drainage on streamflow. *Agronomy Monograph* 38. *Agricultural Drainage* 38, 767–800.

Ross, J. A., Herbert, M. E., Sowa, S. P., Frankenberger, J. R., King, K. W., Christopher, S. F., ... & Yen, H. (2016). A synthesis and comparative evaluation of factors influencing

the effectiveness of drainage water management. *Agricultural Water Management*, 178, 366-376.

Rousseau M, Di Pietro L, Angulo-Jaramillo R, Tessier D, Cabibel B. 2004. Preferential transport of soil colloidal particles: physicochemical effects on particle mobilization. *Vadose Zone Journal* 3: 247–261.

Ruark, M., Madison, A., Cooley, E., Stuntebeck, T., & Komiskey, M. (2012, January). Phosphorus loss from tile drains: Should we be concerned?. In *Proceedings of the 2012 Wisconsin crop management conference* (Vol. 51, pp. 9-14).

Saadat, S., Bowling, L., Frankenberger, J., Kladvko, E., 2018. Nitrate and phosphorus transport through subsurface drains under free and controlled drainage. *Water Res.* 142, 196–207.

Sadhukhan, D., Qi, Z., 2018. RZWQM2 Phosphorus Model (Technical Report). Department of Bioresource Engineering, McGill University, Quebec, Canada.

Salehi, A.A., Navabian, M., Varaki, M.E., Pirmoradian, N., 2017. Evaluation of HYDRUS- 2D model to simulate the loss of nitrate in subsurface controlled drainage in a physical model scale of paddy fields. *Paddy water Environ.* 15, 433–442.

Schwab, G. O., Nolte, B. H., & Brehm, R. D. (1977). Sediment from drainage systems for clay soils. *TRANSACTIONS of the ASAE*, 20(5), 866-0868.

Shedekar, V., King, K.W., Fausey, N.R., Islam, R.R., Soboyejo, A.B.O., Brown, L.C., 2017. Modeling effects of drainage water management in fields with rolling topography. In: Paper No. 1701282). 2017 ASABE Annual International Meeting. Spokane, Washington, USA.

Shedekar, V. S., King, K. W., Fausey, N. R., Islam, K. R., Soboyejo, A. B., Kalcic, M. M., & Brown, L. C. (2021). Exploring the effectiveness of drainage water management on water budgets and nitrate loss using three evaluation approaches. *Agricultural Water Management*, 243, 106501.

Schelde K, Moldrup P, Jacobsen OH, de Jonge H, de Jonge LW, Komatsu T. 2002. Diffusion-limited mobilization and transport of natural colloids in macroporous soil. *Vadose Zone J.* 1: 125–136.

Schelde, K., de Jonge, L. W., Kjaergaard, C., Laegdsmand, M., & Rubæk, G. H. (2006). Effects of manure application and plowing on transport of colloids and phosphorus to tile drains. *Vadose Zone Journal*, 5(1), 445-458.

Sherriff, S. C., Rowan, J. S., Fenton, O., Jordan, P., Melland, A. R., Mellander, P. E., & Huallachain, D. O. (2016). Storm event suspended sediment-discharge hysteresis and controls in agricultural watersheds: implications for watershed scale sediment management. *Environmental Science & Technology*, 50(4), 1769-1778.

Schilling, K. E. and M. Helmers (2008). Tile drainage as karst: Conduit flow and diffuse flow in a tile-drained watershed. *Journal of Hydrology* 349(3): 291-301.

- Schilling, K. E., Streeter, M. T., Vogelgesang, J., Jones, C. S., & Seeman, A. (2020). Subsurface nutrient export from a cropland field to an agricultural stream: Implications for targeting edge-of-field practices. *Agricultural Water Management*, 241, 106339.
- Shipitalo, M. J., & Edwards, W. M. (1998). Runoff and erosion control with conservation tillage and reduced-input practices on cropland watersheds. *Soil and Tillage Research*, 46(1-2), 1-12.
- Sidle, R. C., Noguchi, S., Tsuboyama, Y., & Laursen, K. (2001). A conceptual model of preferential flow systems in forested hillslopes: Evidence of self-organization. *Hydrological Processes*, 15(10), 1675-1692.
- Simard, R. R., Beauchemin, S., & Haygarth, P. M. (2000). Potential for preferential pathways of phosphorus transport. *Journal of Environmental Quality*, 29(1), 97-105.
- Sims, J. T., Simard, R. R., & Joern, B. C. (1998). Phosphorus loss in agricultural drainage: Historical perspective and current research. *Journal of environmental quality*, 27(2), 277-293.
- Singh, R., et al. (2006). "Calibration and validation of DRAINMOD to design subsurface drainage systems for Iowa's tile landscapes." *Agricultural Water Management* 85(3): 221-232.
- Singh, R., Helmers, M. J., Crumpton, W. G., & Lemke, D. W. (2007). Predicting effects of drainage water management in Iowa's subsurface drained landscapes. *Agricultural water management*, 92(3), 162-170.
- Skaggs, R. W., Youssef, M. A., Gilliam, J. W., & Evans, R. O. (2010). Effect of controlled drainage on water and nitrogen balances in drained lands. *Transactions of the ASABE*, 53(6), 1843-1850.
- Skaggs, R. W., Fausey, N. R., & Evans, R. O. (2012). Drainage water management. *Journal of soil and water conservation*, 67(6), 167A-172A.
- Sklash, M. G., & Farvolden, R. N. (1979). The role of groundwater in storm runoff. *Journal of Hydrology*, 43(1-4), 45-65.
- Slattery, M.C., Burt, T.P., 1997. Particle size characteristics of suspended sediment in hillslope runoff and stream flow. *Earth Surf. Process. Landf.* 22, 705–719.
- Smith, E.P., 2002. BACI design. In: El-Shaarawi, A., Piegorsch, W. (Eds.), *Encyclopedia of Environmetrics*. John Wiley i Sons, Ltd, The Atrium, Southern Gate, Chichester, West Sussex, pp. 141–148.
- Smith, D. R., King, K. W., Johnson, L., Francesconi, W., Richards, P., Baker, D., & Sharpley, A. N. (2015). Surface runoff and tile drainage transport of phosphorus in the midwestern United States. *Journal of Environmental Quality*, 44(2), 495-502.
- Smith, E. A. and P. D. Capel (2018). Specific Conductance as a Tracer of Preferential Flow in a Subsurface-Drained Field. *Vadose Zone Journal* 17(1).

Snyder, L., Potter, J. D., & McDowell, W. H. (2018). An evaluation of nitrate, fDOM, and turbidity sensors in New Hampshire streams. *Water Resources Research*, 54(3), 2466-2479.

Soil Survey Staff, Natural Resources Conservation Service, United States Department of Agriculture. *Web Soil Survey*. Accessed [07/31/2019]. Available online at <https://websoilsurvey.nrcs.usda.gov/>.

Stadler, D., Flühler, H., & Jansson, P. E. (1997). Modelling vertical and lateral water flow in frozen and sloped forest soil plots. *Cold Regions Science and Technology*, 26, 181–194.

Stadler, D., Staehli, M., Aeby, P., & Flühler, H. (2000). Dye tracing and image analysis for quantifying water infiltration into frozen soils. *Soil science society of america journal*, 64(2), 505-516.

Stamm, C. H., Flühler, H., Gächter, R., Leuenberger, J., & Wunderli, H. (1998). Preferential transport of phosphorus in drained grassland soils, *Journal of Environmental*, 27(3), 515-522.

Stone, M., & Krishnappan, B. G. (2002). The effect of irrigation on tile sediment transport in a headwater stream. *Water Research*, 36(14), 3439-3448.

Stone, W. W., & Wilson, J. T. (2006). Preferential flow estimates to an agricultural tile drain with implications for glyphosate transport. *Journal of Environmental Quality*, 35(5), 1825-1835.

Stone M, Emelko MB, Droppo IG, Silins U. Biostabilization and erodibility of cohesive sediment deposits in wildfire-affected streams. *Water Res.* 2011; 45: 521–534. pmid:20970822

Strock, J. S., Kleinman, P. J., King, K. W., & Delgado, J. A. (2010). Drainage water management for water quality protection. *Journal of soil and water conservation*, 65(6), 131A-136A.

Tessier, D., Bigorre, F., & Bruand, A. (1999). The exchange capacity, a prevision tool of the physical soil characteristics. *Comptes Rendus de l'Academie d'Agriculture de France (France)*.

Thorp, K.R., Jaynes, D.B., Malone, R.W., 2008. Simulating the long-term performance of drainage water management across the midwestern United States. *Trans. ASABE* 51, 961–976.

Tokunaga, T. K., & Wan, J. (1997). Water film flow along fracture surfaces of porous rock. *Water Resources Research*, 33(6), 1287-1295.

Tsuboyama, Y., Sidle, R. C., Noguchi, S., & Hosoda, I. (1994). Flow and solute transport through the soil matrix and macropores of a hillslope segment. *Water Resources Research*, 30(4), 879-890.

- Turtola, E., Alakukku, L., Uusitalo, R., 2007. Surface runoff, subsurface drainflow and soil erosion as affected by tillage in a clayey Finnish soil. *Agric. Food Sci.* 16, 332–351.
- Turunen, M., Warsta, L., Paasonen-Kivekäs, M., & Koivusalo, H. (2017). Computational assessment of sediment balance and suspended sediment transport pathways in subsurface drained clayey soils. *Soil and Tillage Research*, 174, 58-69.
- Ulén, B., 2004. Size and settling velocities of phosphorus-containing particles in water from agricultural drains. *Water Air Soil Pollut.* 157, 331–343.
- Upadhayay, H. R., Bodé, S., Griepentrog, M., Huygens, D., Bajracharya, R. M., Blake, W. H., ... & Boeckx, P. (2017). Methodological perspectives on the application of compound-specific stable isotope fingerprinting for sediment source apportionment. *Journal of Soils and Sediments*, 17(6), 1537-1553.
- USEPA. (1983). *Methods for chemical analysis of water and wastes* (USEPA Report 600/4-79-020). Cincinnati, OH: USEPA.
- Uusitalo, R., Turtola, E., Kauppila, T., & Lilja, T. (2001). Particulate phosphorus and sediment in surface runoff and drainflow from clayey soils. *Journal of Environmental Quality*, 30(2), 589-595.
- Van den Bogaert, R., Cornu, S., & Michel, E. (2016). To which extent do rain interruption periods affect colloid retention in macroporous soils? *Geoderma*, 275, 40-47.
- Van Esbroeck, C. J., Macrae, M. L., Brunke, R. I., & McKague, K. (2016). Annual and seasonal phosphorus export in surface runoff and tile drainage from agricultural fields with cold temperate climates. *Journal of Great Lakes Research*, 42(6), 1271-1280.
- Vanni, M. J., Renwick, W. H., Headworth, J. L., Auch, J. D., & Schaus, M. H. (2001). Dissolved and particulate nutrient flux from three adjacent agricultural watersheds: a five-year study. *Biogeochemistry*, 54(1), 85-114.
- Verbree, D. A., Duiker, S. W., & Kleinman, P. J. (2010). Runoff losses of sediment and phosphorus from no-till and cultivated soils receiving dairy manure. *Journal of Environmental Quality*, 39(5), 1762-1770.
- Vidon, P. and P. E. Cuadra (2010). Impact of precipitation characteristics on soil hydrology in tile-drained landscapes. *Hydrological Processes* 24(13): 1821-1833.
- Vogel, T., Gerke, H. H., Zhang, R., & Van Genuchten, M. T. (2000). Modeling flow and transport in a two-dimensional dual-permeability system with spatially variable hydraulic properties. *Journal of hydrology*, 238(1-2), 78-89.
- Warsta, L., Taskinen, A., Koivusalo, H., Paasonen-Kivekäs, M., & Karvonen, T. (2013). Modelling soil erosion in a clayey, subsurface-drained agricultural field with a three-dimensional FLUSH model. *Journal of hydrology*, 498, 132-143.
- Warsta, L., Taskinen, A., Paasonen-Kivekäs, M., Karvonen, T., Koivusalo, H., 2014. Spatially distributed simulation of water balance and sediment transport in an agricultural

field. *Soil Tillage Res.* 143, 26–37.

Watanabe, K., & Kugisaki, Y. (2017). Effect of macropores on soil freezing and thawing with infiltration. *Hydrological Processes*, 31, 270-278.

Weiler, M., & Naef, F. (2003). An experimental tracer study of the role of macropores in infiltration in grassland soils. *Hydrological Processes*, 17(2), 477-493.

Wilhelm, W. W., and Charles S. Wortmann. "Tillage and rotation interactions for corn and soybean grain yield as affected by precipitation and air temperature." *Agronomy Journal* 96.2 (2004): 425-432.

Williams, G. P. (1989). Sediment concentration versus water discharge during single hydrologic events in rivers. *Journal of Hydrology*, 111(1-4), 89-106.

Williams, M. R., King, K. W., & Fausey, N. R. (2015). Drainage water management effects on tile discharge and water quality. *Agricultural Water Management*, 148, 43-51.

Williams, M. R., King, K. W., Ford, W., & Fausey, N. R. (2016). Edge-of-field research to quantify the impacts of agricultural practices on water quality in Ohio. *Journal of Soil and Water Conservation*, 71(1), 9A–12A.

Williams, M. R., King, K. W., Ford, W., Buda, A. R., & Kennedy, C. D. (2016). Effect of tillage on macropore flow and phosphorus transport to tile drains. *Water Resources Research*, 52(4), 2868-2882.

Williams, M. R., et al. (2018). Fertilizer placement and tillage effects on phosphorus concentration in leachate from fine-textured soils. *Soil and Tillage Research* 178: 130-138.

Wilson GV, Rigby JR, Ursic M, Dabney SM. 2016. Soil pipe flow tracer experiments: 1. Connectivity and transport characteristics. *Hydrological Processes* 30: 1265–1279.

Wilson, G. V., Wells, R., Kuhnle, R., Fox, G., & Nieber, J. (2018). Sediment detachment and transport processes associated with internal erosion of soil pipes. *Earth Surface Processes and Landforms*, 43(1), 45-63.

Wilson, R. S., Beetstra, M. A., Reutter, J. M., Hesse, G., Fussell, K. M. D., Johnson, L. T., ... & Winslow, C. (2019). Commentary: Achieving phosphorus reduction targets for Lake Erie. *Journal of Great Lakes Research*, 45(1), 4-11.

Wilson, G. V., Ursic, M., Fox, G. A., & Nieber, J. L. (2020). Internal erosion of soil pipes: Sediment rating curves for soil pipes. *Earth Surface Processes and Landforms*, 45(15), 3902-3916.

Wittenberg, H. (1999). Baseflow recession and recharge as nonlinear storage processes. *Hydrological Processes*, 13(5), 715-726.

- Wilson, G. V., Wells, R., Kuhnle, R., Fox, G., & Nieber, J. (2018). Sediment detachment and transport processes associated with internal erosion of soil pipes. *Earth Surface Processes and Landforms*, 43(1), 45-63.
- Wilson, G. V., Ursic, M., Fox, G. A., & Nieber, J. L. (2020). Internal erosion of soil pipes: Sediment rating curves for soil pipes. *Earth Surface Processes and Landforms*, 45(15), 3902-3916.
- Woodhouse, J.M., Johnson, M.S. 1991. Effects of soluble salts and fertilizers on water storage by gel forming soils conditioners. *Acta Horticulture* 294, 261-269.
- Wright, R. B., Lockaby, B. G., & Walbridge, M. R. (2001). Phosphorus availability in an artificially flooded southeastern floodplain forest soil. *Soil Science Society of America Journal*, 65(4), 1293-1302.
- Wu, Z., Huang, N. E., Long, S. R., & Peng, C. K. (2007). On the trend, detrending, and variability of nonlinear and nonstationary time series. *Proceedings of the National Academy of Sciences*, 104(38), 14889-14894.
- Xu, S., Gentry, L., Chen, K. Y., & Arai, Y. (2020). Intensive agricultural management-induced subsurface accumulation of labile phosphorus in Midwestern agricultural soils dominated by tile lines. *Soil Science Society of America Journal*, 84(4), 1094-1109.
- Xylem/YSI incorporation. 2020. EXO User Manual, <https://www.ysi.com/file%20library/documents/manuals/exo-user-manual-web.pdf>
- Youssef, M.A., Skaggs, R.W., Chescheir, G.M., Gilliam, J.W., 2005. The nitrogen simulation model, DRAINMOD-NII. *Trans. ASAE* 48, 611–626.
- Zhu, J., Li, M., & Whelan, M. (2018). Phosphorus activators contribute to legacy phosphorus availability in agricultural soils: A review. *Science of the Total Environment*, 612, 522-537.
- Zuecco, G., Penna, D., Borga, M., & Van Meerveld, H. J. (2016). A versatile index to characterize hysteresis between hydrological variables at the runoff event timescale. *Hydrological Processes*, 30(9), 1449-1466.
- Zhao, S. L., Gupta, S. C., Huggins, D. R., & Moncrief, J. F. (2001). Tillage and nutrient source effects on surface and subsurface water quality at corn planting. *Journal of Environmental Quality*, 30(3), 998-1008.



## VITA

### **Education**

- Ph.D. Biosystems and Agricultural Engineering, University of Kentucky** 2017-2021
- *Dissertation title:* Impacts of Preferential Flow, Source Water Connectivity, and Agricultural Management Practices on Sediment and Particulate Phosphorus Dynamics in Midwestern Tile-Drained Landscapes
  - *Advisor:* William Ford
- M.Sc. Civil and Environmental Engineering, University of Kentucky** 2015-2017
- *Dissertation title:* Assessment of Watershed Nutrient Loads and Effectiveness of Best Management Practices
  - *Advisor:* Lindell Ormsbee
- M.Sc. Water Engineering, Tehran Polytechnic** 2012-2015
- B.Sc. Civil Engineering, Shahid Bahonar University of Kerman** 2008-2012

### **Professional Positions**

#### *Teaching assistant:*

- BAE 502: Modeling of Biological Systems (University of Kentucky)** 2018-2019
- Teaching Assistant, Instructor: Dr. William Ford
- CE 534: Pavement Design (University of Kentucky)** 2016
- Teaching Assistant, Instructor: Dr. Kamyar Mahboub
- CE 211: Surveying (University of Kentucky)** 2016
- Teaching Assistant, Instructor: Todd Saladin

#### *Research assistant:*

- Civil and Environmental Engineering Department (University of Kentucky)** 2015-2017
- Graduate Research Assistant
- Biosystems and Agricultural Engineering Department (University of Kentucky)** 2017-2021
- Graduate Research Assistant

### **Honors and Certificates**

- Student scholarship award (\$1000) of NCERA 217 to present in “drainage design and management practice to improve water quality” annual meeting, Fargo, SD, 2019.
- Stream and Watershed Science Graduate Certificate, Biosystems and Agricultural Engineering Department at University of Kentucky, 2017.

## **Presentations**

- Nazari, S., Ford, W. I., & King, K. W. (2020). Using continuous high-frequency sensing to elucidate sediment sources and pathways to tile drainage. ASABE Conference, Omaha, NE.
- Nazari, S., Ford, W. I., & King, K. W. (2019). Quantifying Particulate Phosphorus Fluxes and Dynamics in Fine-textured Tile Drained Landscapes of Ohio. ASABE Conference, Boston, MA.
- Nazari, S., Ford, W. I., & King, K. W. (2018). Edge-of-Field Modeling to Quantify the Contribution of Macropore Flow into Nitrogen Loading for Poorly Drained Agricultural Fields, ASABE Conference, Detroit, MI.
- Nazari, S., & Ormsbee, L. Urban and Agricultural Nutrient Event Mean Concentration and Export Load Data for Watershed Quality Assessment Models. (2017). In World Environmental and Water Resources Congress (pp. 273-282).
- Nazari, S., Mousavi, S. J., Behzadian, K., & Kapelan, Z. (2014). Sustainable urban water management: a simulation optimization approach, Hydroinformatics Conference, New York.
- Nazari, S., Mousavi, S. J., Behzadian, K., & Kapelan, Z. (2014). Compromise programming based scenario analysis of urban water systems management options: Case study of Kerman City. Hydroinformatics Conference, New York.
- Behzadian, K., Kapelan, Z., Morley, M. S., Venkatesh, G., Brattebø, H., Sægrov, S., ... & Mousavi, S. J. (2015). Quantitative assessment of future sustainability performance in urban water services using watermet2. In IWA/TRUST Cities of the Future Conference, Mülheim, An Der Ruhr, Germany.

## **Publications**

- Nazari, S., Ford, W. I., & King, K. W. (2020). Impacts of preferential flow and agroecosystem management on subsurface particulate phosphorus loadings in tile-drained landscapes. *Journal of Environmental Quality*, P1370-1383.
- Nazari, S., Ford, W. I., & King, K. W. (2021). Elucidating the impact of preferential flow on sediment transport in tile-drainage. *Vadose Zone Journal*, <https://doi.org/10.1002/vzj2.20154>
- Nazari, S., Ford, W. I., & King, K. W. (2021). Impacts of drainage water management on flow pathway-connectivity and sediment phosphorus dynamics in a tile-drained agroecosystem, (To be submitted).
- Nazari, S., Ford, W. I., & King, K. W. (2021). The role of flow pathway, source water connectivity, and environmental gradients on tile-drain sediment transport dynamics (To be submitted).
- Nazari, S., Ebadi, T., & Khaleghi, T. (2015). Assessment of the nexus between groundwater extraction and greenhouse gas emissions employing aquifer modelling. *Procedia Environmental Sciences*, 25, 183- 190.

- Shojaee, S., Izadpanah, E., & Nazari, S. (2014). Imposition of the essential boundary conditions in transient heat conduction problem based on Isogeometric analysis. *scientiairanica*, 21(6), 1962-1972.

Saeid Nazari